

# **Dendritic Polyglycerolsulfate Micelles for the Targeted Delivery of Chemotherapeutics**

Inaugural-Dissertation  
to obtain the Academic Degree  
**Doctor rerum naturalium (Dr. rer. nat.)**

Submitted to  
Department of Biology, Chemistry, Pharmacy  
Institute of Chemistry and Biochemistry  
Freie Universität Berlin

by  
*Daniel Braatz*  
from Berlin, Germany

Berlin, 2023

The following results and thesis were accomplished from **April 2019** until **August 2023** under the supervision of Prof. Dr. Rainer Haag at the Institute of Chemistry and Biochemistry of Freie Universität Berlin.

**1<sup>st</sup> Reviewer:** Prof. Dr. Rainer Haag,  
Freie Universität Berlin

**2<sup>nd</sup> Reviewer:** Prof. Dr. Matthias Ballauff,  
Freie Universität Berlin

**Day of Defense:** 04. December 2023

## STATUTORY DECLARATION

I, Daniel Braatz, declare that I have independently authored this submitted thesis titled "*Dendritic Polyglycerolsulfate Micelles for the Targeted Delivery of Chemotherapeutics*". Further, it is understood that this work or parts of it have not been previously presented or submitted for the award of any other degree or diploma in any university or tertiary institution to my knowledge.

Berlin, 7 August 2023

---

*Daniel Braatz*

## ACKNOWLEDGMENTS

First things first, great thanks go to Prof. Dr. Rainer Haag for giving me the opportunity to conduct my doctoral studies in his research group; being part of this has been an immense pleasure. I acknowledge that you always allowed me to develop my own ideas and that I could always count on your support to turn them into reality. Thanks for supporting me financially and scientifically over the past years.

Another big thanks to Prof. Dr. Matthias Ballauff for being my second reviewer and for his continuous support and guidance during my thesis. I am grateful that you always lend me a hand while preparing my manuscripts.

Also, I appreciate the possibility offered by Prof. Dr. Timothy E. Kennedy to join his research group at McGill University in Montréal, Canada. You broadened my scientific horizon and gave me unique insights into your country; I will always keep these things in good memory. Thanks to all my Canadian, French, American, Turkish, and Argentinian TEK-lab members, to name only a few: Gaby Kennedy, Nathalie Marcal, Jean-Pierre Clément, Daryan Chitsaz, Jean Madranges, Dr. Jean-David Gothié, Teddy Fisher, Emma van den Busch, Melissa Pestemalciyan and Dr. Nonthue Ucelli; I acknowledge all of you for your hospitality and creating such a lovely and wicked good atmosphere. In this regard, I also must thank Prof. Dr. Janine Mauzeroll and Dr. Danny Chhin for allowing me to conduct parts of my lab work in their laboratories. Dr. Bastian Krüger, Mathieu Rivard, and Jeremy Dawkins are thanked for the warm welcome and all the funny adventures in and outside the Pulp and Paper Research Institute.

Prof. Dr. Kevin Pagel, in this role as the IRTG2662 spokesperson, is thanked for appointing me as the temporary scientific coordinator of his “International Research Training Graduate School: Charging into the Future; Understanding the Interaction of Polyelectrolytes with Biosystems”.

Prof. Dr. Michael Schirner is greatly thanked for his strong support in discussing pharmacological questions regarding *in vitro* cell experiments and *in vivo* animal studies.

Moreover, I thank Dr. Mathias Dimde for his interest and passion in supporting and guiding me during our longstanding cooperation. He is also greatly thanked for performing the cryo-EM studies. I acknowledge Dr. Ehsan Mohammadifar for inviting me to be his fume hood’s mate; thanks for introducing me to lab 34.02. With that, I want to thank all my other lab members for the great camaraderie in our laboratory: Dr. Alexander Oehrl, Dr. Magda Ferraro, Dr. Maiko Schulze, Mariam Cherri, Sebastian Schötz, Björn Goerisch, and Adele Griepe.

I am grateful that I could supervise such excellent students for either their Bachelor’s, Master’s, research internships, and/or during their stays as working students; names are

Guoxin Ma, Maximilian Braun, Alexandros Mavroskoufis, Justus Peer Heinrich Peter, Patricia Petsch, Gideon Noelte, Carmen Olivares, and Yizhe Pan.

Large parts of this thesis were only possible due to the great help of my bio-lab colleagues: Dr. Katharina Achazi, Elisa Quaas, and Johanna Scholz. For their support from behind the scenes, thanks to all technicians in the working group: Anja Stöshel, Cathleen Hudziak, Katharina Goltsche, and Marleen Selent. Whenever I felt lost in administrative stuff and related paperwork, I knew I could count on the help of Anna Wolf and Dr. Svenja Herzinger; thanks a bunch to both of you.

Special thanks go out to all former and current members and associates of AG Haag for creating such a lovely and enjoyable atmosphere, to only name a few not already mentioned: Dr. Felix Reisbeck, Dr. Michael Tully, Dr. Isabelle Heing-Becker, Dr. Stephanie Wedepohl, Dr. Yannic Kerkhoff, Clemens Krage, Ann-Cathrin Schmitt, Hanna Koeppe, Lasse Kalle Riediger, Weronika Malicka, and Thomas Hohmann. Dr. Wiebke Fischer, who always knew the solution to every-mentionable problem, is thanked for troubleshooting.

Knowing to have friends on this planet Earth you can go through thick and thin with, whom you knew so well, who nevertheless could surprise you, who see themselves as complementary and who want to act together by sharing a vision to achieve a common goal: Kais Belkahla, Suvrat Chowdhary, Pascal Hinz, Maurice Zantop, and Alexander Vogler. Thank you for enriching my life and for reinforcing this sentiment by having such great partners on your side.

The following comes from the bottom of my heart and is meant for my parents, Regina and Detlef Braatz: Thank you for your support and unwavering faith in me. Arnim and Cordula Schoor, it did not go unnoticed that you care for me like I am one of your children.

They say the best always comes at last; with that, my sincerest appreciation to Anja 'Mein Mausi' Schoor: your endless love has always guided me - I can't wait to welcome Emi into our life.

Für meine Familie

# Table of Contents

STATUTORY DECLARATION.....	III
ACKNOWLEDGMENTS.....	IV
<b>1 INTRODUCTION.....</b>	<b>1</b>
<b>2 THEORETICAL BACKGROUND.....</b>	<b>3</b>
2.1 POLYMERIC DRUG DELIVERY SYSTEMS: THE HOLY GRAIL OF CHEMOTHERAPY?.....	3
2.2 DRUG DELIVERY SYSTEMS: DESIGN OF BLOCK COPOLYMER MICELLES.....	4
2.2.1 <i>Hydrophilic Polymers: Shell Forming Segment</i> .....	6
2.2.2 <i>The “Gold Standard”: Polyethylene Glycol</i> .....	7
2.2.3 <i>Alternatives to PEG</i> .....	7
2.2.3.1 Linear and Hyperbranched Polyglycerol Architectures.....	8
2.2.3.2 Dendritic Polyglycerolsulfate.....	11
2.2.3.3 Natural Biopolymers: Polysaccharides.....	12
2.2.3.4 Hydrophilic Poly(oxazoline)s: PMeOx and PEtOx.....	12
2.2.4 <i>Hydrophobic Polymer: Core Forming Segment</i> .....	14
2.2.4.1 Polyesters: PCL, PLGA, and PLA.....	15
2.2.4.2 Polyether: Polypropylene oxide.....	16
2.2.4.3 Polyaminoacids: Drug-Conjugates and Metal-Complexation.....	16
2.2.4.4 Poly[N-(2-hydroxypropyl) Methacrylamide].....	18
2.2.4.5 Hydrophobic Poly(2-oxazoline).....	19
2.2.4.6 Poly(ester-co-amide)s: New Platform for Drug Delivery.....	20
2.2.5 <i>Delivery of Nanomedicine: Passive and Active Targeting</i> .....	20
2.2.6 <i>Stimuli-Responsive Drug Release in Nanotherapeutics</i> .....	21
2.2.6.1 Endocytic Pathway: Acidic and Enzymatic Hydrolysis.....	22
2.2.6.1.1 Ester Linkages.....	23
2.2.6.1.2 Amide Linkages.....	23
2.2.6.1.3 Hydrazone Linkages.....	24
2.2.6.2 Reductive Drug Release via Disulfide Exchange.....	24
2.2.6.3 Orthogonal Drug Release: Photochemical Sensitivity.....	25
2.3 NONCOVALENT INTERACTIONS IN SUPRAMOLECULAR DRUG DELIVERY SYSTEMS.....	26
2.4 MORPHOLOGY OF DRUG DELIVERY SYSTEMS: CONTROLLING PACKING PARAMETERS.....	29
2.5 ORGANOCATALYSIS IN POLYMER CHEMISTRY.....	30
<b>3 SCIENTIFIC GOALS.....</b>	<b>33</b>
<b>4 PUBLICATIONS AND MANUSCRIPTS.....</b>	<b>36</b>
4.1 TOOLBOX OF BIODEGRADABLE DENDRITIC (POLY GLYCEROL SULFATE)–SS–POLY(ESTER) MICELLES FOR CANCER TREATMENT: STABILITY, DRUG RELEASE, AND TUMOR TARGETING.....	36
4.2 DENDRITIC POLYGLYCEROLSULFATE–SS–POLY(ESTER AMIDE) MICELLES FOR THE SYSTEMIC DELIVERY OF DOCETAXEL: PUSHING THE LIMITS OF STABILITY THROUGH THE INSERTION OF $\pi$ – $\pi$ INTERACTIONS.....	37
<b>5 CONCLUSION AND OUTLOOK.....</b>	<b>38</b>
<b>6 ZUSAMMENFASSUNG.....</b>	<b>42</b>
<b>7 REFERENCES.....</b>	<b>47</b>
<b>LIST OF ABBREVIATIONS.....</b>	<b>57</b>
<b>SCIENTIFIC OUTREACH: PUBLICATIONS, PATENTS, CONFERENCES.....</b>	<b>60</b>
PUBLICATIONS.....	60
PATENTS.....	60
CONFERENCE CONTRIBUTIONS.....	60

# 1 Introduction

In 2023, the American Cancer Society approximates almost two million new cancer cases in the United States – another 600,000 patients will die – making it the second leading cause of death after cardiac arrest.<sup>[1]</sup> These numbers indicate that the development of high-performance chemotherapeutics still plays a significant role in maintaining global health. The current state of chemotherapy is based on administering highly hydrophobic small-molecule drugs to kill the cancer cell or stop it from dividing. However, the minimal water solubility of cancer medicines challenges their intravenous administration. The fast pace and success of macro- and microscale polymeric drug delivery systems from the 1960s drove the further downsizing of functional carrier systems by understanding the self-assembly of polymers able to form systems in the nanoscale size regime.<sup>[2]</sup> An answer to this question could be given thanks to the pioneering works of Kataoka and Kabanov in the early 1980s, which paved the way for polymeric micelles to take their part in the fight against cancer.<sup>[3]</sup> Their works were the first milestones demonstrating that polymeric micelles can find their niche in a clinical application acting as solubilization enhancers, so-called “nanocapsules”. Besides, the development of polymeric micelles, the urge for suitable nanosized carrier systems also led to the design of several other architectures, such as unimolecular micelles,<sup>[4]</sup> or polymeric liposomes - so-called polymersomes<sup>[5]</sup> (see Figure 1). However, given their dynamic and versatile nature, polymeric micelles were the identified candidates for this thesis.

Still, nowadays, the design of polymeric micelles challenges scientists from chemistry, biology, pharmacy, and medicine in equal measure. Over 100 years after Paul Ehrlich’s vision of the “Magic Bullet”<sup>[6]</sup> and Helmut Ringsdorf’s proposal of the “Ringsdorf Model” in 1975,<sup>[7]</sup> the significant challenges remain unchanged, which can be summarized with the following four key points: (i) polymeric micelles are in equilibrium with their unimers; so dilution in the bloodstream must not lead to disassembly; (ii) nonspecific interactions with the reticuloendothelial system (RES) and blood compartments must be avoided; (iii) the carrier must deliver its therapeutic cargo selectively to its site of action with no accumulation in healthy tissue; and (iv) upon cellular uptake, the cargo must be released from the carrier system. Thus, the first border of self-assembled systems is to resist the high dilution in the bloodstream, which can cause the concentration to fall below the critical micelle concentration (CMC). Further, nonspecific interactions with serum proteins and other compartments of the patient’s blood can lead to forming of a biomolecular layer around the particle, where this event has been shown to adversely alter the stabilities and targeting properties of the systems.<sup>[8]</sup>

The urgent demand for high-performance drug delivery systems has attracted the attention of academia and industry, resulting in eleven amphiphilic block copolymer micelles



that have undergone clinical trials.<sup>[9]</sup> The variety of hydrophobic polymers for the construction of these systems ranges from polyether to poly(amino acid N-carboxy anhydrides) (NCA)s and over polyesters to methacrylates; what all of them have in common is the hydrophilic shell made of poly(ethylene glycol) (PEG).<sup>[10]</sup> Today, the only two candidates that have entered the market and are used in clinical applications are both based on methoxy poly(ethylene glycol)-*block*-poly(lactide) (mPEG-*b*-PDLLA; Genexol<sup>®</sup>: Paclitaxel; Nanoxel<sup>®</sup>: Docetaxel).<sup>[11]</sup> Yet, there is no second candidate in close consideration for market authorization. Using PEG promises inert, so-called “stealth particles”, and its approval by the Food and Drug Administration (FDA) and European Medicine Agency (EMA) for food, cosmetic, and pharmaceutical usage suggests excellent biocompatibility. However, there are indications that systematic overexposure to PEG has caused the formation of anti-PEG antibodies in the population, the so-called accelerated blood clearance (ABC) phenomenon,<sup>[12]</sup> which counteracts the therapeutic effect of nanomedicines. Further, numerous reports indicate strong interactions with serum proteins questioning PEG's stealth effect.<sup>[13]</sup> Thus, these systems do not meet their high therapeutic advantages due to insufficient *in vivo* stabilities and uncontrolled biodistributions.<sup>[14]</sup> Finding a suitable replacement for PEG in amphiphilic block copolymer systems holds great promise to overcome these roadblocks.<sup>[15]</sup>

The present thesis aims at overcoming the various problems of drug delivery systems enumerated above. In this background, dendritic polyglycerolsulfate (dPGS) will be evaluated as an alternative polymer to PEG as the shell-forming segment with the goal of biocompatible and tumor-targeting micelles. Moreover, it investigates the influence of the core-polymer's nature to beneficially alter the stability and drug-loading capacity of these systems to boost the therapeutic potential of dPGS-based drug delivery systems.

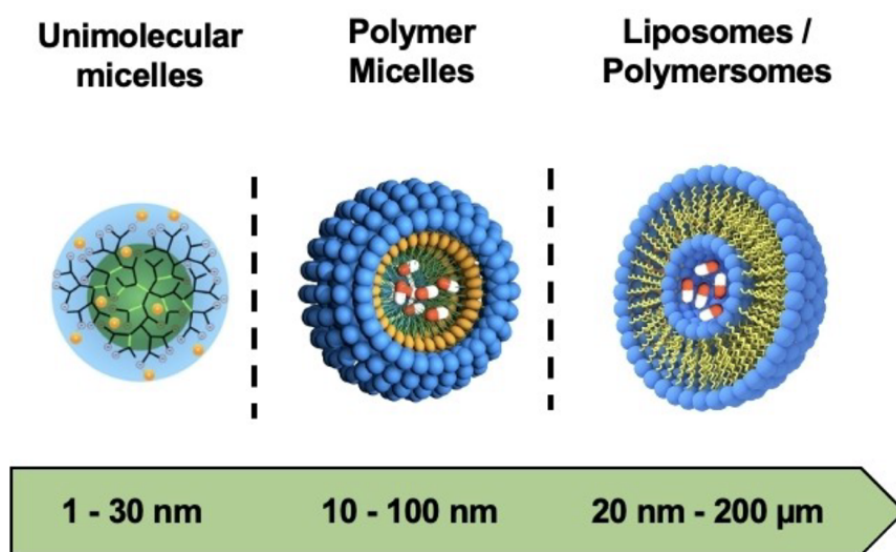


**Figure 1.** Schematic depiction on the different architectures and categories of polymeric drug delivery systems. Reprinted from Ref. <sup>[16]</sup> Copyright 2022, Wiley-VCH Verlag GmbH & Co. KGaA, Weinheim.

## 2 Theoretical Background

### 2.1 Polymeric Drug Delivery Systems: The Holy Grail of Chemotherapy?

Chemotherapy is a part of medical oncology that refers to the intravenous injection of chemotherapeutics. Since anti-cancer drugs don't discriminate between cancerous and healthy cells, altering their pharmacokinetics and pharmacodynamics is indispensable, ensuring selective accumulation on the site of action. Additionally, to that, the drug's extremely high hydrophobicity and fast degradation in the *in vivo* environment further challenge intravenous administration. The encapsulation in drug delivery systems promises to overcome these problems by facilitating the water-solubility of the agents, enhancing their half-time by shielding them from the outer environment, and thus guaranteeing a good patient's life quality by altering the drug's pharmacokinetics. After the approval of the very first nanomedicine DOXIL® in 1995<sup>[17]</sup> - a liposomal formulation of Doxorubicin - different strategies have been exploited to improve the therapeutic index of chemotherapy. Several have led to market-authorized systems, such as protein-drug conjugates (Abraxane®, albumin-bound PTX),<sup>[18]</sup> low molecular weight surfactants (Taxol®),<sup>[19]</sup> and polymeric micelle formulations (Genexol®, Nanoxel®). Comparing the self-assembled systems, the major limitation of low molecular weight surfactants lies in their insufficient stability, causing rapid disaggregation *in vivo*; thus, the substitution of low molecular weight surfactants by polymeric micelles promises superior stabilities due to the increased interfacial interaction of the larger hydrophobic segments. However, many systems don't match their high therapeutic expectations drawn from *in vitro* results if translated to *in vivo* settings.<sup>[20]</sup>

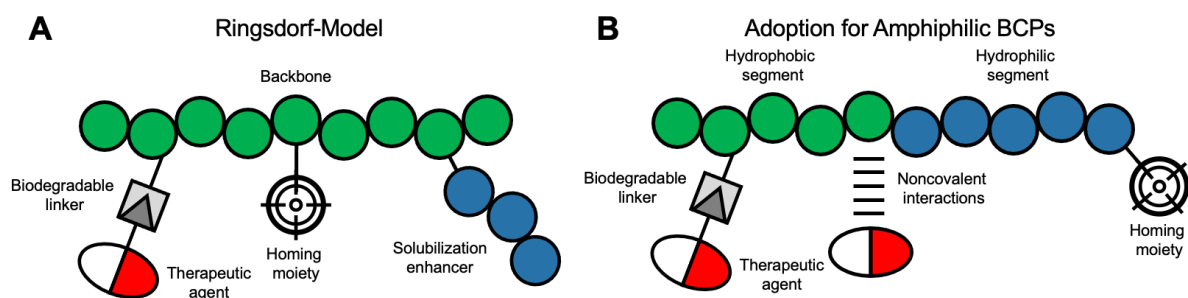


**Figure 2. (A)** Concept drawing of the original proposed Ringsdorf-Model by Helmut Ringsdorf in 1975;<sup>[7]</sup> **(B)** The Ringsdorf-Model after adoptions that have been made for the design of amphiphilic block copolymer polymers; the significant variation can be found in the installment of noncovalent interactions encapsulating the drug rather than exclusively conjugating them *via* biodegradable linkers.

According to the Ringsdorf-Model, a “pharmacologically active polymer”, such as a drug delivery system, must fulfill the following characteristics: (i) a hydrophilic unit must ensure the water solubility of the whole system; (ii) the drug must be covalently attached to the polymeric backbone *via* a stimuli-sensitive linker; and (iii) a homing-device - a targeting unit - must facilitate the selective accumulation of the system on its site of action (Figure 2A).<sup>[7]</sup> The last characteristic proposed by Ringsdorf – the targeting unit - also satisfies Paul Ehrlich’s vision of the “Magic Bullet”, describing a medication that explicitly kills its target without harming the body itself.<sup>[21]</sup> However, until today, no system can fulfill the claims of Ringsdorf and Ehrlich to their full extent. For example, for amphiphilic block copolymers, two different classes of systems have been established:<sup>[22]</sup> (i) amphiphilic polymer-drug conjugates carrying the drug *via* stimuli-sensitive linkers; or (ii) encapsulation of the drug *via* noncovalent interactions between the hydrophobic block and the drug, acting as “solubilizers” (Figure 2B). The only micellar system that offers active targeting is BIND-014, but it follows the second approach by physically entrapping the drug; therefore, it is not a Ringsdorf-Model-like system.

## **2.2 Drug Delivery Systems: Design of Block Copolymer Micelles**

Block copolymer micelles (BCM) are constructed by self-assembling amphiphilic block copolymers built from biocompatible synthetic polymers or natural macromolecules.<sup>[23]</sup> Given their core-shell structure, these systems can carry several chemotherapeutics in their hydrophobic inner core, wherein the outer-hydrophilic shell facilitates water solubility. The respective block copolymer's nature determines the drug delivery system's structure and function. The self-assembly, drug-loading capacity, stability, and performance in biological fluids can be controlled by tailoring the identity of the block copolymer composition. In addition to their properties determining the structural and functional role, the safety and accessibility of the segments are other criteria to be considered. The critical challenge lies in carefully selecting the suitable hydrophilic component with the appropriate hydrophobic part to design high-performance drug delivery systems. Over the past years, several hydrophilic (Table 1) and hydrophobic polymers (Table 2) have been investigated as shell-forming or core-forming segments, respectively. They will be further discussed in the following chapters in more detail.

The fate of polymeric micelles is mainly determined by their physiochemical characteristics, which alter the *in vivo* performance of the later system, including size, size distribution, morphology, and stability. The stability can be divided into two different components: (i) thermodynamic; and (ii) kinetic stability; thermodynamic stability gives insights into how the system behaves in equilibrium, giving the CMC; kinetic stability describes the behavior of the systems over time; e.g., during long-term storage or blood circulation.<sup>[24]</sup> The most common techniques to measure stability are based on absorbance, fluorescence, or light

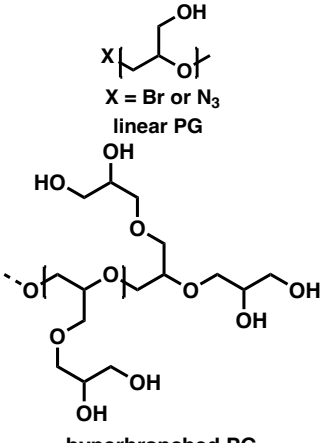
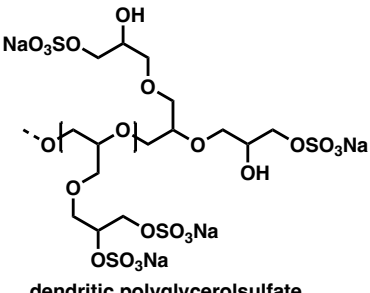
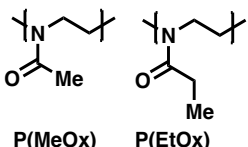
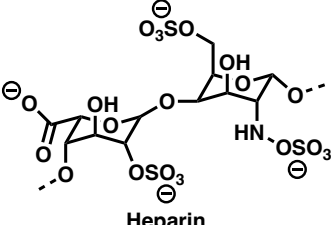
scattering approaches.<sup>[25]</sup> Over the last years, light scattering has become a considerable alternative to absorbance or fluorescence techniques; since a label-free measurement enables high-throughput CMC determination of drug-unloaded and drug-loaded systems.<sup>[26]</sup> By varying the molecular weight and density of the shell-forming segment, the stability of self-assembled systems can be controlled; e.g., it was demonstrated that a dendritic PEG-outer shell enhanced the stability significantly compared to its linear PEG-analogs.<sup>[27]</sup> More, the CMC can be further manipulated by controlling the core-crystallinity, revealing that semicrystalline cores exhibited higher stability over amorphous cores.<sup>[28]</sup> Also, the implementation of  $\pi$ - $\pi$  stacking, host-guest, coordination, or hydrogen interaction up to chemical crosslinking by disulfide exchange, free radical polymerization, or click-reactions in the core has been extensively used to enhance the stability of polymeric micelles.<sup>[29]</sup>

The size and the size distribution play another fundamental role in understanding the performance of polymer micelle. It has been found that the larger-sized micelles have prolonged blood circulation times, resulting in enhanced accumulations in the cancerous tissue; however, larger particles between 100 – 160 nm have shown poorer intra-cellular penetrations compared to smaller micelles around 30 nm; thus, larger particles did not show significantly improved therapeutic efficacy compared to the smaller analogs.<sup>[30]</sup> As a matter of fact, control over the size is another criterion in the design of functional micellar drug delivery systems.

Further, the surface charge determines the particle's blood circulation duration and tumor penetration, giving negatively charged particles prolonged circulation times; in contrast to positively charged particles, which show rapid sequestration in the spleen and liver.<sup>[31]</sup> An central and mainly unresolved question in this regard is the response of the surrounding biological medium to the injected particles.<sup>[32]</sup> Upon administration into the patient's blood, the formation of a biomolecular layer around the particle is eventually caused by the interaction with the patient's blood compartments. Electrostatic interactions between the different biomacromolecules and the polymeric material mainly govern this interaction.<sup>[33]</sup> This opsonization has been shown to adversely alter the stability and pharmacokinetics of the systems,<sup>[34]</sup> decreasing their therapeutic index dramatically; thus, there has been emerging interest in overcoming the undesired interaction of polymeric materials with biological media.<sup>[8b]</sup>

## 2.2.1 Hydrophilic Polymers: Shell Forming Segment

**Table 1.** Overview of the most frequently used hydrophilic shell-forming segment used to construct amphiphilic block copolymers.

Polymer	Chemical structure	Synthesis	Advantages / Limitations
Polyether	$\alpha \text{ X-O} \left[ \text{CH}_2\text{CH}_2\text{O} \right]_n \text{CH}_2\text{CH}_2\text{Y} \omega$ <p>X = H, CH<sub>3</sub> Y = OH, NH<sub>2</sub></p>	aROP of ethylene oxide	<ul style="list-style-type: none"> <li>+ Clinically approved</li> <li>+ Low molecular weight distributions</li> <li>- Non-degradable</li> <li>- PEG-antibodies / Allergic reaction</li> </ul>
Polyglycerols	 <p>X = Br or N<sub>3</sub> linear PG</p> <p>hyperbranched PG</p>	aROP of glycidol or its protected analogs	<ul style="list-style-type: none"> <li>+ Post modifications</li> <li>+ Multifunctionality</li> <li>+ Linear and hyperbranched architectures</li> <li>- Non-degradable</li> <li>- Structure similarities to PEG</li> <li>- Immunogenicity unclear</li> <li>- Research use only</li> </ul>
Polyglycerolsulfate	 <p>dendritic polyglycerolsulfate</p>	Sulfation of hyperbranched PG	<ul style="list-style-type: none"> <li>+ Intrinsic tumor targeting</li> <li>+ No interaction with blood serum proteins</li> <li>+ Multifunctionality</li> <li>+ Gram-scale synthesis</li> <li>- Immunogenicity unclear</li> <li>- Non-degradable</li> <li>- Research use only</li> </ul>
Polyoxazoline	 <p>P(MeOx) P(EtOx)</p>	Living-controlled cationic ROP of oxazolines	<ul style="list-style-type: none"> <li>+ High water solubility</li> <li>+ Control over end-group chemistry</li> <li>? Degradation to PEI</li> <li>- Research use only</li> </ul>
Polysaccharides	 <p>Heparin</p>	Enzymatic synthesis	<ul style="list-style-type: none"> <li>+ Clinically approved</li> <li>+ Biodegradable</li> <li>+ Binds to cell adhesion proteins</li> <li>- Undefined molecular weight distributions and structure</li> <li>- Batch-to-batch variety</li> <li>- Challenging conjugation chemistry</li> </ul>

## 2.2.2 The “Gold Standard”: Polyethylene Glycol

By today, PEG (also known as poly(ethylene oxide (PEO))), originally introduced to the biomedical field to be conjugated to therapeutic proteins leading to PEG-protein conjugates extending the half-time of the proteins,<sup>[35]</sup> is the only hydrophilic polymer in amphiphilic block copolymers that has found its way into clinical investigations. This can be attributed to the fact of PEG’s classification by the FDA as “Generally Regarded as Safe” (GRAS) and its approval for oral, topical, and intravenous use. Also, its hydrophilicity, linearity, chain flexibility, lack of charge, and well-defined structure with a low dispersity of 1.01 obtained by anionic ROP of ethylene oxide have propelled PEG’s wide range of applications.<sup>[36]</sup> By varying the initiator, the PEG’s  $\alpha$ -end-group can be controlled, whereas methoxy (mPEG) is the most prominent one; by choosing an appropriate  $\omega$ -capping moiety, several functional groups, such as alcohols (mPEG-OH) or amines (mPEG-NH<sub>2</sub>) can further be introduced to the polymer structure. These modifications led to the basis for the development of the preparation of block copolymers using mPEG-OH or mPEG-NH<sub>2</sub> as so-called macro-initiators for the polymerization of several cyclic monomers. Further, the  $\omega$ -pending groups can couple several other molecules, such as radical initiators, also enabling the radical polymerization of vinyl-containing monomers.<sup>[37]</sup> However, since PEG only bears a maximum of two functional groups on each polymer chain, the post-modification of its block copolymers by attaching different ligands, such as targeting, or imaging agents, is strictly limited to a maximum of one molecule per chain. Due to their structural similarities to PEG, polyglycerols are increasingly recognized as an alternative albeit their multi-hydroxy-functional nature.<sup>[38]</sup>

## 2.2.3 Alternatives to PEG

The overexposure of the population to PEG, which is used in biomedical and in numerous everyday products such as food, hygiene, or skin care products, has caused the formation of anti-PEG antibodies.<sup>[39]</sup> Due to this, several PEG-alternative hydrophilic macromolecules have been investigated and will be discussed below. Current indications are that polymers sharing structural similarities to PEG, namely the C-C-O backbone, show cross-reactivity and bind to anti-PEG antibodies.<sup>[40]</sup> A head-to-head comparison of PEGylated liposomes with many herein-discussed PEG-alternative polymers, including p(HPMA) and poly(2-methyl-2-oxazoline), revealed increased blood circulation times for all polymers compared to non-modified PEG-liposomes; however, the second injection for the PMeOx-modified liposomes also induced ABC phenomena, which was not the case of the p(HPMA)-liposomes.<sup>[41]</sup> In preclinical studies comparing PEG-liposomes and PEG-micelles, it has been found that anti-PEG antibodies did not affect the pharmacokinetics of polymeric PEG-micelles. In contrast,

the circulation time was markedly decreased for the PEG-liposomes, upon repeated dosing.<sup>[42]</sup> It is believed that the binding of anti-PEG antibodies is also controlled by the core-forming segment's nature and the hydrophilic shell's density, which is higher for polymeric micelles over liposomes.<sup>[43]</sup> Whether or not the ABC phenomenon also applies to polymeric micelles is still unclear. Still, the search for replacements for PEG must be continued to achieve highly functional, customized polymers, enhancing the therapeutic index. These observations strongly support the need for more studies to understand the patient's immune response to applied nanomedicines.

### 2.2.3.1 Linear and Hyperbranched Polyglycerol Architectures

In 1952, Paul Flory published his theory on hyperbranched polymers obtained from AB<sub>2</sub>-type monomers.<sup>[44]</sup> In 1966, Sandler and Berg showed for the first time that glycidol, an AB<sub>2</sub>-type monomer, could easily be polymerized at room temperature in the presence of triethylamine, pyridine, lithium hydroxide, potassium hydroxide, sodium hydroxide, sodium methoxide, sodium amide, and other catalysts.<sup>[45]</sup> 30 years later, Dworak *et al.* described the cationic polymerization of glycidol in the presence of Lewis or Bronsted acids.<sup>[46]</sup> They also introduced two new mechanistic pathways of this polymerization: active chain end and activated monomer.<sup>[47]</sup> To overcome the limitations of cationic polymerization, Sunder *et al.* employed anionic ring-opening multi-branching polymerization in combination with slow monomer addition to the polymerization of glycidol.<sup>[48]</sup> The slow addition of glycidol to the partially deprotonated initiator 1,1,1-Tris(hydroxymethyl)propane (TMP) at temperatures of 90-100°C avoided the intra-cyclization of low molecular weight hPGs, which would lead to chain termination reactions. This has led to hyperbranched polymers in the 1250-6500 g/mol range and dispersity of 1.13-1.47.<sup>[48]</sup> Figure 3 shows the schematic synthetic pathway and mechanism of the anionic ring-opening polymerization of glycidol initiated by various initiators. Given the AB<sub>2</sub>-type manner of the monomer glycidol, the hyperbranched structure contains three different structural motifs: (i) terminal (T); (ii) linear (L); and (iii) dendritic (D) glycerol subunits.

Due to its polyether backbone, hyperbranched polyglycerol lacks degradable moieties, so the synthesis of biodegradable hPGs has been investigated, leading to hPG scaffolds containing a variety of stimuli-sensitive groups, including acetal,<sup>[49]</sup> ketal,<sup>[50]</sup> ester,<sup>[51]</sup> and disulfide linkages.<sup>[52]</sup> Since then, hPGs have attracted tendinous interest due to their dendrimer-like structure, excellent bio- and blood-compatibility, low intrinsic viscosity, compact size, multi-functionality, and ease of gram-to-kilogram synthesis, and were investigated for numerous biomedical applications.<sup>[53]</sup>

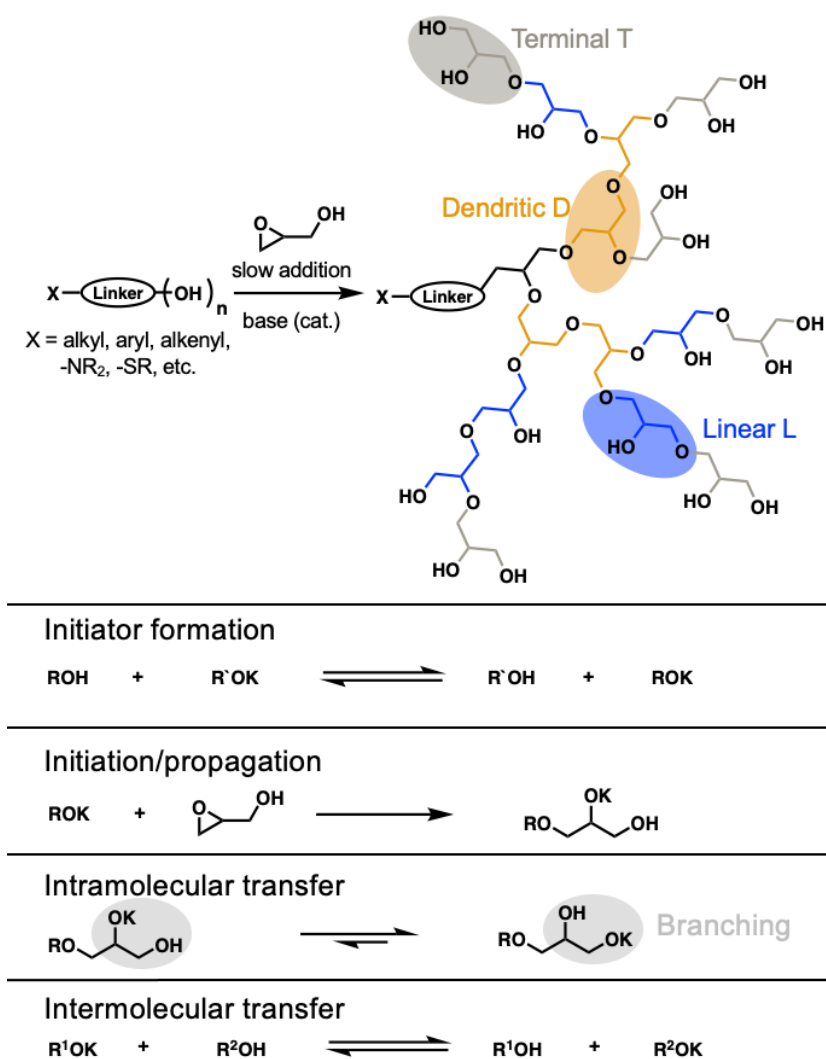


**Figure 3.** Synthetic scheme for the preparation of dendritic polyglycerol *via* slow monomer addition of glycidol to an activated alcohol initiator acquires dendritic polyglycerol.

While the polymerization of glycidol obtains hyperbranched polyglycerols, its linear polymeric analogs require the protection of the hydroxy group with later deprotection again, preventing branching in the first step, see Figure 4. The commonly used monomers for the synthesis of linear polyglycerol are trimethylsilyl glycidyl ether (TMSGE), ethoxyethyl glycidyl ether (EEGE), *tert-butyl* glycidyl ether (tBGE), and allyl glycidyl ether (AGE). Even though EEGE is the only non-commercially available monomer, the facile removal of the acetal-protecting group under mildly acidic conditions has made it the most frequently used monomer in this list.<sup>[38]</sup> In 1968, Koenuma *et al.* described the first polymerization of epoxyorganosilanes.<sup>[54]</sup> After the first hurdles of the base catalysis and the coordination-polymerization of linear polyglycerol; in 1993, Taton *et al.* reported the first successful anionic ring-opening polymerization of EEGE using CsOH as an initiator. However, in anionic polymerization, the



chain transfer reaction between the propagating chain or the initiator oxyanion and EEGE, which leads to the formation of an allyl alkoxide, limits the molecular weight and dispersity. Thus, Deffieux *et al.* described a new strategy where they activated the monomer toward nucleophilic attacks and reduced the basicity of the growing chain by using triisobutyl aluminum (*i*-But<sub>3</sub>Al).<sup>[55]</sup> In 2009, this approach, called “monomer-activated anionic polymerization”, was also employed in the polymerization of EEGE and tBGE leading to well-defined, high molecular weight linear polyglycerols.<sup>[56]</sup> Indeed, PEG and linear polyglycerol share structural similarities; PEG is given a highly crystalline material, whereas, due to the steric hindrance of the pending hydroxy groups, linear polyglycerol is a viscous and amorphous material. Nevertheless, its high water solubility, good bio- and blood compatibility,<sup>[57]</sup> and multi-functionality have attracted linear polyglycerol's great potential for replacing PEG in diblock copolymers, triblock copolymers, and other biomedical applications.<sup>[58]</sup>

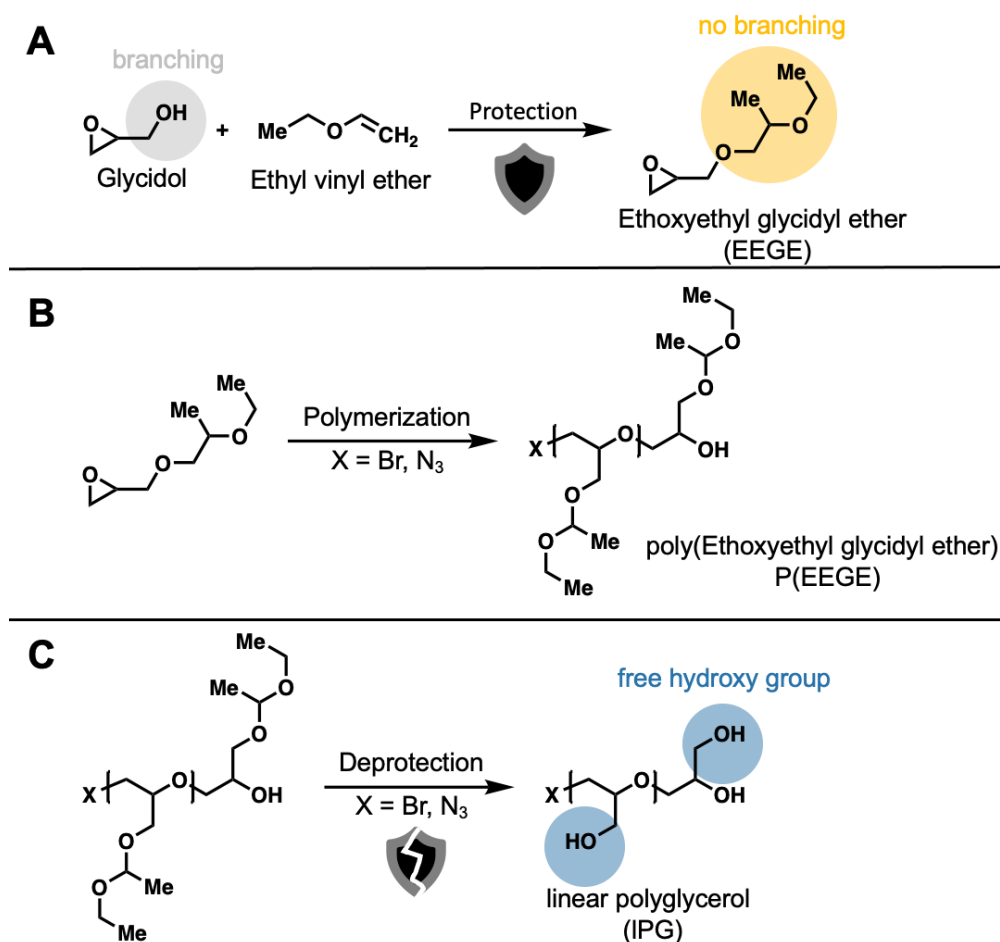


**Figure 4.** Synthetic scheme for the preparation of linear polyglycerol **(A)** prior protection of the AB<sub>2</sub> monomer glycidol to avoid the formation of a hyperbranched polymer forming EEGE; **(B)** polymerization of the acetal-protected monomer EEGE; **(C)** Deprotection of the acetals acquiring linear polyglycerol.

### 2.2.3.2 Dendritic Polyglycerolsulfate

Dendritic polyglycerolsulfate is a hyperbranched, highly water-soluble, biocompatible, synthetic polyelectrolyte originally synthesized for the first time by Türk *et al.* in 2004, who were on the search for a potential replacement for heparin, which was dPGS.<sup>[59]</sup> They found increased anticoagulant and anticomplementary activities for dPGS by up to 2-fold compared to unfractionated heparin (UFH). Upon sulfation of the polyol dendritic polyglycerol using a sulfur trioxide-pyridine complex and subsequently quenching of the reaction with aqueous sodium hydroxide, the polyanionic dPGS was obtained in high gram-scale with a broad range of adjustable sulfation degrees and molecular weights. Due to its low anticoagulant activity and high anticomplementary effect, dPGS has emerged with great potential over the last years for biomedical applications,<sup>[60]</sup> such as an anti-inflammatory agent but incredibly as selective tumor-targeting nanomedicine. Since then, dPGS has been widely studied for targeted nanomedicine of drug-conjugates<sup>[61]</sup> and so-called “unimolecular” micelles.<sup>[62]</sup> But its implementation onto polymeric micellar drug delivery systems acting as the hydrophilic segment has been its most substantial approach to date, as demonstrated by Zhong *et al.* in 2016,<sup>[63]</sup> where this approach will further be exploited in the frame of this thesis.

In 2010, Dervede *et al.* revealed that the cancer-homing ability of dPGS could be traced down to its multivalent and electrostatically interaction with L-selectine,<sup>[64]</sup> a positively-charged, overexpressed cell adhesion protein during cancer progression.<sup>[65]</sup> Comparing several anions, it has been demonstrated that the sulfate anions show the strongest binding affinity towards L-selectine in the following order carboxylate < phosphate < phosphonate ≈ sulfonate < bisphosphonate < sulfate.<sup>[66]</sup> Further, it has been demonstrated that the larger the dendritic polyglycerol core and the higher the degree of sulfation, the higher the binding potential of the polymers, as revealed by SPR binding assays.<sup>[64]</sup> To further understand the high therapeutic outcomes of the dPGS-functionalized systems, Ballauff *et al.* performed several ITC experiments revealing that dPGS does not interact with HSA under physiological conditions (150 mM, 37°C, pH 7.4).<sup>[67]</sup> This finding is crucial for understanding the targeting ability of the dPGS-functionalized systems, as the formation of a biomolecular layer has been demonstrated to adversely influence the pharmacokinetic and cellular uptake of intravenously injected particles.<sup>[68]</sup>

Based on these findings, dPGS-functionalized polymeric micelles are believed to exhibit extraordinarily high therapeutic efficacy and tumor-targeting ability due to the installment of an additional dimension of multivalency due to their supramolecular nature.<sup>[69]</sup>

### 2.2.3.3 Natural Biopolymers: Polysaccharides

Several polysaccharides, such as chitosan, hyaluronic acid, heparin, alginate, and chondroitin sulfate have been investigated as the shell-forming segment of amphiphilic block copolymers.<sup>[70]</sup> Compared to synthetic macromolecules, biopolymers, such as polysaccharides, promise excellent biocompatibility and biodegradation; however, for using biopolymers, their availability, stability, and, mostly, safety and batch-to-batch variability need to be considered, as they are derived from natural sources like animal, plant, or algal origins.

Heparin, discovered in 1916, is a negatively charged polysaccharide that has been used as an anticoagulant in clinics since 1935.<sup>[71]</sup> Nowadays, it is also investigated for inhibiting angiogenesis and tumor growth.<sup>[72]</sup> For example, mixed micelles of heparin-conjugates and Pluronics showed that the permeability of PTX through rat small intestine was 5- to 6-fold higher with heparin-conjugated micelles than that of pure Taxol.<sup>[73]</sup> Also, hyaluronic acid has shown a strong binding affinity to the CD44 receptor that is overexpressed in cancerous and inflammatory tissue.<sup>[74]</sup> For example, hyaluronic acid-functionalized and PEGylated nanoparticles have shown improved cancer inhibition efficacy and high tumor accumulation of DOX in SCC7 tumor xenograft mice models.<sup>[75]</sup>

Even though some polysaccharides, such as heparin or hyaluronic acid, have shown the capability as target ligand molecules and hydrophilic segments, the research for their therapeutic use is mainly in an academic setting due to the various drawbacks mentioned above, slowing down their entry into clinical investigations.<sup>[76]</sup> Therefore, e.g., in the case of heparin, researchers spotlighted the search for synthetic polysulfated heparin mimetics, where a promising candidate was found in dendritic polyglycerolsulfate (dPGS), see Chapter 2.2.3.2.

### 2.2.3.4 Hydrophilic Poly(oxazoline)s: PMeOx and PEtOx

Today, no poly(oxazoline) containing amphiphilic block copolymer systems has entered clinical trials. In the 1960s, the water-soluble polymers poly(2-methyl-2-oxazoline) (PMeOx) and poly(2-ethyl-2-oxazoline) (PEtOx) were described for the first time.<sup>[77]</sup> Depending on the 2-substituent of the 2-oxazoline monomer, the solubility of the resulting polymer can be tailored, ranging from highly hydrophilic (PMeOx, PEtOx) to highly hydrophobic (see chapter 2.2.4.5). Due to their structural similarities to naturally occurring peptides, this class of polymers is often regarded as “pseudo-peptide”.<sup>[78]</sup> The living-controlled cationic polymerization of 2-oxazolines, employing electrophilic tosylate initiators, acquires strictly linear polymer architectures with high control on the molecular weight distribution and degree of polymerization. A broad variety of functional polymers is achievable by controlling the end

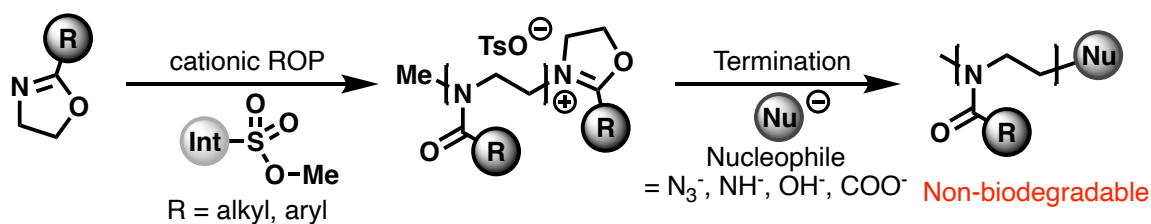


**Figure 5.** Synthetic scheme towards poly(2-oxazoline) (POx) polymers via cationic ROP of 2-oxazoline monomers.

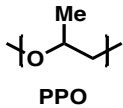
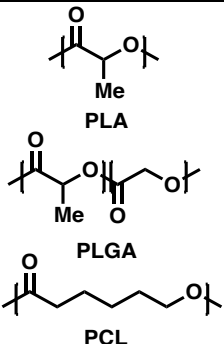
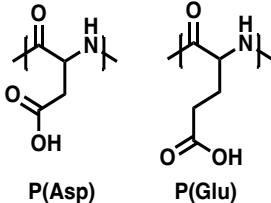
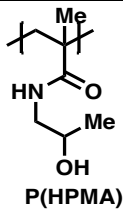
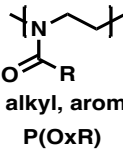
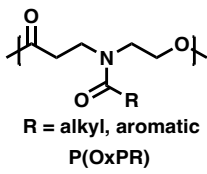
group chemistry by varying the terminating agents, including several nucleophiles such as  $\text{N}_3^-$ ,  $\text{OH}^-$ ,  $\text{COO}^-$ , or  $\text{NH}^-$ <sup>[79]</sup>, see Figure 5.

Currently, PEtOx is FDA-approved as an indirect food additive.<sup>[80]</sup> Most micellar drug delivery systems containing poly(oxazoline)s either feature a hybrid poly(oxazoline)-poly(ester) diblock copolymer or an A-B-A triblock copolymer synthesized by sequential addition of hydrophilic and hydrophobic 2-oxazoline monomers., where A represents the hydrophilic, and B the hydrophobic segment. For the second approach, Kabanov *et al.* designed doubly amphiphilic triblock copolymers based on methyl-poly(MeOx-*b*-BuOx-*b*-MeOx)-piperidine, which showed extremely high drug loading capacities of up to 45 wt% of the formulation. Further, the triblock copolymer provides superior tumor inhibition compared to the commercial micellar formulation Taxol<sup>®</sup>.<sup>[80]</sup> The first approach, e.g., was followed by Zhao *et al.*, who synthesized folate-modified diblock copolymer consisting of poly(EtOx)-*b*-PCL micelles, showing better therapeutic efficacy and reduced toxicity than DOX when administered to nude mice bearing KB tumors.<sup>[81]</sup>

Since the long-term accumulation of the polymer must be avoided and POx devoid of degradable bonds, the modification of poly(oxazoline)s has been studied by Schubert *et al.*, where they introduced statistically distributed peptide groups to the polymer backbone. By partial oxidation of the POx scaffold, the amide groups were statistically oxidized to glycine moieties. Then by subsequent reacylation of the secondary amines, they reintroduced N-acyl ethylene imine repeating units onto the polymer achieving degradable analogs of poly(oxazoline);<sup>[82]</sup> however, a peptide bond is limited to enzymatic hydrolysis. Another potential issue of poly(oxazoline) materials is the hydrolysis of the amide side chain forming toxic linear polyethylene imine (I-PEI), limiting their biomedical application. A non-human enzyme, proteinase K, showed the degradation of PEtOx to I-PEI,<sup>[83]</sup> whereas human digestive enzymes do not show significant hydrolysis,<sup>[84]</sup> thus, biodegradation to I-PEI in the human body remains unknown.

## 2.2.4 Hydrophobic Polymer: Core Forming Segment

**Table 2.** Overview of the most frequently used hydrophobic core-forming segment used to construct amphiphilic block copolymers.

Polymer	Chemical structure	Synthesis	Advantages / Limitations
Polyether	 <p>PPO</p>	Anionic or monomer activated ROP of PO	<ul style="list-style-type: none"> <li>+ PEG-block copolymers (e.g., Poloxamer) are commercially available</li> <li>+ Low molecular weight distributions</li> <li>- High CMC</li> <li>- Low drug-loading</li> <li>- Non-degradable</li> </ul>
Polyester	 <p>PLA PLGA PCL</p>	Metal-coordinated or organo-catalytic ROP of lactones	<ul style="list-style-type: none"> <li>+ Biodegradable</li> <li>+ Clinically approved</li> <li>- Metal impurities <ul style="list-style-type: none"> <li>• can be overcome by Organo-Catalysts</li> </ul> </li> <li>- Burst release</li> </ul>
Poly(amino acid)s	 <p>P(Asp)      P(Glu)</p>	Anionic ROP of NCAs	<ul style="list-style-type: none"> <li>+ Biodegradable</li> <li>+ Clinically approved</li> <li>+ Postmodifications possible <ul style="list-style-type: none"> <li>+ High affinity with the drug</li> <li>+ Polymer-Drug Conjugates</li> <li>+ Low CMC</li> </ul> </li> <li>- Slow degradation due to amide backbone</li> </ul>
Polymethacrylates	 <p>P(HPMA)</p>	FRP of methacrylates	<ul style="list-style-type: none"> <li>+ Clinically approved</li> <li>+ Postmodifications possible <ul style="list-style-type: none"> <li>+ Chemical-Crosslinking</li> </ul> </li> <li>- Non-degradable</li> </ul>
Poly(2-oxazoline)s	 <p>R = alkyl, aromatic P(OxR)</p>	Cationic ROP of 2-oxazolines	<ul style="list-style-type: none"> <li>+ Custom-made monomers possible <ul style="list-style-type: none"> <li>+ High affinity with the drug</li> <li>+ Low CMC</li> </ul> </li> <li>+ Introduction of terminal groups</li> <li>- Polymer backbone is non-degradable</li> <li>- Research use only</li> </ul>
Poly(ester amide)s	 <p>R = alkyl, aromatic P(OxPR)</p>	Organo-catalytic ROP of OxPs	<ul style="list-style-type: none"> <li>+ Biodegradable</li> <li>+ Custom-made monomers possible <ul style="list-style-type: none"> <li>+ High affinity with the drug</li> <li>+ Customizable CMCs</li> </ul> </li> <li>- Research use only</li> </ul>

### 2.2.4.1 Polyesters: PCL, PLGA, and PLA

Aliphatic polyesters are one of the most studied hydrophobic polymers in the biomedical field and find applications as surgical sutures, tissue engineering scaffolds, and controlled drug delivery systems.<sup>[85]</sup> The most prominent examples that are also found in amphiphilic block copolymers are poly( $\epsilon$ -caprolactone) (PCL), poly(D,L-lactic acid)-*co*-(glycolic acid) (PLGA), and poly-(D,L-lactic acid) (PDLLA), where the last one is the only hydrophobic segment with market authorization as a drug delivery systems, Nanoxel<sup>®</sup> and Genexol<sup>®</sup>. The use of the homopolymer of glycolic acid, called poly(glycolic acid) (PGA), has been challenging due to the limited solubility in common solvents; hence it is difficult to process.<sup>[86]</sup> The degradation of poly(ester) materials is accompanied by bulk degradation with random hydrolytic scission of the hydrolytically labile polymer backbone by either (i) passively acidic or basic or (ii) actively by enzyme-catalyzed hydrolysis.<sup>[87]</sup> It has been found that an interplay of the hydrophilicity, molecular weight, crystallinity, processing, and polymer composition has an influence on the hydrolysis rate of the later material.<sup>[88]</sup> A rule of thumb is: that shorter chains degrade faster, and the hydrolysis rate drops with increased hydrophobicity.

This class of polymers has been widely synthesized by metal-coordinated ROP of the respective lactone using Tin(II) octoate. Even though Tin(II) octoate has found FDA approval as a food stabilizer, tin catalysts lack control of dispersity, and traces can cause toxicity of the later product.<sup>[89]</sup> With the first report of the living polymerization of lactide by Hedrick *et al.* in 2001,<sup>[90]</sup> the use of organo-catalyst has been widely exploited in the preparation of well-defined, non-toxic polyesters.<sup>[91]</sup> For more details see Chapter 2.5. Due to PEG's well-controllable  $\alpha$ - and  $\omega$ -end-group chemistry, e.g., terminal hydroxy groups can be used as macro-initiators for several lactones forming well-defined diblock PEG-*b*-poly(ester) or triblock poly(ester)-*b*-PEG-*b*-poly(ester) copolymers. Also, the synthesis of highly functional biodegradable polymers *via* ROP of functionalized monomers with several chemical functionalities has been widely studied.<sup>[92]</sup>

Contrary to the homopolymers poly-(D,L-lactic acid) (PDLLA) and poly( $\epsilon$ -caprolactone) (PCL), Poly(lactic-*co*-glycolic acid) (PLGA) is a copolymer of the two cyclic ester monomers, lactones, lactide and glycolide. Meyer *et al.* exploited the influence of the copolymer's sequence on the hydrolysis behavior, where they found that alternately distributed lactic and glycolic acid units in the copolymer sequence undergo chain degradation 2-times slower than block-like architectures of the copolymer.<sup>[93]</sup> Since the burst release is a major limitation of polyester materials, the approach of Hoye *et al.* on the "random" copolymerization of lactide and glycolide mediated by the organo-base DBU was used for the preparation of the materials in this thesis.<sup>[94]</sup> In this approach, glycolide is constantly added to the organo-base-mediated polymerization of lactide, resulting in a "random" PLGA copolymer. The higher reactivity of

glycolide requires slow monomer addition to avoid the homopolymerization of the glycolide monomers, resulting in unwanted block-like structures in the later material, see Figure 6.

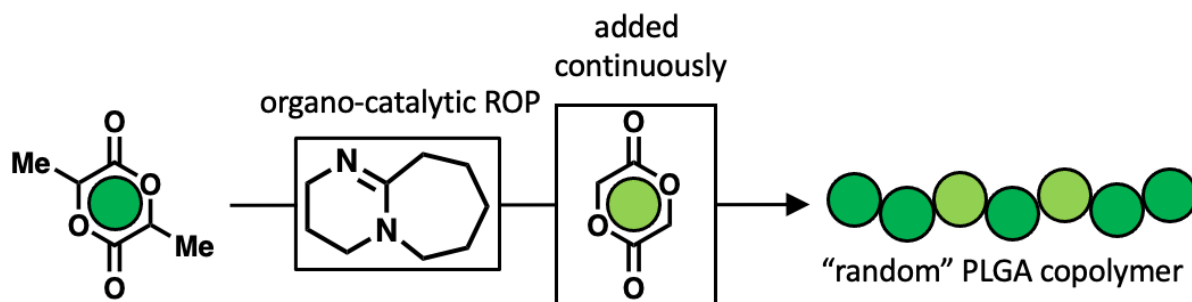


**Figure 6.** Synthetic approach acquiring “random” PLGA copolymers achieved by slow-monomer addition of the monomer with higher reactivity, here glycolide, to an organo-base, e.g., DBU, mediated ROCP of lactide and glycolide.

#### 2.2.4.2 Polyether: Polypropylene oxide

So far, polypropylene oxide is the only polyether under clinical trials preparing the core-forming segment of amphiphilic block copolymers. Although their readily accessible synthesis by telechelic anionic ring-opening polymerization of propylene oxide initiated by propylene glycol and subsequent addition of ethylene oxide;<sup>[95]</sup> its copolymers lack biodegradability and only offer a low affinity with the drug molecules; thus, giving insufficient drug-loading capacities and undesired drug-leaching.<sup>[96]</sup> In the late 1980s, Kabanov published the first example of an A-B-A triblock copolymer consisting of PEO-*b*-PPO-*b*-PEO used as a drug delivery system for Doxorubicin.<sup>[97]</sup> This type of triblock copolymer is also called poloxamer and trademarked by BASF, formerly as Pluronic<sup>®</sup>, now Kolliphor<sup>®</sup>, as a drug emulsifier for topical applications.<sup>[98]</sup>

In 1999, this triblock copolymer entered clinical trials as the first polymeric micelle drug delivery system, named SPC1049C; however, its quick dissociation in the bloodstream consequently resulted in comparable toxicities and pharmacokinetics compared to the injection of free Doxorubicin.<sup>[99]</sup> Currently, SPC1049C is in clinical phase 2 investigations for the treatment of multi-resistant cancer.<sup>[3b]</sup>

#### 2.2.4.3 Polyaminoacids: Drug-Conjugates and Metal-Complexation

Considering their participation as the core-forming segment of amphiphilic block copolymers entering clinical trials, this class of polymers can be seen as the most successful candidate, as it can be found in six of the eleven candidates. Polyaminoacids can be prepared by anionic ring-opening polymerization of the N-carboxy anhydride of amino acids (NCA)s, which have high control over the molecular weight and dispersity of the reaction.<sup>[100]</sup>

The first example of a polyaminoacid containing amphiphilic block copolymer is based on mPEG-*b*-poly( $\alpha,\beta$ -aspartic acid-DOX) covalently carrying Doxorubicin and was described by Kataoka *et al.* in 1989.<sup>[101]</sup> Besides the amide-bounded drug, the drug delivery system was also physically loaded with Doxorubicin, having the conjugated DOX served as an agglomerate facilitating  $\pi$ - $\pi$  stacking between the molecules, enhancing the system's stability and drug loading capacity. This candidate entered clinical trials in 2001 and can be considered the first milestone in the clinical translation of polymeric micelles. It was found that this system showed higher tumor uptake than clinically approved DOXIL<sup>®</sup>; however, the covalently conjugated drug exerted no antitumor activity, most likely due to the slow hydrolysis of the amide bonds.<sup>[102]</sup> This study, on the one hand, revealed the requirement of cohesive forces in the core; on the other, it marked the need for degradable bonds between the polymer and the drug.<sup>[103]</sup> The next systems, NK012<sup>[104]</sup> and NC-6300<sup>[105]</sup>, conjugated the drugs, SN-38 or Epirubicin, to the carboxylic acid of the polyaminoacid segment *via* ester or hydrazone linkages, respectively. Both linkages were designed to be selectively cleavable under physiological conditions found in the early to late endosomes to lysosomes,<sup>[106]</sup> but stable in the bloodstream at pH 7.4 (for more details, see Chapter 2.2.6.1). Further, in NK105, introducing aromatic units by attaching 4-phenyl-1-butanol onto the hydrophobic segment again enabled  $\pi$ - $\pi$  stacking between the physically loaded drug and the carrier system.<sup>[107]</sup> This candidate recently completed a clinical phase 3 study comparing the efficacy and safety of NK105 and PTX in metastatic or recurrent breast cancer, which revealed lower peripheral sensory neuropathy (PSN) toxicity for the polymer-supported treatment than free PTX. However, the candidate could not pass the final end goals of the study and will be considered for new trials in the future.<sup>[108]</sup>

On the WHO Model List of Essential Medicines, besides Docetaxel, Paclitaxel, and Doxorubicin, there is also Cisplatin; a very powerful chemotherapy medication used for the treatment of several cancer types including testicular, bladder, and brain tumors. In 2004, cisplatin was FDA-approved in the combinatorial treatment of advanced colorectal cancer in combination with 5-FU and LV. Since the intravenous injection of Cisplatin has several side effects, such as nephrotoxicity (kidney damage), neurotoxicity, nausea, and vomiting, among others; its implementation into polymer drug delivery systems has been widely studied.<sup>[109]</sup> Formulations based on polymer-drug conjugates or liposomes showed undesired high leaching events and solubility issues upon a high degree of platinum complexation. The group of Kataoka *et al.* took advantage of the increased hydrophobicity upon platinum-complexation and designed two polymeric micelles based on mPEG-*b*-poly( $\alpha,\beta$ -glutamic acid), NC-6004<sup>[110]</sup> and NC-4016<sup>[111]</sup>, incorporating cis-platinum(II) and (trans-1-1,2-diaminocyclohexane)-platinum(II) (DACHPt), respectively. The polymer-metal complex formation is based on the ligand exchange of reaction of the Pt(II)-Chlorides with the carboxylates of the polymer chain.



However, since this reaction is in equilibrium, exposure to saline solutions, such as blood, can trigger the dissociation of the carboxylate-platinum complex.<sup>[112]</sup>

#### **2.2.4.4 Poly[N-(2-hydroxypropyl) Methacrylamide]**

Poly[N-(2-hydroxypropyl) Methacrylamide] P(HPMA) is a hydrophilic, biocompatible, and non-immunogenetic polymer,<sup>[113]</sup> which can be synthesized by free or controlled radical polymerization of [N-(2-hydroxypropyl) Methacrylamide]. P(HPMA) was originally introduced to the biomedical field as a plasma expander,<sup>[114]</sup> however, its high density of functional groups on the sidechains propelled its application as the first clinically investigated polymer-drug conjugate, p(HPMA)-Doxorubicin (PK1).<sup>[115]</sup> Even with p(HPMA)'s high water-solubility, it barely finds application as the shell-forming segment in amphiphilic block copolymers; indeed, it is readily used in preparing the core-forming segment by introducing several functional groups to the sidechain. The group around Hennink *et al.* designed several HPMA-modified derivatives ranging from thermosensitive lactide moieties,  $\pi$ -electron rich aromatic units, to cross-linkable methacrylates.

Since most polymeric micelles suffer from insufficient *in vivo* stability, they designed  $\pi$ -electron stabilized block copolymer micelles based on methoxy poly(ethylene glycol)-*b*-(N-(2-benzoyloxypropyl)methacrylamide) (mPEG-*b*-p(HPMAm-Bz) showing enhanced drug-loading capacities and stabilities compared to non-aromatic systems.<sup>[116]</sup> They also tested the *in vivo* performance on different mice models, finding excellent tolerability to different doses. The treatment with Paclitaxel-loaded micelles induced complete tumor regression in two different xenograft models (*i.e.*, A431 and MDA-MB-468)<sup>[117]</sup> or potentiated chemotherapy responses in multiple advanced-stage GI cancer mouse models.<sup>[118]</sup> Further, the group of Hennink *et al.* also investigated the influence on the pharmaceutical properties of the synthetic pathway affording the drug delivery systems, finding no significant difference between systems obtained by free or controlled radical polymerization.<sup>[119]</sup> These studies demonstrate the potential of  $\pi$ -electron stabilization applied to micellar drug delivery systems.

The introduction of monolactate or dilactate side groups into the HPMA monomer aimed for amphiphilic block copolymers with decreased lower critical solution temperature (LCST) if, for example, compared to poly(N-isopropylacrylamide) (PNIPAAm) with its cloud point of around 32 °C in water.<sup>[120]</sup> It has been demonstrated that the poly(HPMAm-dilactate) copolymers have an LCST far beyond body temperature at 10°C.<sup>[121]</sup> Thus, it is expected that mPEG-poly(HPMAm-dilactate) copolymers form micelles at the given body temperature of 37°C, but due to hydrolysis of the lactate groups in the core,<sup>[122]</sup> the micelles start to gradually disassemble, triggering the drug release. However, polymeric micelle based on mPEG-poly(HPMAm-dilactate) showed low tumor accumulation and short blood circulation times,<sup>[123]</sup>

most likely as a result of insufficient stability causing premature disassembly. Based on these findings, they developed core-cross linkable methacrylated thermosensitive mPEG-*b*-p((HEMAm-Lac) copolymers that can covalently entrap several chemotherapeutics *via* pH-sensitive linkers. In 2010, they synthesized mPEG-*b*-p((HEMAm-Lac) copolymers covalently entrapping 30-40 wt% Doxorubicin. These micelles showed better antitumor activity in mice bearing B16F10 melanoma carcinoma than free DOX, with low leaching of only 5% after 24 hours.<sup>[124]</sup> These findings paved the avenue for core-linked micelles in the clinics.<sup>[125]</sup> Currently, this technology is in clinical phase 2 under the trademark CriPec634 held by Cristal Therapeutics located in the Netherlands.<sup>[126]</sup>

#### 2.2.4.5 Hydrophobic Poly(2-oxazoline)

In the homolog series of poly(2-alkyl-2-oxazoline)s, poly(2-*n*-butyl-2-oxazoline) (PBUx) is the first homophobic POx. The use of different hydrophobic POxs segments preparing the core-forming segment in amphiphilic block copolymer has been widely exploited in the literature.<sup>[127]</sup> It became apparent that short *n*-alkyl POxs derivatives, such as PBUx, are not very sufficient in shielding the repeating polar amide motif in each monomer unit of the polymer backbone, which results in an unexpected polar micelle core for the short *n*-alkyl POxs. In contrast, for the long *n*-alkyl poly(2-*n*-nonyl-2-oxazoline) (PNOx) analogs, a rather nonpolar core environment is obtained, as proven by pyrene fluorescence assays.<sup>[80, 128]</sup> It has been found that the polarity of the resulting micellar core drastically influences the drug-loading capacity of PTX with higher drug-loading with higher polarity.<sup>[129]</sup> Luxenhofer *et al.* also presented a library of different POxs amphiphiles in which they altered the aromatic character systematically by introducing several core-forming segments, including poly(2-butyl-2-oxazoline) (A-pBUx-A), poly(2-butyl-2-oxazoline-co-2-benzyl-2-oxazoline) (A-p(BUx-co-BzOx)-A), poly(2-benzyl-2-oxazoline) (A-pBzOx-A), and poly(2-phenyl-2-oxazoline) (A-pPheOx-A), with A being poly(2-methyl-2-oxazoline) (pMeOx), investigating the solubilization capacity for several drugs. Interestingly, they found the highest drug-loading capacity for the more polar core when PTX is incorporated, whereas more aromatic cores favored CUR loading.<sup>[130]</sup> Further, the interaction of the drug with the POx core-forming segment can induce morphology transitions from originally spherical micelles to worm-like micelles.<sup>[129, 131]</sup> These transitions can impact the pharmacokinetics of the later drug delivery systems as it has been shown that the particle's shape and morphology determine the particle's cellular uptake and *in vivo* performance.<sup>[132]</sup>

### 2.2.4.6 Poly(ester-co-amide)s: New Platform for Drug Delivery

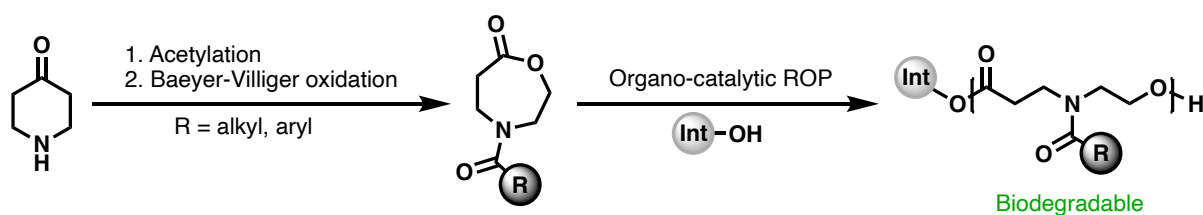


**Figure 7.** Synthetic scheme towards poly(ester amide) polymers *via* organo-catalytic ROP of N-acylated-1,4-oxazepan-7-one (OxP) monomers.

This class of polymer was first described by Hadjichristidis *et al.* in 2020, who aimed to substitute poly( $\beta$ -amino esters) for their use as gene delivery systems.<sup>[133]</sup> Indeed, poly( $\beta$ -amino esters), first described in the late 1970s, reincarnated by Langer *et al.* in 2000,<sup>[134]</sup> are widely studied as a replacement for viral vectors;<sup>[135]</sup> however, their synthesis by step-growth polymerization of primary amines and diacrylates, also limits their potential due to a lack of controlled molecular weights and dispersity, which ROP can overcome. Over the past years, poly (amino ester)s have emerged as a potential biomedical platform in several applications.<sup>[134]</sup> The so-called N-acylated-1,4-oxazepan-7-one (OxP) monomers are readily accessible using the Baeyer-Villiger oxidation of N-acylated-4-piperidones with prior acetylation of the amine, where the acylate can be of alkyl or aryl origin, see Figure 7. This novel class of polymers shares structural similarities with poly(2-oxazoline)s, both having a lateral tertiary amide group ( $-\text{CONH}-$ ), but due to the ester group ( $-\text{COO}-$ ) in the backbone; these polymers can be seen as their degradable analogs. For this type of monomer, organo-catalytic-driven ROP has been demonstrated to be extremely powerful, leading to well-defined linear polymer architectures.<sup>[136]</sup> Thus, this class of polymers offers biodegradability due to the ester groups and allows the introduction of various pending groups provided by the tertiary amine.

The toolbox-like manner of this class of monomers enabled the preparation of  $\pi$ -electron rich amphiphilic block copolymers, which led the way for understanding the influence of  $\pi$ -electron stabilization on the stability and performance of self-assembled drug delivery systems.

### 2.2.5 Delivery of Nanomedicine: Passive and Active Targeting

Drug delivery systems aim to enhance the accumulation of the applied chemotherapeutic on its site of action, e.g., cancerous tissue. Two different strategies can be followed to achieve this goal: (i) passive; and (ii) active targeting. The first one is governed by the enhanced permeability and retention (EPR) effect that determines the accumulation of polymeric nanoparticles in tumorous tissue, as Maeda *et al.* described already 40 years ago.<sup>[137]</sup> This

effect is caused by the leakiness of blood vessels in cancerous tissue, which allows the nanoparticles to accumulate in cancerous cells. The retention time of the intravenously injected particles upon enrichment in the tumor is prolonged by the lack of lymphatic drainage.<sup>[138]</sup> However, this concept has been criticized recently and could only resolve some doubts in the academic community till today.<sup>[139]</sup>

The other approach follows the attachment of targeting ligands onto the drug delivery systems that can undergo specific interactions with defined receptors on the cell surface. This strategy is known as the so-called “actively targeted nanomedicine” approach and exemplifies the previously reported Models by Ringsdorf and Ehrlich, see Chapter 2.1. Several targeting ligands, ranging from peptides to proteins and antibodies, have been discovered and established for the construction of targeted drug delivery systems.<sup>[140]</sup> Further, bioorthogonal click chemistry has been demonstrated to be a powerful tool in conjugating targeting ligands onto polymeric particles.<sup>[141]</sup> To date, the only amphiphilic block copolymer system under clinical trials that possess active targeting is BIND-014, which is based on a PEG-*b*-PLA block copolymer that is conjugated to an ACUPA ligand targeting a specific protein in the extracellular domain of prostate-specific membrane antigen (PSMA). The completion of a clinical phase 2 study has been reported; however, the company behind this technology, BIND Therapeutics, declared bankruptcy in 2016; thus, ongoing investigations on this system are unclear.<sup>[142]</sup>

In 2016, Chan *et al.* published a literature analysis that deals with the targeting and the accumulation of drug delivery systems published over the past 10 years since this very time. They found that a delivery efficiency on the drug dose of 0.6% is achieved for drug delivery systems relying on passive targeting. For systems exploiting active targeting, the delivery efficiency was indeed found to increase by 50%, at 0.9%,<sup>[143]</sup> but this disappointing low value has also led to doubts about this concept. Whether or not the idea of targeted nanomedicine and the construction of drug delivery systems may need to be reconsidered.<sup>[144]</sup>

### **2.2.6 Stimuli-Responsive Drug Release in Nanotherapeutics**

The degradability of drug delivery systems is a key figure in their wide range of applications.<sup>[145]</sup> On one side, selective degradation ensures the release of the cargo exerting the drug's therapeutic activity. On the other, it ensures the digestion of the delivery platform, avoiding the long-term accumulation of and exposure to the material. Control over the degradation can be achieved by taking advantage of the different pathophysiological features and subcellular conditions that are specified for diseased cells, e.g., cancer tissue. For example, the lowered intracellular pH can be used to cleave pH-sensitive bonds, such as hydrazones. Further, the overexpression of disease-associated enzymes can cascade the enzymatic hydrolysis of ester

or amide bonds. The upregulation of glutathione, a unique feature for cancer cells, can be exploited for the reductive cleavage of disulfide bonds in the cell interior. Another emerging field is applying photochemistry to trigger drug release and degradation. Figure 8 summarizes all these different strategies along with the corresponding linker structure. Following the rational design of drug delivery systems will be further discussed in more detail:

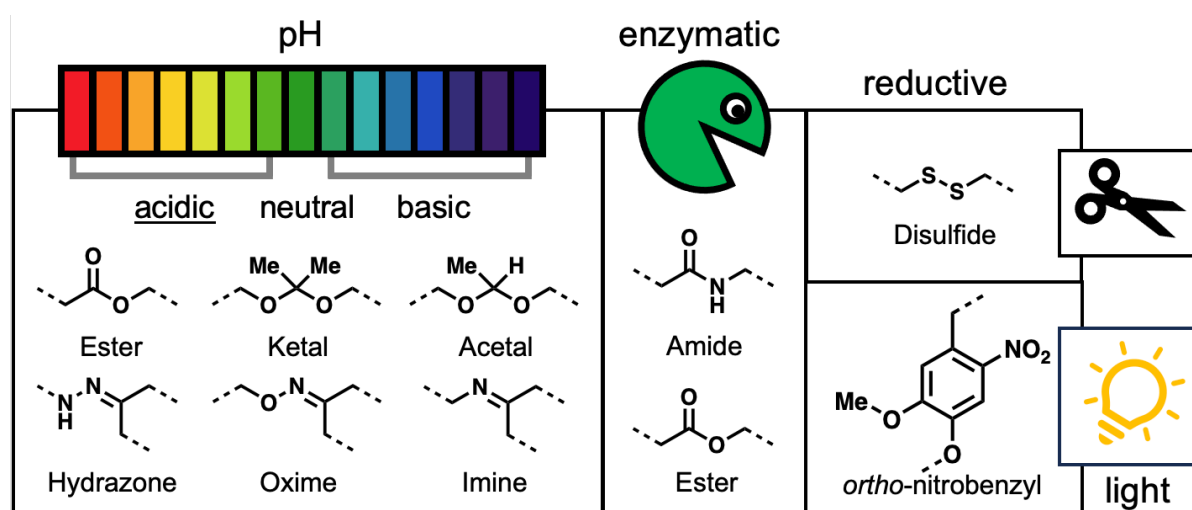


**Figure 8.** Schematic overview of different (bio)-degradable bonds and their respective stimuli for the preparation of drug delivery systems capable of selectively releasing their chemotherapeutic cargo.

### 2.2.6.1 Endocytic Pathway: Acidic and Enzymatic Hydrolysis

The cellular uptake of nanosized drug delivery systems primarily occurs *via* receptor-mediated endocytosis.<sup>[146]</sup> As depicted in Figure 9A, a binding-ligand decorated drug delivery system, e.g., a dendritic polyglycerolsulfate micelle, binds to the surface receptor of a mammalian cell, such as a cancer cell, followed by insertion into the cytosol *via* endocytosis.

Upon cellular internalization, the particle undergoes the so-called endocytic pathway, ending up in the different cell compartments: (i) starting with the early endosome; (ii) then sorted to the late endosome; and (iii) lastly being fused into the lysosome. Compared to plasma (pH 7.4) or other cell compartments, such as the nucleus (pH 7.7) or the cytosol (pH 7.3), the cascade of the endocytic pathway exposes the particles to different acidic environments, see Figure 9B. Further, these subcellular compartments contain numerous hydrolases, which are typically involved in the hydrolysis of ester- or amide-containing drug delivery systems.<sup>[147]</sup>

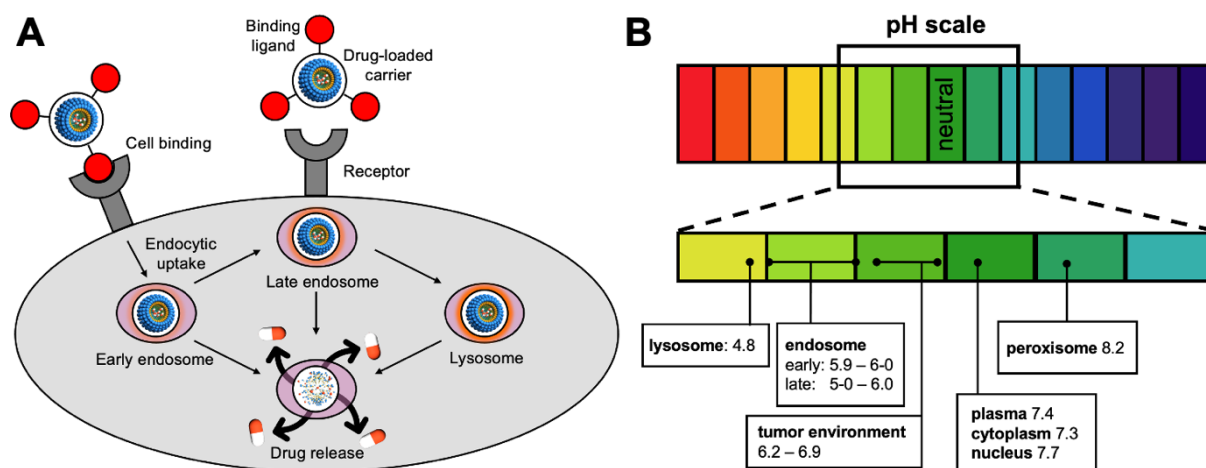


**Figure 9.** (A) Schematic depiction of the cell-targeted delivery of a drug-loaded polymeric system undergoing selective cell binding to the cancer cell dictated by the nanoparticle's surface binding ligand; Followed by the cell binding, the particle is inserted into the cell by endocytic uptake; subsequently, the nanoparticle undergoes the endocytic pathway, being exposed to different pH values in the early endosome, late endosome, and lysosome (B) Summary of the different pH values found in representative subcellular compartments upon endocytic uptake altering the hydrolysis rate of applied drug delivery systems triggering the drug release.<sup>[148]</sup>

### 2.2.6.1.1 Ester Linkages

The ester bond can serve two different roles in amphiphilic drug delivery systems: (i) it builds up the hydrophobic segment, see Genexol<sup>®</sup> and Nanoxel<sup>®</sup>; or (ii) it conjugates the drug covalently to the hydrophobic segment *via* an ester-linkage, see NK012.<sup>[104]</sup>

Indeed, ester bonds have been associated with chemical hydrolysis catalyzed by the acidic intracellular environment, but it has also been indicated that the ester bond is more susceptible to base-catalyzed hydrolysis; thus, chemical hydrolysis may play only a minor role in facilitating the drug release, unless basic subcellular compartments, such as the peroxisome (pH 8.2) were targeted. In cancer cells, esterases play an important role in maintaining tumor growth; as a result, the esterase activity in cancerous tissue is 2.6- to 3.7-fold higher than in normal tissue.<sup>[149]</sup> This hydrolytic stress can readily catalyze the cleavage of ester bonds upon internalization into the cancer tissue and has paved the way for developing esterase-responsive drug delivery systems.<sup>[150]</sup>

### 2.2.6.1.2 Amide Linkages

To date, six of the eleven amphiphilic block copolymers that have been under clinical trials consist of polyamide bonds, either given by their poly amino acid-based backbone or due to the drug-conjugation *via* amide bonds, see NK911.<sup>[101]</sup> Due to their structural similarities to naturally occurring biomaterials, poly(amide)s promise excellent biocompatibility with no

toxicity of their degradation products.<sup>[151]</sup> The amide bond is less subject to chemical hydrolysis under physiological conditions than ester bonds, giving it a benefit in biomedical applications, such as extended blood circulation times. However, for NK911, it was found that the slow hydrolysis of the amide bond suppresses the therapeutic activity of the conjugated drug. Also, slow hydrolysis can cause long-term toxicity due to extended exposure of the material to the organisms. In general, the drug release of amides is triggered by different hydrolytic proteases,<sup>[152]</sup> with their site-specific action is directly altering the rate and site of the drug release. For studying the proteolytic degradation of polymeric drug delivery systems *in vitro*, the application of surface-immobilized lipases, such as Novozyme 435, has been demonstrated to be powerful as they allow, e.g., the separation of the degradation products from the enzyme.<sup>[153]</sup>

### **2.2.6.1.3 Hydrazone Linkages**

The slow hydrolysis of amide bonds, such as in NK911, has driven forwards the development of NC-6300, in which the chemotherapeutic Epirubicin (the 4'-epimer of DOX) is covalently conjugated to the hydrophobic segment *via* a hydrazone linkage.<sup>[105]</sup> This class of linkers has demonstrated some tolerance to hydrolytic cleavage at the given physiological pH of 7.4, which ensures the system's intactness during systemic circulation in the bloodstream. The controlled drug release of hydrazone linkages can be triggered by the exposure of the conjugates to lower pH in the extracellular tumor environment or after their entrance into the tumor cells *via* endocytosis.<sup>[154]</sup> The hydrazone cleavage has been reported to occur at a given pH of 5.5 – 6.0. For the preparation of hydrazone-drug conjugates, two synthetic pathways have been developed: (i) first is the generation of a hydrazone-terminated linker prior to its coupling to the carbonyl-containing (ketone or aldehyde) drug molecule; or (ii) first installing of a hydrazone-linker onto the molecule followed by chemoselective coupling of the ketone-bearing linker molecule, e.g., polymer.<sup>[155]</sup>

### **2.2.6.2 Reductive Drug Release *via* Disulfide Exchange**

Different from the above-discussed materials based on, e.g., ester or amide, the disulfide (-S-S-) is not subject to enzymatic or acidic hydrolysis, but it is cleaved through a disulfide exchange reaction triggered by endogenous thiol-containing molecules, such as glutathione (L- $\gamma$ -glutamyl-L-cysteinyl-L-glycine; GSH). GSH is a tripeptide consisting of glutamic acid, cysteine, and glycine and is the most abundant nonprotein thiol-containing reducing agent in biological systems.<sup>[156]</sup> It is produced in the cytosol where the intra-cellular abundance of its

reduced “physiological active” form (GSH) is maintained by the glutathione redox couple of (GSSG/GSH) between the oxidized (GSSG) and reduced form.<sup>[157]</sup>

Since the extracellular concentration of GSH is indispensable low with only micromolar contents, its level increases in the cytosol of cancerous tissue up to 10 mM,<sup>[158]</sup> which allows a precise drug release upon cellular uptake while not being triggered in the bloodstream. Over the past years, several drug delivery systems containing disulfides have been investigated,<sup>[159]</sup> where two approaches were studied for a larger extent on polymeric micelles: (i) shell-sheddable; or (ii) core-crosslinked micelles. Following the first approach (Figure 10), the hydrophobic and hydrophilic segments were connected *via* a disulfide bridge, forming an amphiphilic system. Upon cleavage of the disulfide bridge, the amphiphilicity of the systems is no longer given, triggering the disassembly, and the cargo is released.<sup>[63, 160]</sup> The second strategy undergoes thiol-initiated ring-opening cascade polymerization of cyclic disulfides of so-called 1,2-Dithiolanes forming a well-defined, reversible disulfide network within the micellar core.<sup>[161]</sup>

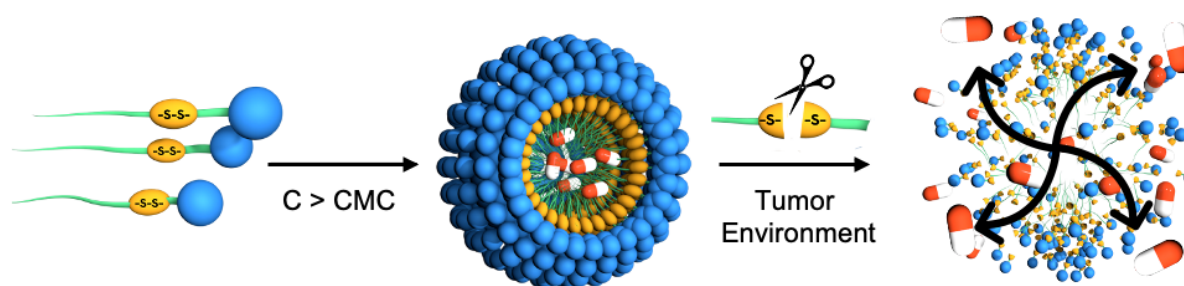


**Figure 10.** Schematic depiction of the cleavage mechanism of shell-sheddable amphiphiles used in drug delivery application; the cleavage of the disulfide, e.g., induced by GSH, destroys the amphiphilic nature of the block copolymer, triggering the drug release within the cancerous tissue.

### 2.2.6.3 Orthogonal Drug Release: Photochemical Sensitivity

Among the various types of external stimuli relying on either chemical or enzymatic degradation, the photochemical drug release from photo-responsive polymer micelles has attracted much attention over the last years due to its on-off profile, enabling the orthogonal drug release on the site of action.<sup>[162]</sup> By derivatizing a drug molecule to a photon-cleavable linker, the pharmaceutical activity of the drug is suppressed. Still, after the cleavage, the active drug is regenerated, giving this approach the name “photocaging”.<sup>[163]</sup> Several UV-light-responsive linkers have been established for the preparation of light-responsive nanocarriers for controlled drug delivery systems, including coumarin, quinoline, xanthene, benzophenone, and *ortho*-nitrobenzyl (ONB), among others.<sup>[164]</sup> Even though photon-induced drug release has



promising features; its clinical potential is still limited due to the predominant use of UV light, which does not penetrate deeper tissue.<sup>[165]</sup>

## 2.3 Noncovalent Interactions in Supramolecular Drug Delivery Systems

The bond length between two covalently connected atoms is described with a distance less than 0.2 nm, and the applied strength to break these bonds can vary from 149 kJ/mol for an I-I bond to 411 kJ/mol for a C-H bond.<sup>[166]</sup> Since covalent chemistry is limited in its capability for generating well-defined, functional architectures beyond a nanometer's tens or hundreds-size regime, noncovalent interactions can occur over a much longer distance, enabling the construction of nanosized supramolecular architectures.<sup>[167]</sup> For constructing supramolecular, self-assembled systems capable of delivering pharmaceuticals cargos, hydrophobic,  $\pi$ - $\pi$  stacking, electrostatic, and hydrogen bond interactions have been demonstrated to be powerful tools. Compared to covalent interaction, noncovalent interactions are 10-100 times weaker (Figure 11);<sup>[167]</sup> however, polyvalent interactions and the cooperativity interplay of several different noncovalent interactions can compensate for the weaker bonds.

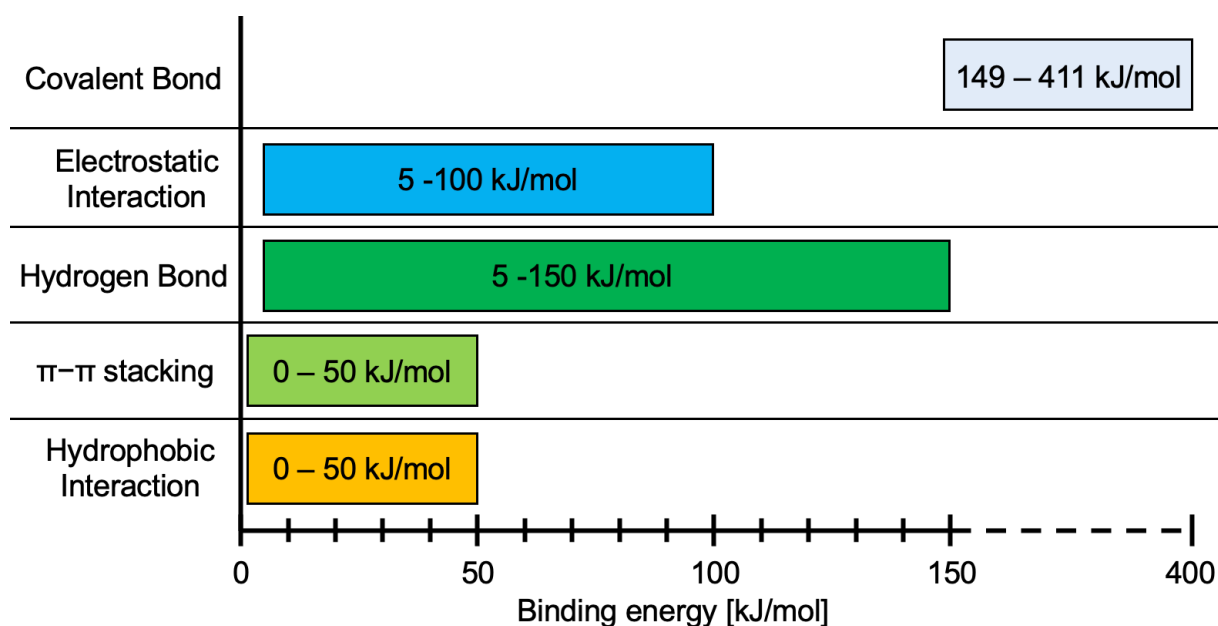


**Figure 11.** Overview of the most important non-covalent interactions and their binding strength found in amphiphilic block copolymer systems; for comparison, there is also the binding strength of covalent bonds listed; please note that the x-axis has been cropped for visualizing the covalent bond; Adapted from Ref.<sup>[167]</sup>

The hydrophobic effect describes the tendency of nonpolar molecules – or parts of them, such as for amphiphilic block copolymers – to aggregate in an aqueous environment. This aggregation is mainly driven by the minimization of the energy penalty caused by the insertion of nonpolar molecules into the water network, which disrupts the hydrogen bonds between the water molecules. In order to minimize this disordering effect of the water network, the water molecules are forced into a 3D network around the nonpolar surfaces, reorientating their hydrogen bonds. This solvation leads to a well-structured water “cage” around the particle called “clathrate”, in which the water molecules have restricted mobility. Since this process would lead to a loss of entropy of the water molecules, the nonpolar molecules tend to aggregate; thus, excluding water and minimizing this energy penalty. For amphiphilic block copolymers, the enlarged area of their hydrophobic segments can compensate the rather weak binding strength of this type of interaction, having a maximum of 50 kJ/mol (Figure 11). The hydrophobic effect contributes to many different biological and live processes,<sup>[168]</sup> including the construction of the cell membrane or the formation of subcellular compartments, such as vesicles.<sup>[169]</sup> An uncountable amount of drug delivery systems have been published exploiting the hydrophobic effect, but notably, it has also led to the first approval of nanomedicine, which was DOXIL®.<sup>[17]</sup> In 2005, another drug delivery system gained market authorization, Abraxane®, in which Paclitaxel is bounded *via* hydrophobic interactions into the hydrophobic pocket of Albumin.<sup>[170]</sup>

Noncovalent interactions involving aromatic groups containing  $\pi$ -bonds are defined as  $\pi$ - $\pi$  stacking<sup>[171]</sup> and are associated with binding strengths of up to 50 kJ/mol.<sup>[167]</sup> In Figure 12, their stacking geometry is depicted, which can be separated into three different categories: (i) edge-to-face (T-shape); (ii) offset stacked; or (iii) face-to-face (sandwich-shape).<sup>[172]</sup> However, the last situation is only energetically favored for a mixture of per-fluorinated and nonfluorinated systems. These non-covalent, intermolecular interactions play important roles, e.g., in protein-folding,<sup>[173]</sup> RNA and DNA base stacking,<sup>[174]</sup> drug design, and numerous other biological molecular recognition processes, such as receptor-ligand binding.<sup>[175]</sup> The implementation of noncovalent  $\pi$ - $\pi$  stacking onto drug delivery systems has emerged with great potential over the last years.<sup>[176]</sup> It has been used in the systems NK911, NC-6300, NK105, NK102 and dPGS-SS-POxPPh-Py.

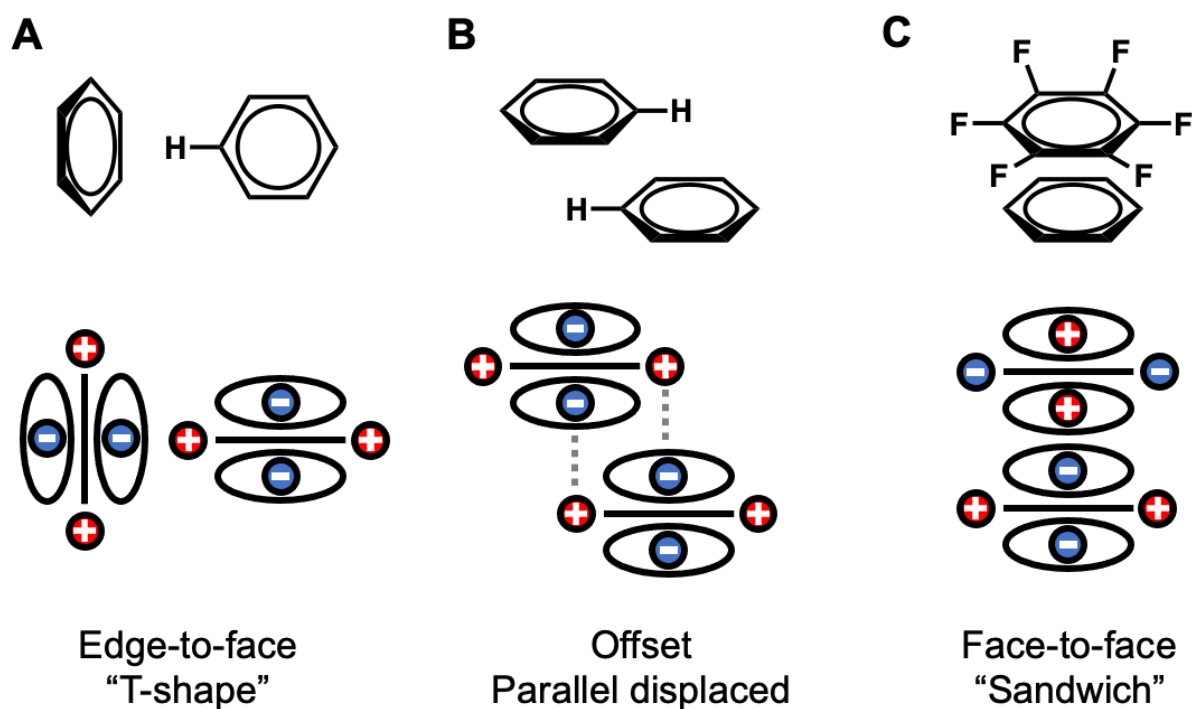


**Figure 12.** Schematic overview of the different geometric configurations between two aromatic rings **(A)** Edge-to-face or T-shape **(B)** Offset or parallel displaced stacking **(C)** Face-to-face stacking.

An electron-rich atom, such as nitrogen or oxygen, can undergo interaction in the role of a hydrogen acceptor with another atom, a hydrogen donor. Even though hydrogen bonds are associated with relatively low binding energies, the multiplication by multivalent interactions gives this type of interaction a fundamental role in understanding biomolecular processes, such as protein folding.<sup>[177]</sup> Further, hydrogen bonding gets exploited for the preparation of highly stable polymeric drug delivery systems.<sup>[178]</sup>

The solvation of ions by surrounding molecules decreases the energy cost dramatically to separate oppositely charged species compared to the required energy needed in a vacuum. For example, this shielding effect on the Coulomb interaction between two-point charges, e.g., induces by water molecules, brings the electrostatic interactions down to the same energy scale as the other noncovalent interactions, see Figure 11. In biological systems, electrostatic interaction plays an important role in cell-cell interactions, ligand-receptor binding, and nucleic acid condensation;<sup>[179]</sup> in drug delivery systems, this concept enabled the development of polyion complex (PIC) micelles for the delivery of pharmaceuticals proteins.<sup>[180]</sup> In this approach, amphiphilic block copolymers having a charged block are used to complex an oppositely charged therapeutic protein; thereby forming protein-complexing micelles.<sup>[181]</sup>

## 2.4 Morphology of Drug Delivery Systems: Controlling Packing Parameters

The self-assembly of amphiphiles is one of the most studied fields in the biological area given by the bilayer manner of the cellular membrane built up from natural lipids. The attractive hydrophobic interaction between the hydrophobic segment and the head groups' repulsive electrostatic and steric interaction with each other mainly governs the self-assembly of amphiphilic structures, for a more detailed explanation, see Chapter 2.3. Predicting the shape and size of the aggregates is crucial since the morphology significantly affects the performance and capability of the drug carrier system and must be carefully evaluated in advance for the desired application.<sup>[182]</sup> For example, for the delivery of hydrophilic cargos, such as proteins, the aqueous lumen of polymersomes is superior over the hydrophobic core of polymeric micelles.<sup>[183]</sup> In contrast, delivering hydrophobic cargos, their encapsulation into polymeric micelles is preferred as they allow higher drug-loading capacities over polymersomes.

For determining the preferred supramolecular architecture, Israelachvili *et al.* developed a model-based theory that considers the volume of the hydrophobic chain ( $v$ ), the optimum area of the hydrophilic headgroup ( $a_0$ ), and the critical length of the hydrophobic chain ( $l_c$ ) of the amphiphilic building block, giving rise to the critical packing parameter ( $CPP$ ).<sup>[184]</sup> This value is a theoretical framework that allows for determining the aggregates' later morphology, see Figure 13. For example, a cone-shaped amphiphile having a large hydrophilic head, such as dendritic polyglycerolsulfate, and a proportional to that short hydrophobic chain prefers the formation of spherical micelles ( $CPP = 1/3$  or smaller). If one wants to alter the morphology of dPGS-based amphiphiles from spherical to something like vesicle structures, such as polymersomes, the area of the hydrophilic head must be somewhat smaller than the volume of the hydrophobic chain; meaning the molecular weights of the hydrophobic segment must be increased if the area of the hydrophilic heads wants to be kept constant.

It has also been demonstrated that the morphology is not only determined by the geometry of the amphiphilic building block itself but also by drug loading the system morphology changes can be induced. This can, for example, convert an empty micelle, with an originally given spherical shape, into worm-like particles upon drug-loading.<sup>[131]</sup> Further, the interaction with serum albumin, the most abundant protein in human blood, can also lead to the deformation of spherical into spheroidal micelles.<sup>[185]</sup> All these factors must be considered in designing and screening drug delivery systems, making it eventually even more challenging. Besides the “first-level self-assembly” of amphiphilic block copolymers into supramolecular structures, there has also been emerging interest in higher hierarchical structures built up from

self-assembled structures themselves; however, such systems are limited to an academic setting.<sup>[186]</sup>

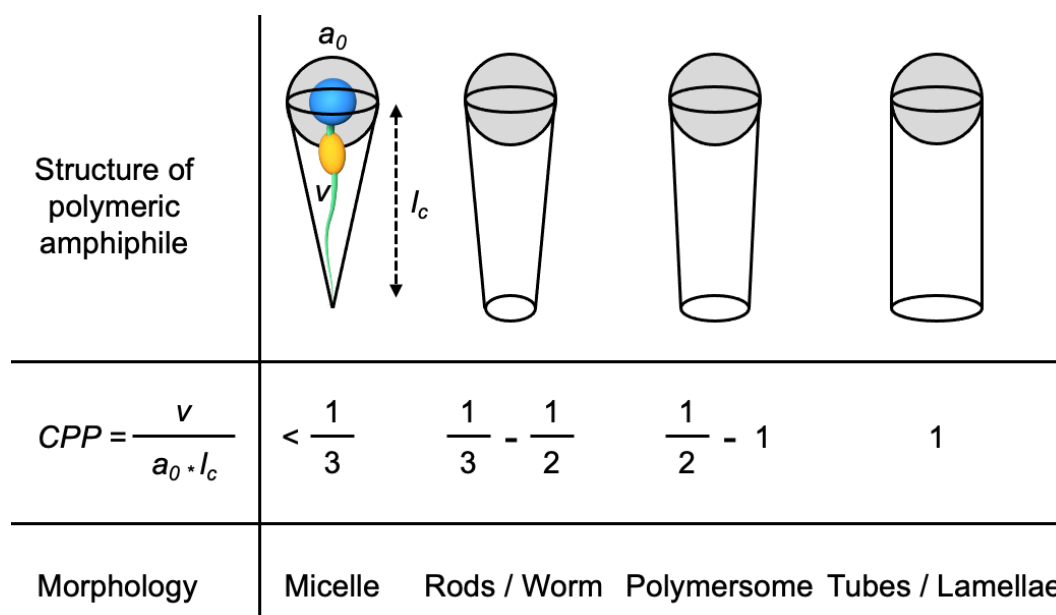


**Figure 13.** Influence of the Critical Packing Parameter ( $CPP$ ) on the morphology and shape of self-assembled polymeric amphiphiles;  $v$  is the volume of the hydrophobic chain,  $a_0$  is the optimum area of the hydrophilic headgroup, and  $l_c$  is the critical length of the hydrophobic chain.<sup>[187]</sup>

## 2.5 Organocatalysis in Polymer Chemistry

In 2021, Benjamin List and David MacMillan were awarded the Nobel Prize in Chemistry for their contributions to the development of asymmetric organocatalysts.<sup>[188]</sup> Whereas their works were focused on the catalysis of small-molecule reactions, the first polymerization of cyclic monomers initiated by simple molecules such as 4-(dimethylamino)pyridine (DMAP) was reported by Hedrick *et al* in 2001.<sup>[90]</sup> Since their pioneering work, organocatalysis has become a popular and powerful tool in polymer science for constructing well-defined polymeric architectures ranging from linear to cyclic polymers.<sup>[189]</sup> The use of organocatalysts is superior to the use of metal-based catalysts since they show some tolerance to moisture, lower toxicity profiles, are easier to be removed, and allow to operate the reaction under milder conditions, which all makes them widely studied candidates in the academic setting. However, due to their low thermal stability and required high catalyst loading, their application in the industry still needs to be improved compared to the conventional metal-based alternatives.<sup>[190]</sup>

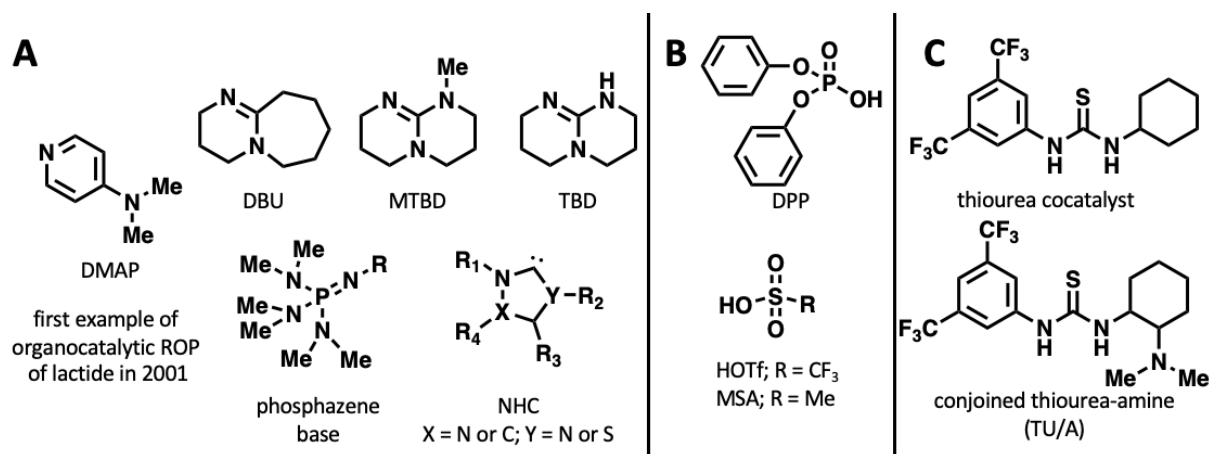


**Figure 14.** Schematic overview of the most used organocatalysts in polymer chemistry **(A)** nucleophilic catalysts such as 4-dimethylaminopyridine (DMAP), 1,8-diazabicyclo[5.4.0]undec-7-ene (DBU), 7-methyl-1,5,7-triazabicyclo[4.4.0]dec-5-ene (MTBD), 1,5,7-triazabicyclo[4.4.0]dec-5-ene (TBD), the general structure of a phosphazene base, and general structure of an N-heterocyclic carbene (NHC); **(B)** acidic catalysts, such as diphenyl phosphate (DPP), trifluoromethanesulfonic acid (HOTf), and methanesulfonic acid (MSA); **(C)** “supramolecular” catalysts, such as thiourea cocatalyst, and conjoined thiourea-amine (TU/A).

Based on the first report of DMAP facilitating the polymerization of lactide, other nucleophilic bases were investigated for the polymerization of many cyclic monomers, where the widest studied bases are N-heterocyclic carbenes (NHCs).<sup>[191]</sup> This type of catalyst revealed extremely high activities in the ROP of lactones, epoxides, and cyclic carbonates, among others;<sup>[192]</sup> however, their air sensitiveness and easy deactivation by water motivated researchers to look out for more robust alternatives. This search led to the discovery of strong nitrogen bases, such as guanidine, and amidine organocatalysts, for the ROP of several cyclic monomers, including 1,5,7-Triazabicyclo[4.4.0]dec-5-ene (TBD), N-methyl-TBD (MTBD), and 1,8-diazabicyclo[5.4.0]-undec-7-ene (DBU).<sup>[193]</sup> Notably, other organocatalysts based on, e.g., thiourea-derivates, phosphazene bases, and acidic catalysts, also found their widespread application in the polymerization of cyclic monomers.<sup>[91]</sup> For a summary, see Figure 14.

The mechanism of the ring-opening polymerization of, e.g., cyclic esters, is governed by the involved catalyst; in which always, the lactone monomer is electrophilic, and the initiator (or propagating chain end) is nucleophilic. For example, metal-based catalysts operate by a “coordination-insertion” mechanism,<sup>[194]</sup> in which the transformation into a metal alkoxide activates the alcohol initiator. Depending on the Lewis acidity and the availability of open binding sites on the coordinating metal center, the metal alkoxides can also activate the lactone *via* coordination with the carbonyl of the monomer, see Figure 15.

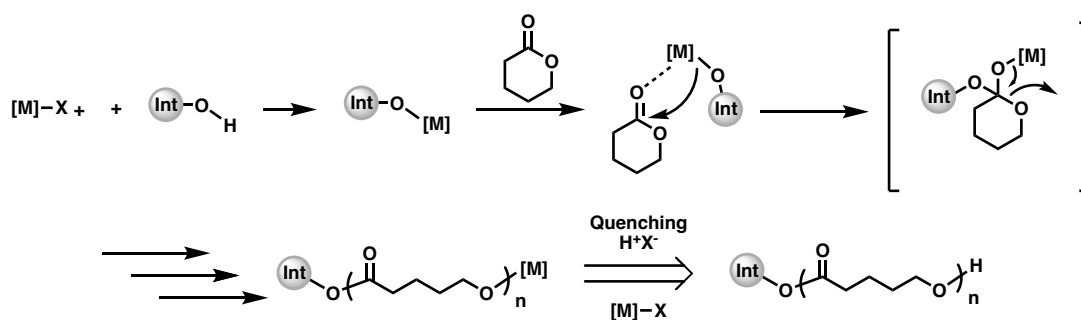
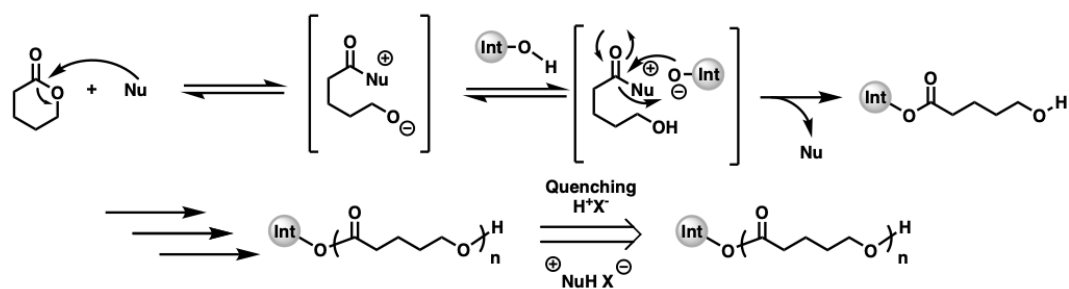


**Figure 15.** Coordination-Insertion Mechanism for Metal-catalyzed ROP of cyclic monomers, e.g.,  $\delta$ -Valerolactone, whereas  $[M]-X$  stands for the metal catalyst, and  $Int-OH$  for the alcohol initiator.

Whether TBD follows the hydrogen-bonding mechanism, also called bifunctional activation, or the nucleophilic mechanism has been debated, and it still needs to be fully unwrapped. TBD's strong basicity and high reactivity initially led to the conclusion that it undergoes a nucleophilic attack on the carbonyl atom<sup>[195]</sup> (Figure 16); however, theoretical calculations support the theory behind the hydrogen bonding mechanism.<sup>[196]</sup>

#### Nucleophilic Monomer Activation Mechanism for ROP



OR

#### Bifunctional Activation Using Hydrogen Bonding for ROP

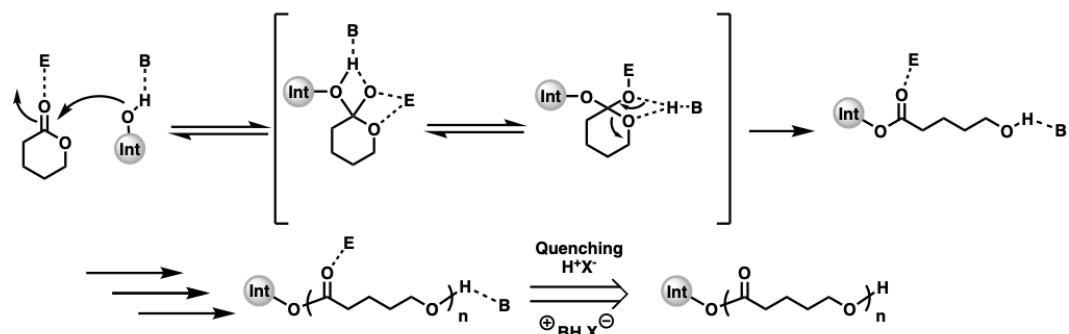


**Figure 16.** Two proposed mechanistic pathways for the organocatalyzed ROP through TBD; top: nucleophilic monomer activation *via* a nucleophilic attack, Nu = nucleophile; bottom: bifunctional activation using hydrogen bonding to the monomer, e.g.,  $\delta$ -Valerolactone, B = base, E = electrophile.

### 3 Scientific Goals

The strong hydrophobicity of the most frequently used chemotherapeutics requires solubilization enhancers, such as polymeric micelles, to enable the intravenous injection into the patient's bloodstream. However, even market-authorized drug delivery systems bring only a little benefit compared to the administration of the free drug, ending up in an uncontrolled distribution of the drug all over the patient's body, which on the one side, brings additional suffering to the already worn-out patients; on the other, it lowers the therapeutic efficacy and can cause the failure of the therapy.

The present work aims to establish dendritic polyglycerolsulfate, an extremely water-soluble, biocompatible polymer with the intrinsic ability to target cancerous tissue, as the polymer to replace PEG in the construction of amphiphilic block copolymer micelles. Various biodegradable polymers were investigated as the hydrophobic segment, ranging from FDA-approved candidates, such as PCL, PLA, or PLGA, to recently published poly(ester amide)s polymers. By employing different cohesive forces to the micellar core, such as hydrophobic or  $\pi$ - $\pi$  interactions, the critical micelle concentration (CMC) was altered to obtain highly stable drug delivery systems, the major shortcoming of conventional drug delivery systems. For exerting the therapeutic action of the pharmaceutical cargo, the drug must be released upon cellular uptake from the carrier systems, which was ensured by implementing a reductive-sensitive disulfide bridge onto the polymer structure (Figure 17).

The synthesis of the hydrophobic and hydrophilic segments must be conducted with high control over the molecular weight and ease of purification to ensure the biocompatibility of the later material; thus, organo-base mediated ROP of the cyclic monomers and anionic ROP of glycidol acquired the hydrophobic and hydrophilic segments. Before forming the amphiphilic block copolymers, a prior amide coupling reaction must introduce the redox-sensitive disulfide bridge to the hydrophilic segment (Figure 18A). Since the administration route of these drug delivery systems is an intravenous injection, the systems were tested for their ability to undergo the so-called "CAPIR" cascade, including the following 5-steps: Circulation in the bloodstream and its compartments, Accumulation, and Penetration into the cancerous tissue, followed by cellular Internalization, and finally, precise drug Release.<sup>[197]</sup> An interplay of different physical and chemical characteristics determines the success of particles in undergoing the complete cascade, including size, morphology, surface charge, and stability. To our understanding, insufficient stability is the major limitation of self-assembled systems to their clinical application; therefore, light scattering experiments systematically studied the extraordinarily low CMCs of the systems (Figure 18B). Further understanding their fate upon injection, the serum protein interaction and the systems' stability in a serum-rich environment were investigated by light scattering and size exclusion



experiments. Other critical parameters in the drug development process are to gather information on the efficacy, toxicity, and pharmacokinetics; thus, suitable *in vitro* models using human immortalized cell lines, both non- and tumor-derived, studied the excellent cell compatibility and substantial cancer growth inhibition of the empty and drug-loaded systems (Figure 18C). All herein-used chemotherapy medications were medically approved, including Sunitinib, a receptor tyrosine kinase (RTK) inhibitor used for the treatment of renal cell carcinoma (RCC) and imatinib-resistant gastrointestinal stromal tumor (GIST), and Docetaxel, a microtubule inhibitor used to treat several types of cancer, such as breast, lung, and prostate cancer. An angiogenesis assay was established for Sunitinib to understand the enhanced therapeutic efficacy of the encapsulated drug. Further, the *in vitro* fate upon cellular uptake on different cell lines was monitored by fluorescence-labeled dPGS-SS-micelles. As a proof of concept, the biodistribution of the herein-developed systems was monitored in tumor-bearing mice models to understand the cancer-homing ability of the dPGS-functionalized systems. The final goal of this thesis was to underline the substantial therapeutic efficacy and safety of a dPGS-SS-micelle-supported therapy administrating Sunitinib (Figure 18D). For this study, a HeLa-tumor-bearing mice model was established with the aim of proofing the enhancement of the chemotherapy by using a significantly lower dosage of the encapsulated-chemotherapeutic compared to the free drug. The body weight and other organ tissues, such as the heart, liver, and tumor, were also analyzed for any unwanted side effects caused by the treatments.

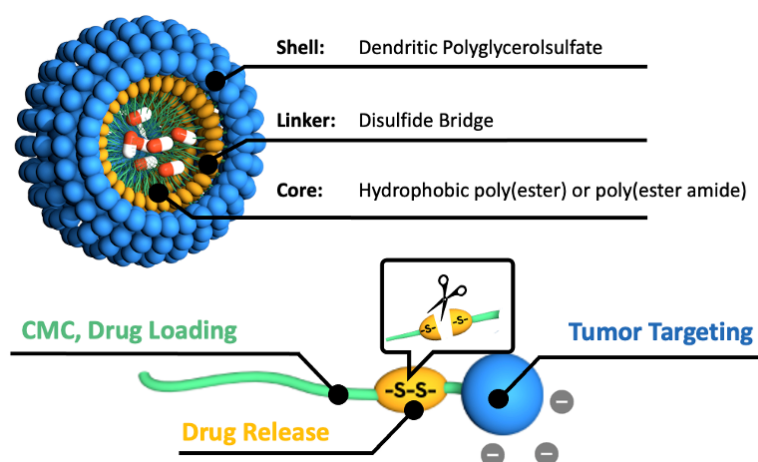


**Figure 17.** Conceptual depiction of the toolbox-like manner of the dPGS-SS-micelles investigated in this thesis; the hydrophilic shell is given as dPGS, facilitating the water solubility of the whole systems along with the intrinsic ability to selectively target cancerous tissue; the hydrophobic block is either given by poly(ester) or poly(ester amide)s copolymers, which allows altering the CMC and drug-loading capacity of the systems; the drug-release of the amphiphilic block copolymers micelles is ensured *via* the implementation of a disulfide bridge connecting the hydrophilic and hydrophobic block forming the amphiphilic block copolymer.

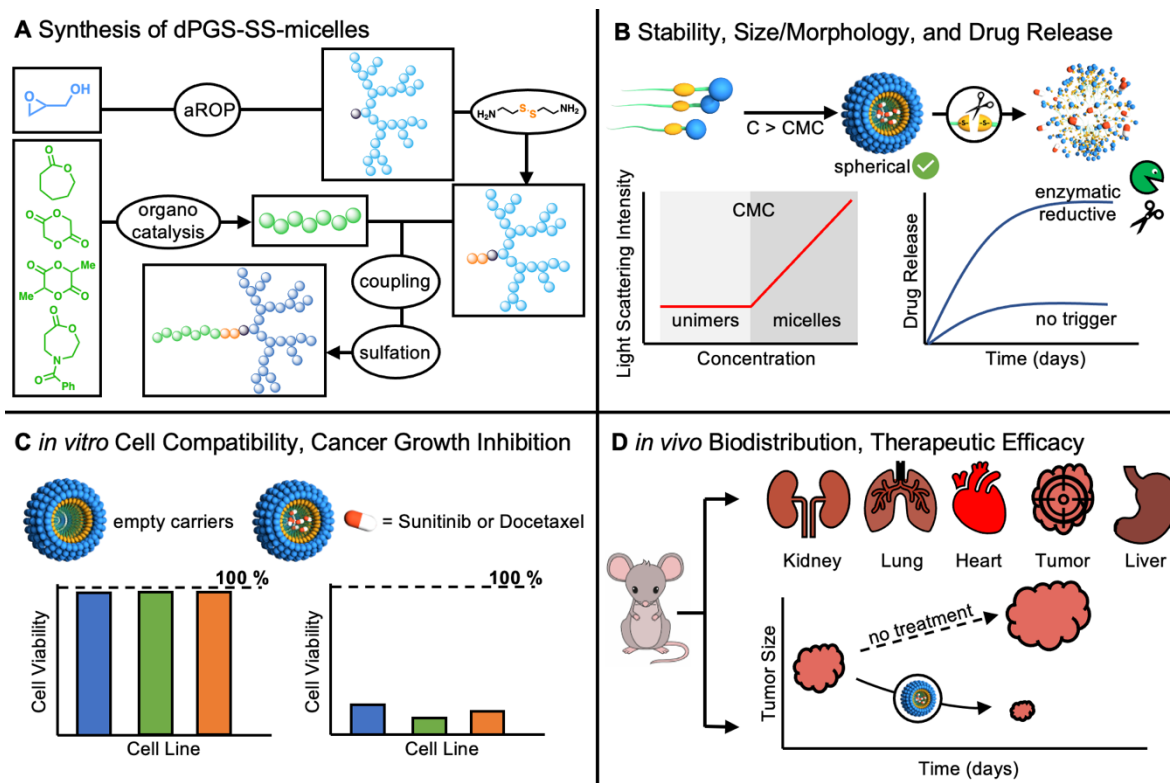


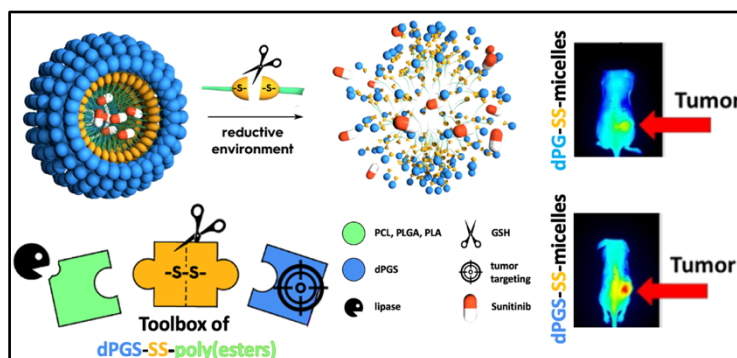
**Figure 18.** Schematic representation of the work packages, and the projects covered in this thesis. **(A)** synthetic pathway towards functional amphiphilic block copolymers; Synthesis of the hydrophobic homopolymers poly(caprolactone) (PCL), poly(lactide) (PLA), poly(lactide-co-glycolide) (PLGA), and poly(4-benzoyl-1,4-oxazepan-7-one) (POxPPH), starting from the respective monomer caprolactone, lactide, glycolide/lactide, and 4-benzoyl-1,4-oxazepan-7-one catalyzed by organo-catalysts, such as 1,8-Diazabicyclo[5.4.0]undec-7-en (DBU) or 1,5,7-Triazabicyclo(4.4.0)dec-5-en (TBD); in parallel, anionic ring-opening polymerization (aROP) of glycidol and subsequent coupling of cysteamine acquired the hydrophilic polymer segment (dPG-SS-NH<sub>2</sub>); the connection of both blocks and following sulfation leads to the targeted amphiphilic block copolymers (dPGS-SS-hydrophobic polymer); **(B)** the stability, size/morphology, and drug release kinetics under physiological conditions were systematically studied by light scattering, cryo-EM, and dialysis experiments, respectively; **(C)** the *in vitro* cell compatibility of the empty carrier systems was studied on both non- and tumor-derived cell lines; further, the cancer growth inhibition of the drug-loaded systems was also investigated; **(D)** suitable *in vivo* models investigated the biodistribution of fluorescence-dye loaded dPGS-SS-micelles, and further, drug-loaded micelles were tested for their therapeutic efficacy in tumor-bearing mice.

## 4 Publications and Manuscripts

### 4.1 *Toolbox of Biodegradable Dendritic (Poly glycerol sulfate)–SS-poly(ester) Micelles for Cancer Treatment: Stability, Drug Release, and Tumor Targeting*

**Daniel Braatz**, Mathias Dimde, Guoxin Ma, Yinan Zhong, Michael Tully, Carsten Grötzinger, Yuanyuan Zhang, Alexandros Mavroskoufis, Michael Schirner, Zhiyuan Zhong, Matthias Ballauff\*, and Rainer Haag\* *Biomacromolecules* **2021**, 22, 6, 2625–2640.

<https://doi.org/10.1021/acs.biomac.1c00333>



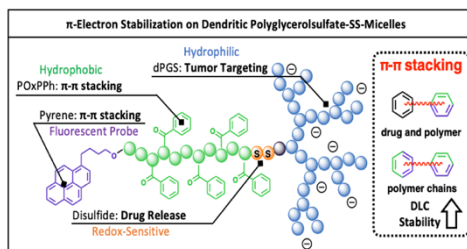
**Abstract:** In this paper, we present well-defined dPGS-SS-PCL/PLGA/PLA micellar systems demonstrating excellent capabilities as a drug delivery platform in light of high stability and precise in vitro and in vivo drug release combined with active targetability to tumors. These six amphiphilic block copolymers were each targeted in two different molecular weights (8 or 16 kDa) and characterized using  $^1\text{H}$  NMR, gel permeation chromatography (GPC), and elemental analysis. The block copolymer micelles showed monodispersed size distributions of 81–187 nm, strong negative charges between  $-52$  and  $-41$  mV, and low critical micelle concentrations (CMCs) of up to 1.13–3.58 mg/L (134–527 nM). The serum stability was determined as 94% after 24 h. The drug-loading efficiency for Sunitinib ranges from 38 to 83% (8–17 wt %). The release was selectively triggered by glutathione (GSH) and lipase, reaching 85% after 5 days, while only 20% leaching was observed under physiological conditions. Both the in vitro and in vivo studies showed sustained release of Sunitinib over 1 week. CCK-8 assays on HeLa lines demonstrated the high cell compatibility (1 mg/mL, 94% cell viability, 48 h) and the high cancer cell toxicity of Sunitinib-loaded micelles ( $IC_{50}$  2.5  $\mu\text{g/mL}$ ). By in vivo fluorescence imaging studies on HT-29 tumor-bearing mice, the targetability of dPGS<sub>7.8</sub>-SS-PCL<sub>7.8</sub> enabled substantial accumulation in tumor tissue compared to nonsulfated dPG<sub>3.9</sub>-SS-PCL<sub>7.8</sub>. As a proof of concept, Sunitinib-loaded dPGS-SS-poly(ester) micelles improved the antitumor efficacy of the chemotherapeutic. A tenfold lower dosage of loaded Sunitinib led to an even higher tumor growth inhibition than the free drug, as demonstrated in a HeLa human cervical tumor-bearing mice model. No toxicity for the organism was observed, confirming the good biocompatibility of the system.

**Contribution of Daniel Braatz to this work:** Design of the system, synthesis of hydrophobic and amphiphilic polymers, characterization of micelles, drug-loading, and release studies, evaluation of data, and preparation of the manuscript.

## 4.2 Dendritic polyglycerolsulfate-SS-poly(ester amide) micelles for the systemic delivery of docetaxel: pushing the limits of stability through the insertion of $\pi$ - $\pi$ interactions

**Daniel Braatz**, Justus H. Peter, Mathias Dimde, Elisa Quaas, Kai Ludwig, Katharina Achazi, Matthias Ballauff\*, and Rainer Haag\* *J. Mater. Chem. B*, **2023**, 11, 3797-3807.

<https://doi.org/10.1039/D3TB00055A> (CC BY-NC 3.0 <https://creativecommons.org/licenses/by-nc/3.0/>)



**Abstract:** Insufficient stability of micellar drug delivery systems is still the major limitation to their systematic application in chemotherapy. This work demonstrates novel  $\pi$ -electron stabilized polyelectrolyte block copolymer micelles based on dendritic polyglycerolsulfate-cystamine-block-poly(4-benzoyl-1,4-oxazepan-7-one)-pyrene (dPGS-SS-POxPPh-Py) presenting a very low critical micelle concentration (CMC) of 0.3 mg/mL (18 nM), 55-fold lower than that of conventional amphiphilic block copolymer micelles. The drug loading capacities of up to 13 wt% allow the efficient encapsulation of the chemotherapeutic Docetaxel (DTX). The spherical morphology of the micelles was proven by cryogenic electron microscopy (cryo-EM). Gaussian Analysis revealed well-defined sizes of 57 nm and 80 nm in the unloaded/loaded state, respectively. Experiments by dynamic light scattering (DLS), ultraviolet-visible spectroscopy (UV-VIS), fluorescence spectroscopy, and cross-polarization solid-state  $^{13}\text{C}$  NMR studied the  $\pi$ - $\pi$  interactions between the core-forming block segment of dPGS-SS-POxPPh-Py and DTX. The findings point to a substantial contribution of these noncovalent interactions to the system's high stability. By confocal laser scanning microscopy (CLSM), the cellular uptake of fluorescein-labelled FITC-dPGS-SS-POxPPh-Py micelles was monitored after one day displaying the successful cell insertion of the cargo-loaded systems. To ensure the drug release in cancerous cells, the disassembly of the micellar DTX-formulations was achieved by reductive and enzymatic degradation studied by light scattering and GPC experiments. Further, no size increase nor disassembly in the presence of human serum proteins after four days was detected. The precise in vitro drug release was also given by the high potency of inhibiting cancer cell growth, finding half-maximal inhibitory concentrations ( $IC_{50}$ ) efficiently reduced to 68 nM coming along with high viabilities of the empty polymer materials tested on tumor-derived HeLa, A549, and McF-7 cell lines after two days. This study highlights the substantial potential of micelles tailored through the combination of  $\pi$ -electron stabilization with dendritic polyglycerolsulfate for targeted drug delivery systems, enabling them to have a significant foothold in the clinical treatment of cancer.

**Contribution of Daniel Braatz to this work:** Design of the system, synthesis of hydrophobic and amphiphilic polymers, characterization of micelles, drug-loading, evaluation of data, and preparation of the manuscript.

# Journal of Materials Chemistry B

Materials for biology and medicine

rsc.li/materials-b





ISSN 2050-750X

**PAPER**

Matthias Ballauff, Rainer Haag *et al.*  
Dendritic polyglycerolsulfate-SS-poly(ester amide) micelles  
for the systemic delivery of docetaxel: pushing the limits of  
stability through the insertion of  $\pi$ - $\pi$  interactions

Cite this: *J. Mater. Chem. B*, 2023, **11**, 3797

# Dendritic polyglycerolsulfate-SS-poly(ester amide) micelles for the systemic delivery of docetaxel: pushing the limits of stability through the insertion of $\pi$ - $\pi$ interactions†

Daniel Braatz,<sup>a</sup> Justus H. Peter,<sup>a</sup> Mathias Dimde,<sup>ab</sup> Elisa Quaas,<sup>a</sup> Kai Ludwig,<sup>b</sup> Katharina Achazi,<sup>a</sup> Michael Schirner,<sup>a</sup> Matthias Ballauff <sup>\*a</sup> and Rainer Haag <sup>\*a</sup>

Insufficient stability of micellar drug delivery systems is still the major limitation to their systematic application in chemotherapy. This work demonstrates novel  $\pi$ -electron stabilized polyelectrolyte block copolymer micelles based on dendritic polyglycerolsulfate-cystamine-*block*-poly(4-benzoyl-1,4-oxazepan-7-one)-pyrene (dPGS-SS-POxPPh-Py) presenting a very low critical micelle concentration (CMC) of 0.3 mg L<sup>-1</sup> (18 nM), 55-fold lower than that of conventional amphiphilic block copolymer micelles. The drug loading capacities of up to 13 wt% allow the efficient encapsulation of the chemotherapeutic Docetaxel (DTX). The spherical morphology of the micelles was proven by cryogenic electron microscopy (cryo-EM). Gaussian Analysis revealed well-defined sizes of 57 nm and 80 nm in the unloaded/loaded state, respectively. Experiments by dynamic light scattering (DLS), ultraviolet-visible spectroscopy (UV-VIS), fluorescence spectroscopy, and cross-polarization solid-state <sup>13</sup>C NMR studied the  $\pi$ - $\pi$  interactions between the core-forming block segment of dPGS-SS-POxPPh-Py and DTX. The findings point to a substantial contribution of these noncovalent interactions to the system's high stability. By confocal laser scanning microscopy (CLSM), the cellular uptake of fluorescein-labelled FITC-dPGS-SS-POxPPh-Py micelles was monitored after one day displaying the successful cell insertion of the cargo-loaded systems. To ensure the drug release in cancerous cells, the disassembly of the micellar DTX-formulations was achieved by reductive and enzymatic degradation studied by light scattering and GPC experiments. Further, no size increase nor disassembly in the presence of human serum proteins after four days was detected. The precise *in vitro* drug release was also given by the high potency of inhibiting cancer cell growth, finding half-maximal inhibitory concentrations (IC<sub>50</sub>) efficiently reduced to 68 nM coming along with high viabilities of the empty polymer materials tested on tumor-derived HeLa, A549, and McF-7 cell lines after two days. This study highlights the substantial potential of micelles tailored through the combination of  $\pi$ -electron stabilization with dendritic polyglycerolsulfate for targeted drug delivery systems, enabling them to have a significant foothold in the clinical treatment of cancer.

Received 10th January 2023,  
Accepted 22nd March 2023

DOI: 10.1039/d3tb00055a

rsc.li/materials-b

## 1. Introduction

In 2022, the American Cancer Society estimated almost two million new cancer cases in the United States<sup>1</sup> – another 600 000 patients will die of cancer – making it the second leading cause of death after cardiac disorders. The current state of chemotherapy is based on administering hydrophobic small-molecule drugs in order to

kill the cancer cells or stop them from dividing.<sup>2,3</sup> Self-assembled carrier systems are often applied to ensure the solubility of these water-insoluble compounds in the formulation and bloodstream.<sup>4,5</sup> The fact that the delivery system gets highly diluted after injection and its simultaneous opsonization by a biomolecular layer has posed a challenge to scientists in chemistry, pharmacy, medicine, and pharmacology for decades.<sup>6–10</sup> Upon administration, the dilution in the bloodstream triggers the disassembly of the system by causing the concentration to fall below the critical micelle concentration (CMC), resulting in a loss of function. Additionally, the nonspecific interaction with blood serum proteins is known to alter the applied systems' stability<sup>10</sup> and targeting properties.<sup>11</sup> Most developed micellar carrier systems do not match their high performances drawn from *in vitro* experiments if tested *in vivo*.<sup>12</sup>

<sup>a</sup> Institute of Chemistry and Biochemistry, Freie Universität Berlin, Berlin 14195, Germany. E-mail: mballauff@zedat.fu-berlin.de, haag@zedat.fu-berlin.de

<sup>b</sup> Institute of Chemistry and Biochemistry, Research Center of Electron Microscopy, Freie Universität Berlin, Berlin 14195, Germany

† Electronic supplementary information (ESI) available. See DOI: <https://doi.org/10.1039/d3tb00055a>



Consequently, the pharmacokinetic and biodistribution of the administered drug delivery system is similar to that of a free drug giving a distribution all over the body with low accumulation on its site of action, *e.g.*, the tumor. In addition, this uncontrolled distribution causes further suffering for the cancer patient who is already worn out by the actual disease. Thus, to ensure therapy's success, the critical challenge lies in systematically improving the screening of the stability and protein interactions to keep the systems in their active states.<sup>13</sup> Recently, biodegradable micelles based on dendritic polyglycerolsulfate (dPGS) demonstrated their high therapeutic potential *in vivo* with selective accumulation in tumor tissue showing no toxicity to the organisms.<sup>14,15</sup> However, remaining is the central question of whether the stability of this system can be further increased to boost its therapeutic potential.

The development of micelles has attracted attention in both academia and industry.<sup>16</sup> Yet, only minor progress has been reported in their clinical translation over the last few years.<sup>17–19</sup> One of the early concepts, which has shown promising results, is the application of so-called  $\pi$ - $\pi$  stabilized systems.<sup>20</sup> This idea was applied in most of the very early systems that went into clinical trials; see NK911<sup>21</sup> or NK105.<sup>22</sup> This principle was adopted by Hennink *et al.*, who again pointed out its high potential.<sup>23–25</sup> In our study, we combine the efficiency of  $\pi$ -electron stabilization and the intrinsic targetability of dendritic polyglycerolsulfate towards inflammation and cancer. The selective accumulation of dPGS-based materials can be traced down to the binding of the sulfates with L-selectin,<sup>26–28</sup> an overexpressed cell adhesion molecule in cancer progression. The hydrophobic  $\pi$ -electron-donating block is synthesized from a

recently developed new class of monomers, the so-called *N*-acylated-1,4-oxazepan-7-one (OxP) monomers, a degradable analogue of poly(oxazoline).<sup>29</sup> The hydrophilic segment is given as dPGS which is connected to the hydrophobic block *via* a disulfide bridge enabling the precise drug release in the reductive environment found in tumor tissue.<sup>30</sup> This novel amphiphilic block copolymer is tailor-made for yielding micelles with (i) high stability; (ii) high drug loading capacity; (iii) a precise release of the payload; and (iv) excellent cell viability with substantial tumor growth inhibition (Fig. 1).

We designed a library of three novel block copolymer micelles (Fig. 2), each with varying amounts of  $\pi$ -electrons (i) dendritic polyglycerolsulfate-cystamine-*block*-poly(caprolactone)-ethyl (dPGS-SS-PCL-Et, Fig. 2(A)) having no  $\pi$ -electrons, (ii) dendritic polyglycerolsulfate-cystamine-*block*-poly(caprolactone)-pyrene (dPGS-SS-PCL-Py, Fig. 2(B)) with moderate  $\pi$ -electrons, and (iii) dendritic polyglycerolsulfate-cystamine-*block*-poly(4-benzoyl-1,4-oxazepan-7-one)-pyrene with high  $\pi$ -electron density (dPGS-SS-POxPPh-Py, Fig. 2(C)). The influence of  $\pi$ - $\pi$  stacking in terms of self-assembly and stability was studied systematically by light scattering and cryo-TEM. The chemotherapeutic drug Docetaxel, which is part of first-line treatment regimens for numerous cancer types in the clinics, such as breast and non-small cell lung cancer, was used as the model compound. DLS measurements found decreased CMC values in the low nanomolar range with an increased density of  $\pi$ -electrons. Also,  $\pi$ -electron-bearing micelles exhibit higher drug-loading capacities than non-aromatic micelles. Furthermore, UV-VIS, fluorescence, and cross-polarization solid-state <sup>13</sup>C NMR measurements

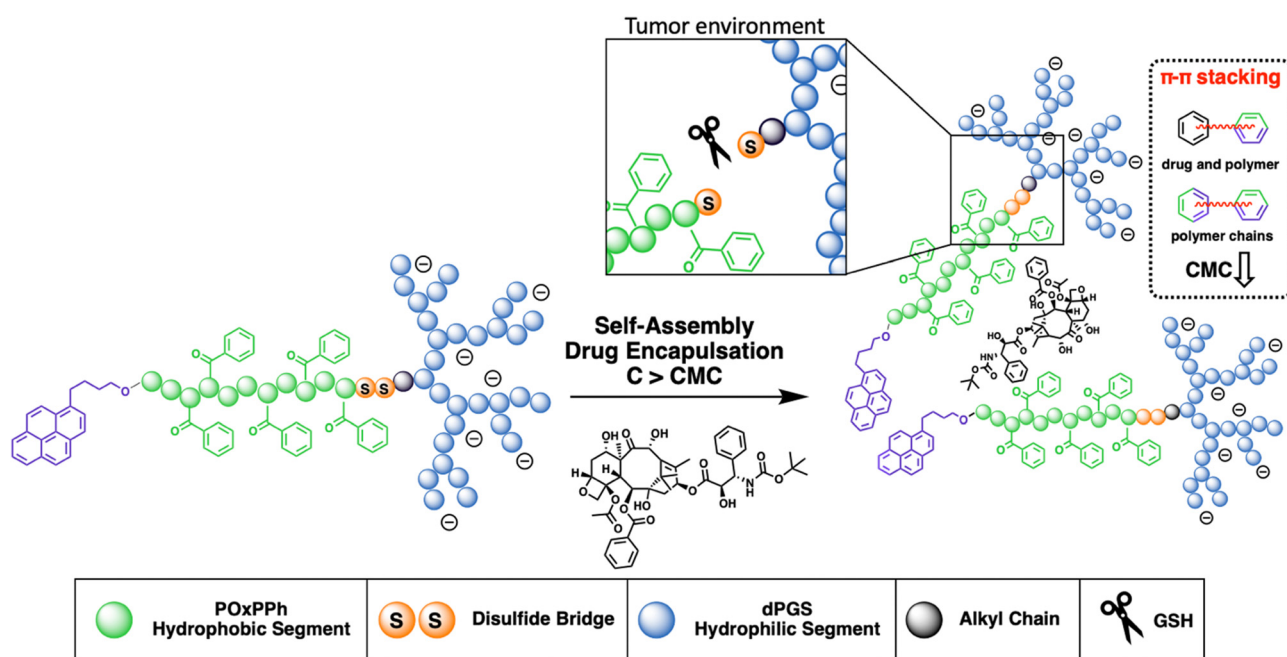


**Fig. 1** Schematic illustration of dPGS-SS-POxPPh-Py amphiphiles undergoing self-assembly in an aqueous solution above their CMC, forming spherical micelles carrying a water-insoluble cargo, here docetaxel, in their hydrophobic inner-core, whereas the anionic-charged dPGS-shell (blue) facilitates the solubility of the system. The hydrophobic polymer, POxPPh (green), bears phenyl-rings on its side chain, facilitating  $\pi$ - $\pi$  stacking in the micellar core between the polymer chains, the drug, and *vice versa*, decreasing CMC values and increasing drug loading capacities. The hydrophobic and hydrophilic segments are connected *via* a disulfide bridge (orange), enabling the polymer chain's reductive cleavage in tumor-mimicking GSH-rich environments.



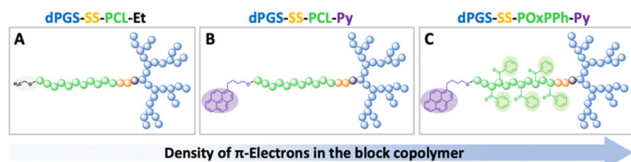


Fig. 2 Schematic overview of the amphiphilic block copolymer library with increasing  $\pi$ -electrons from left to right (A) dPGS-SS-PCL-Et with no  $\pi$ -electrons (B) dPGS-SS-PCL-Py with  $\pi$ -electrons on the chain-end attributed by pyrene (purple), and (C) dPGS-SS-POxPPh-Py with a high density of  $\pi$ -electrons in the presence of sidechain bearing phenyl rings (green) all over the hydrophobic segment and pyrene moiety on the chain end (purple). Notably, for dPGS-SS-POxPPh-Py, each repeating unit of the hydrophobic block carries a benzoyl group; this has been presented in a simplified manner for clarity.

unwrapped the structural morphology of the drug-loaded micelle core. The disassembly of the micelles was selectively triggered by reductive cutting of the disulfide bridge by GSH and by enzymatic cleavage of the esters by surface-immobilized lipases. The micelles were found to absorb no serum proteins on the micelle surface nor disassembly in their presence. FITC-labelled dPGS-

SS-POxPPh-Py were successfully inserted into tumor-thrived cells shown by CLMS. As proof of concept, the polymers' *in vitro* cell viability and *in vitro* cancer cell toxicity were evaluated, indicating low toxicity of the empty polymeric material while their DTX formulations exhibited highly potent anti-tumor performance. This study demonstrates the substantial potential of drug delivery systems achieved by the combination of  $\pi$ -electron stabilization and dendritic polyglycerolsulfate.

## 2. Results and discussion

### 2.1 Synthesis and characterization of dPGS-SS-PCL-Et, dPGS-SS-PCL-Py, and dPGS-SS-POxPPh-Py

To understand the importance of  $\pi$ -electron-rich domains on the stability and efficacy of polymeric micelles, we have designed a library of three different amphiphilic block copolymers (Fig. 2) (i) with no  $\pi$ -electrons (dPGS-SS-PCL-Et, Fig. 2(A)); (ii) with  $\pi$ -electrons located on the chain end (dPGS-SS-PCL-Py, Fig. 2(B)); and (iii) with  $\pi$ -electron distributed along the hydrophobic polymer block (dPGS-SS-POxPPh-Py, Fig. 2(C)). The synthesis of

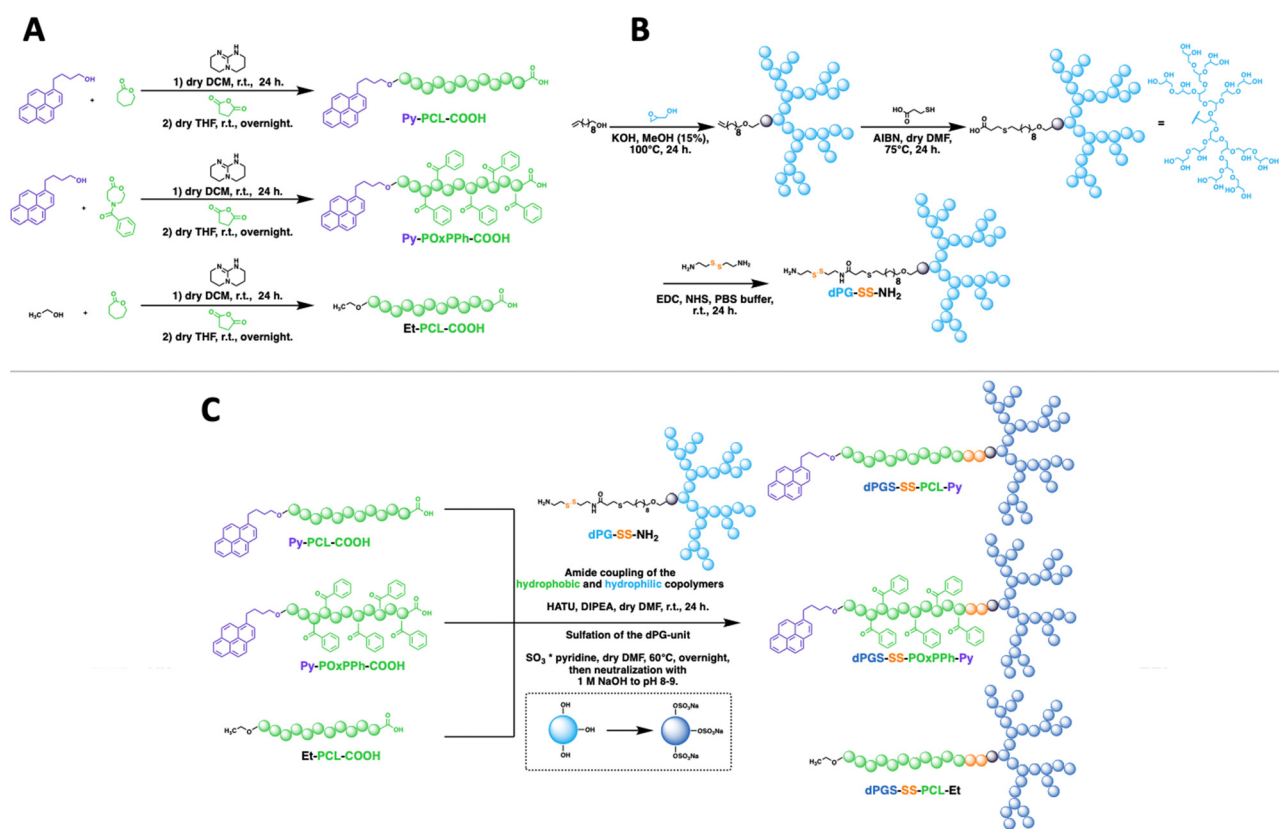


Fig. 3 Synthetic pathway to dPGS<sub>8.6</sub>-SS-POxPPh<sub>7.9</sub>-Py, dPGS<sub>8.6</sub>-SS-PCL<sub>7.9</sub>-Py, and dPGS<sub>7.8</sub>-SS-PCL<sub>7.8</sub>-Et. (A) Synthesis of the hydrophobic polyester segments Py-PCL-COOH, Py-POxPPh-Py, and Et-PCL-COOH by organo-catalyst TBD-mediated ring-opening polymerization of OxPPh or CL monomer initiated by pyrene butanol or ethanol with subsequent quenching *via* the addition of succinic anhydride. (B) Synthesis of the hydrophilic segment dPG-SS-NH<sub>2</sub> *via* an anionic ring-opening polymerization of glycidol initiated by 10-undecenol with following click reaction with mercapto-propionic acid and coupling of cystamine. (C) Synthesis of the amphiphilic block copolymers, first, *via* an amide coupling reaction mediated by HATU; the hydrophobic segments, Py-PCL-COOH, Py-POxPPh-COOH, and Et-PCL-COOH were coupled to the hydrophilic segment dPG-SS-NH<sub>2</sub> (dPG unit represented as light blue branched architecture), leading to amphiphilic block copolymers. Subsequently, sulfation converts the hydroxy groups of the dPG unit to sulfates, as indicated by the dark blue colour of the branched dPG-architecture leading to the final products dPGS-SS-PCL-Py, dPGS-SS-POxPPh-Py, and dPGS-SS-PCL-Et.





4-benzoyl-1,4-oxazepan-7-one (OxPPh) was performed following a Baeyer–Villiger oxidation of 1-benzoyl-4-piperidone (see ESI†). First, the hydrophobic segments Et-PCL-COOH, Py-PCL-COOH, and Py-POxPPh-COOH were synthesized starting from caprolactone (CL) or OxPPh using ethanol (Et-OH) or pyrene butanol (Py-OH) as initiators catalyzed by the organo-base 1,5,7-triazabicyclo(4.4.0)dec-5-en (TBD). Subsequently, the polymer chain ends were reacted with succinic anhydride quenching the polymerization and introducing a carboxylic acid (polymer-COOH) to the chain end (Fig. 3(A)). Since TBD has been demonstrated to be highly efficient in the polymerization of cyclic monomers,<sup>31</sup> all polymers were obtained in their desired molecular weights of 7.8–7.9 kDa and low dispersity ( $D < 1.3$ , see ESI†). A 3-step synthesis formed the hydrophilic segment as follows: (i) anionic ring-opening polymerization of glycidol initiated by 10-undecenol; (ii) thiol-click reaction of mercaptopropionic acid; and (iii) amide-coupling of cystamine to introduce the reductive-sensitive disulfide bridge (Fig. 3(B)). The dPG-SS-NH<sub>2</sub> was characterized by <sup>1</sup>H NMR and GPC, revealing a molecular weight of 4.3 and 4.4 kDa, respectively, with a narrow dispersity of  $D = 1.5$  (see ESI†). The amphiphilic block copolymers were obtained *via* an amide coupling procedure between Et-PCL<sub>7,8</sub>-COOH, Py-PCL<sub>7,9</sub>-COOH, and Py-POxPPh<sub>7,9</sub>-COOH with dPG<sub>4,3</sub>-SS-NH<sub>2</sub> (numbers indicated the molecular weight in kDa) mediated by HATU/DIPEA in DMF at room temperature (Fig. 3(C)). The successful coupling of Py-OxPPh<sub>7,9</sub>-COOH and dPG<sub>4,3</sub>-SS-NH<sub>2</sub> was proven by <sup>1</sup>H diffusion-ordered spectroscopy (DOSY) NMR in DMF-d<sub>7</sub>, finding one significant diffusion species indicating the covalent attachment of the block copolymers with no free homopolymers (Fig. 4(A)). The ESI† shows the <sup>1</sup>H NMR DOSY of the polymer blend with two different diffusion species of the mixed homopolymers (Fig. S11, ESI†). Lastly, the sulfation of the dPG<sub>4,3</sub>-SS-R yielded in dPG<sub>8,6</sub>-SS-R (R = PCL<sub>7,8</sub>-Et, PCL<sub>7,9</sub>-Py, POxPPh<sub>7,9</sub>-Py), where it doubles the molecular weight of the dPG units by the mass increase of alcohols transformed to sulfate groups (see ESI†). From this point onwards, the characterization of the sulfated block copolymers is strongly limited due to the excessive amphiphilicity (see ESI†). In Fig. 4(B) and (C), the solution <sup>1</sup>H NMR of dPG<sub>4,3</sub>-SS-POxPPh<sub>7,9</sub>-Py and dPG<sub>8,6</sub>-SS-POxPPh<sub>7,9</sub>-Py is measured in DMF-d<sub>7</sub> and D<sub>2</sub>O, respectively. Before sulfation, the NMR shows all characteristic structural motifs of the block copolymers. In contrast, the core-forming segments disappear after sulfation due to the micelle formation in D<sub>2</sub>O, the exclusive solvent for this polymer. However, the intact structure was proven *via* IR, GPC, Solid-State NMR (for more details see ESI†), and UV spectroscopy (Fig. 7).

## 2.2 Formation and characterization of micelles: shape, size, charge, and stability

The amphiphilic block copolymers were used to form micelles following a nanoprecipitation protocol from acetone into PBS buffer (150 mM NaCl, pH 7.4) with subsequent organic solvent evaporation. Before light scattering experiments studied the formed micelles intensively, the morphology and size were analyzed by cryo-TEM, finding a spherical morphology (Fig. 5).

By Gaussian analysis of the detected particles, the mean particle size for dPG<sub>8,6</sub>-SS-POxPPh<sub>7,9</sub>-Py was 57 nm in the unloaded state (Fig. 5(A)) and 80 nm upon loading with

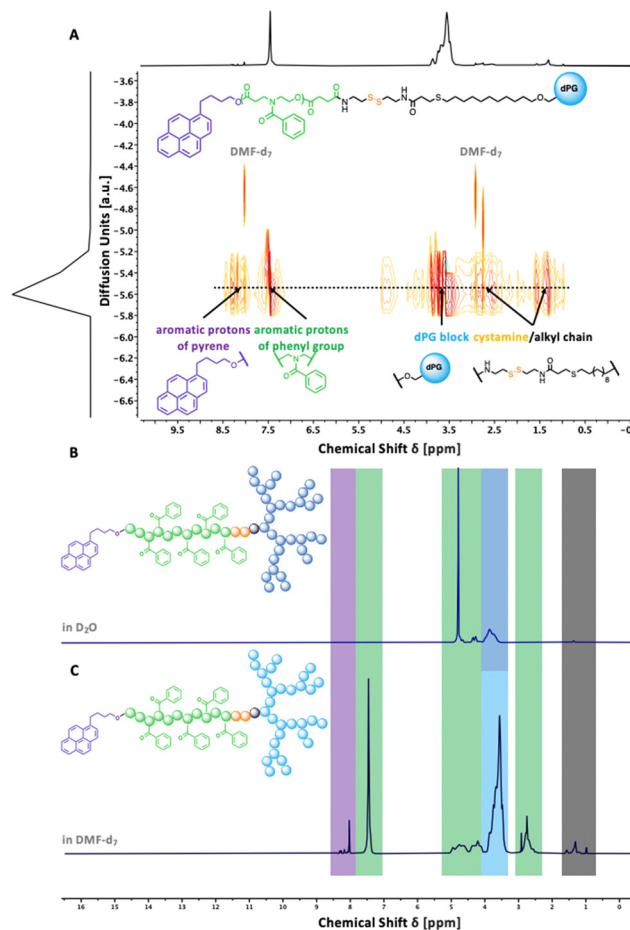


Fig. 4 (A) <sup>1</sup>H-derived DOSY spectrum (500 MHz) in DMF-d<sub>7</sub> after amide coupling of Py-POxPPh<sub>7,9</sub>-COOH and dPG<sub>4,3</sub>-SS-NH<sub>2</sub> showing one significant diffusion species (dotted line) confirming successful coupling to a covalently connected amphiphilic block copolymer with no uncoupled educts. (B) <sup>1</sup>H NMR spectrum of dPG<sub>8,6</sub>-SS-POxPPh<sub>7,9</sub>-Py shows the signals of the shell-forming dPG<sub>8,6</sub>-segment in D<sub>2</sub>O. The signals of the core-forming segments disappear due to the formation of micelles in an aqueous solution. (C) <sup>1</sup>H NMR spectrum of dPG<sub>4,3</sub>-SS-POxPPh<sub>7,9</sub>-Py showing all characteristic peaks of the pyrene butanol-initiator, hydrophobic POxPPh block, alkyl chain/disulfide linker, and of the hydrophilic dPG<sub>4,3</sub>-segment in DMF-d<sub>7</sub>.

Docetaxel according to cryo-TEM (Fig. 5(B)). In DLS, the hydrodynamic diameter for dPG<sub>8,6</sub>-SS-POxPPh<sub>7,9</sub>-Py micelles was found to be in similar ranges with 94 nm in the unloaded and 102 nm in the drug-loaded state. Notably, in the DLS measurements, the size is slightly larger due to the hydration shell around the particles, hence it is not present in cryo-TEM images. The sizes for dPG<sub>8,6</sub>-SS-PCL<sub>7,9</sub>-Py, DTX@dPG<sub>8,6</sub>-SS-PCL<sub>7,9</sub>-Py, and dPG<sub>7,8</sub>-SS-PCL<sub>7,8</sub>-Et were found between 81–130 nm according to DLS. With increased  $\pi$ -electron domains on the polymer, the PDI detected by DLS starts to decrease from 0.17 for dPG<sub>7,8</sub>-SS-PCL<sub>7,9</sub>-Et to 0.08 for DTX@dPG<sub>8,6</sub>-SS-POxPPh<sub>7,9</sub>-Py. The surface charge of all micelles was measured and detected from  $-44$  to  $-33$  mV. For a complete characterization of all colloids and formulations, see Table 1.

The first border of a self-assembled system is in the extreme dilution upon injection; thus, the stability of the micelles under



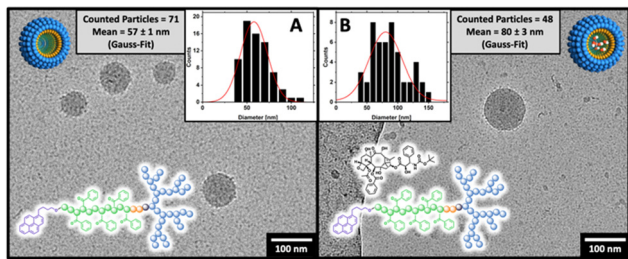


Fig. 5 cryo-TEM images of (A) empty and (B) docetaxel-loaded dPGS<sub>8,6</sub>-SS-POxPPh<sub>7,9</sub>-Py micelles in PBS at 1 mg mL<sup>-1</sup> showing the spherical character of the aggregates. Gauss-analysis of multiple TEM measurements determined the particle size. The detected values show DLS-consistent sizes of 57 and 80 nm for empty/DTX-loaded micelles, respectively. (Scale bar: 100 nm.)

physiological conditions (150 mM NaCl, pH 7.4, 37 °C) was systematically studied. To do so, a DLS-supported dilution experiment was conducted to monitor the evolution of the light scattering intensity, steadily decreasing the concentration of the amphiphiles in the solution. As the light scattering intensity is proportional to the concentration of a scattering species, it allows for the efficient determination of the CMC (Fig. 6(A)). Compared to other techniques, such as fluorescence, DLS allows the label-free determination of the CMC.<sup>32</sup> Since encapsulation of hydrophobic cargos has been shown to alter the stability of polymeric micelles,<sup>33</sup> fluorescence spectroscopy was not applicable in this study since this effect would interfere with the drug-loading stability studies by DTX. The analysis of the CMC of the block copolymer library revealed the trend of significantly decreased CMCs with increased  $\pi$ -electron-density of the systems following the order dPGS<sub>7,8</sub>-SS-PCL<sub>7,9</sub>-Et > dPGS<sub>8,6</sub>-SS-PCL<sub>7,9</sub>-Py > dPGS<sub>8,6</sub>-SS-POxPPh<sub>7,9</sub>-Py. For dPGS<sub>7,8</sub>-SS-PCL<sub>7,9</sub>-Et, the highest CMC of 2.1 mg L<sup>-1</sup> (133 nM) was found. For dPGS<sub>8,6</sub>-SS-PCL<sub>7,9</sub>-Py, the implementation of the pyrene moiety decreased the CMC by 2-fold to 0.9 mg L<sup>-1</sup> (54 nM). As expected, the dPGS<sub>8,6</sub>-SS-POxPPh<sub>7,9</sub>-Py, with a high  $\pi$ -electron density, shows a CMC of 0.7 mg L<sup>-1</sup> (42 nM), which even can be further decreased upon loading with Docetaxel to 0.3 mg L<sup>-1</sup> (18 nM) (Fig. 6(B)). Thus, also the drug contributes  $\pi$ -electron to the micellar core improving the CMC (see the structure of Docetaxel). The drug-loading of dPGS<sub>8,6</sub>-SS-PCL<sub>7,9</sub>-Py showed no influence on the CMC, most likely due to the insufficient loading capacity of only 5 wt% compared to 13 wt%

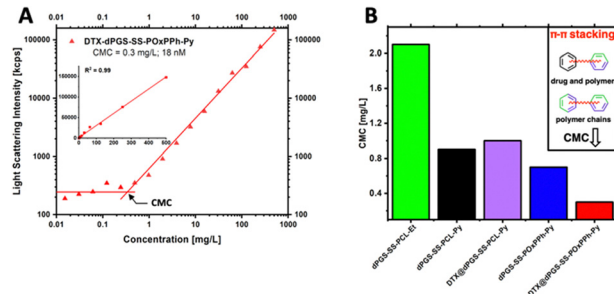


Fig. 6 (A) CMC determination of DTX-loaded dPGS<sub>8,6</sub>-SS-POxPPh<sub>7,9</sub>-Py micelles in PBS at 37 °C by a light scattering experiment with different concentrations ranging from 500 mg L<sup>-1</sup> to 5  $\mu$ g L<sup>-1</sup> (inset: linear dependency of the count rate and concentration;  $R^2 = 0.99$ ); light scattering intensity below CMC was horizontalized according to ISLS  $\sim C_{\text{polymer}}$ . (B) Influence of  $\pi$ -stabilization on dPGS-SS-PCL-Et, empty/DTX-loaded dPGS-SS-PCL-Py, and empty/DTX-loaded dPGS<sub>8,6</sub>-SS-POxPPh<sub>7,9</sub>-Py micelles showing significantly decreased CMC values for  $\pi$ -electron-rich systems.

for dPGS<sub>8,6</sub>-SS-POxPPh<sub>7,9</sub>-Py. The CMC determination of the other amphiphiles is shown in more detail in the ESI† (Fig. S34).

As self-assembled systems are dynamic systems in an equilibrium between their monomeric and polymeric nature, it is essential to correlate the CMC to the minimum required dosage. For example, in Genexol-PM, a clinically approved nanomedicine based on PEG-*b*-PLA micelles, the formulation of one dosage contains 30 mg of taxane.<sup>34</sup> For the DTX@dPGS<sub>8,6</sub>-SS-POxPPh<sub>7,9</sub>-Py systems, the DLC is determined as 13 wt%; thus, a theoretical dose of 230 mg of the polymeric material would be needed for a human application. Considering the total blood volume of an adult as 5 L, the final concentration of the amphiphile is 46 mg L<sup>-1</sup>, which still exceeds the CMC by 150-fold (CMC: 0.3 mg L<sup>-1</sup>). To our knowledge, the lowest CMC described yet is found at 2.7 nM achieved by so-called “sharp polarity contrast” micelles,<sup>35,36</sup> however, typical polymer systems based on PEG-amphiphiles show CMCs in the 1000 nM range.<sup>37</sup> All polymers included in this study, but especially DTX@dPGS<sub>8,6</sub>-SS-POxPPh<sub>7,9</sub>-Py, undercut this value underlining their high stability. In summary, we showed that implementing  $\pi$ -electrons onto a polymeric structure beneficially influences micellar stability.

### 2.3 Drug-loading with docetaxel: influence of $\pi$ -electron density

By HPLC, the drug-loading capacity (DLC in wt%) and drug-loading efficiency (DLE in %) of Docetaxel in dPGS<sub>8,6</sub>-SS-PCL<sub>7,9</sub>-

Table 1 Characteristic of empty/DTX-loaded dPGS-SS-POxPPh-Py, dPGS-SS-PCL-Py, and dPGS-SS-PCL-Et block copolymers and their respective micelles in terms of molecular weight, drug loading efficiency, drug loading capacity, size, PDI, CMC, and surface potential

Polymer	Molecular weight $M_n$ (kDa)		Drug loading docetaxel		Size (nm) <sup>c</sup>	PDI <sup>c</sup>	CMC at 37 °C in PBS		
	Theo.	Calc. <sup>a</sup>	DLE <sup>b</sup> (%)	DLC <sup>b</sup> (wt%)			mg L <sup>-1c</sup>	nM	$\zeta^d$ (mV)
dPGS <sub>7,8</sub> -SS-PCL <sub>7,8</sub> -Et	16.0	15.6	n.s.	n.s.	81.2 ± 1.1	0.17	2.1	133	-44
dPGS <sub>8,6</sub> -SS-PCL <sub>7,9</sub> -Py	16.0	16.5	—	—	111.9 ± 1.8	0.15	0.9	54	-34
DTX@dPGS <sub>8,6</sub> -SS-PCL <sub>7,9</sub> -Py	16.0	16.5	26	5	129.4 ± 18.8	0.13	1.0	55	—
dPGS <sub>8,6</sub> -SS-POxPPh <sub>7,9</sub> -Py	16.0	16.5	—	—	93.7 ± 1.4	0.09	0.7	42	-39
DTX@dPGS <sub>8,6</sub> -SS-POxPPh <sub>7,9</sub> -Py	16.0	16.5	62	13	102.4 ± 7.6	0.08	0.3	18	—

<sup>a</sup> Calculated  $M_n^{\text{NMR,hydrophobic segment}} + (2 \times M_n^{\text{NMR,hydrophilic segment}})$ . <sup>b</sup> Docetaxel-loading, determined by HPLC. <sup>c</sup> Determined by light scattering in PBS at 37 °C. <sup>d</sup> Measured in 10 mM PB buffer at 37 °C at pH 7.4; n.s. = not significant; no detectable drug amount in the formulation.



Py and dPGS<sub>8,6</sub>-SS-POxPPh<sub>7,9</sub>-Py micelles were determined. For micelles with a decent number of  $\pi$ -electrons in their core (dPGS<sub>8,6</sub>-SS-PCL<sub>7,9</sub>-Py), a low DLC of only 5 wt% (DLE: 26%) was detected. For dPGS<sub>7,8</sub>-SS-PCL<sub>7,9</sub>-Et, no significant encapsulation could be detected. The increase of the  $\pi$ -electron density in dPGS<sub>8,6</sub>-SS-POxPPh<sub>7,9</sub>-Py raises the DLC to 13 wt% and 62% loading efficiency (Table 1). This is due to the greater possibility of the drug Docetaxel interacting with the phenyl rings of the POxPPh<sub>7,9</sub> segment, as shown in poly( $\beta$ -benzyl malate)-*b*-polyethylene glycol systems interacting with Doxorubicin by Qiao *et al.*<sup>38</sup>

#### 2.4 $\pi$ - $\pi$ stacking in the micelle core: UV-VIS, cross-polarization solid-state <sup>13</sup>C NMR, and fluorescence spectroscopy

To classify  $\pi$ - $\pi$  interactions, the structural behavior of the aromatic motifs was studied by UV-VIS and fluorescence spectroscopy (Fig. 7). The pyrene moiety on dPGS<sub>8,6</sub>-SS-POxPPh<sub>7,9</sub>-Py and dPGS<sub>8,6</sub>-SS-PCL<sub>7,9</sub>-Py chain ends allows the detection of  $\pi$ - $\pi$  interaction. Due to the greater electron delocalization, the UV bands of dPGS<sub>8,6</sub>-SS-POxPPh<sub>7,9</sub>-Py and dPGS<sub>8,6</sub>-SS-PCL<sub>7,9</sub>-Py

shifted to longer wavelengths (red-shift) compared to free pyrene butanol in PBS, which is also known as bathochromic effect (Fig. 7(A)).<sup>39</sup> Further, pyrene displays the unique ability, besides its known fluorescence emission peaks (375–405 nm, monomer), to show an additional band at *ca.* 460 nm if a so-called excimer is formed.<sup>40</sup> This phenomenon was used to obtain deeper insights into the structural orientation of the micellar core. Fig. 7(B) shows the fluorescence spectra of pyrene butanol, dPGS<sub>8,6</sub>-SS-POxPPh<sub>7,9</sub>-Py, and dPGS<sub>8,6</sub>-SS-PCL<sub>7,9</sub>-Py in PBS ( $\lambda_{\text{ex}}$  350 nm). For pyrene butanol, a strong, and for dPGS<sub>8,6</sub>-SS-PCL<sub>7,9</sub>-Py, a moderate excimer emission at 480 nm was observed. Thus, the excimer emission is called “turn ON”. In contrast, for dPGS<sub>8,6</sub>-SS-POxPPh<sub>7,9</sub>-Py, no significant band was detectable. The high  $\pi$ -electron density of dPGS<sub>8,6</sub>-SS-POxPPh<sub>7,9</sub>-Py forms a more randomly distributed micellar core by stacking the aromatic motifs. In dPGS<sub>8,6</sub>-SS-PCL<sub>7,9</sub>-Py, the  $\pi$ - $\pi$  interaction is limited to the pyrene motifs only (Fig. 7(C)), whereas, in dPGS<sub>8,6</sub>-SS-POxPPh<sub>7,9</sub>-Py, the phenyl rings of the hydrophobic block OxPPh can undergo  $\pi$ - $\pi$  interactions with the pyrene moiety quenching the excimer emission bringing the system in the “turn OFF” mode (Fig. 7(D)).

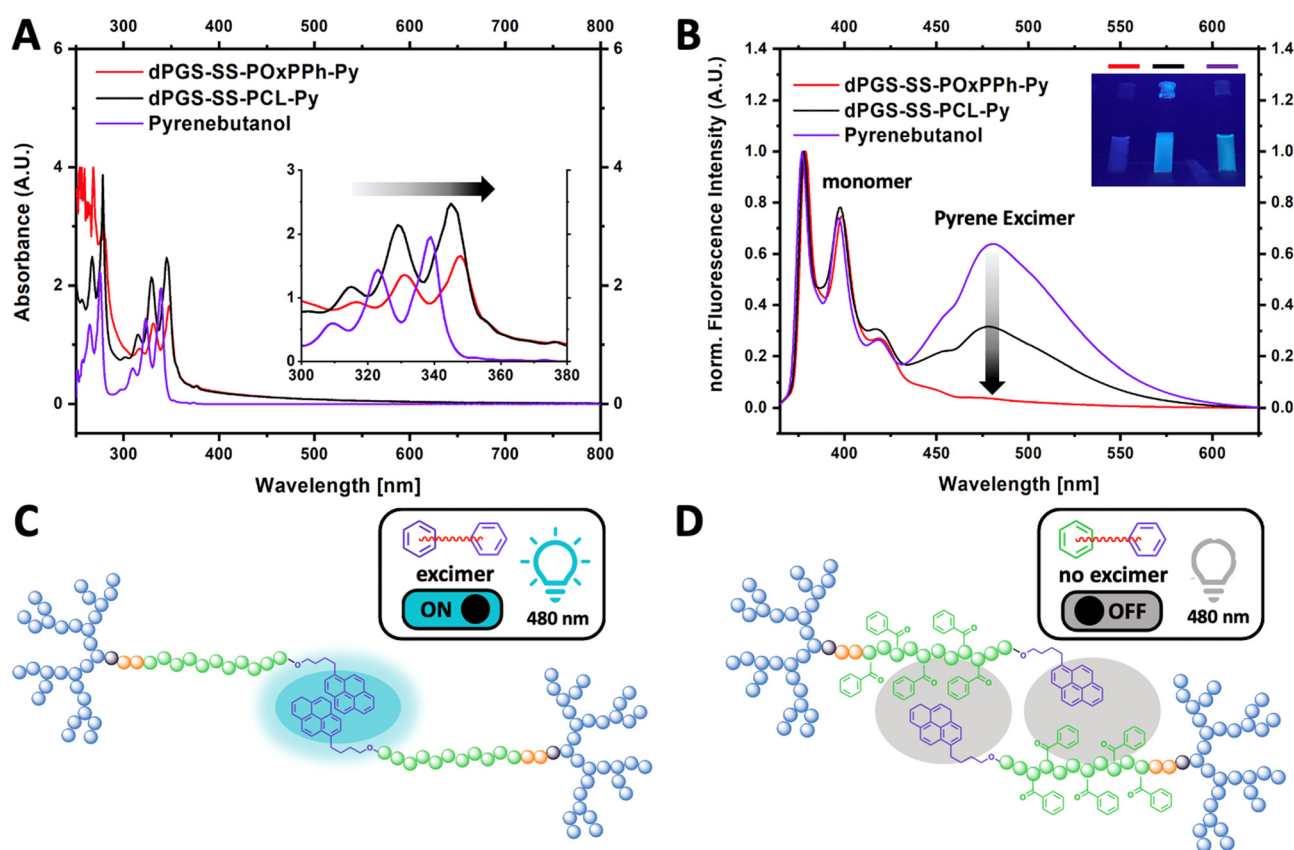


Fig. 7 (A) Absorbance spectra measured in PBS at 37 °C of dPGS<sub>8,6</sub>-SS-POxPPh<sub>7,9</sub>-Py (red), dPGS-SS-PCL-Py (black), and pyrene butanol (purple), inset showing red-shift of micellar formulations (B) normalized fluorescence spectra ( $\lambda_{\text{ex}}$  350 nm) in PBS at 37 °C of dPGS<sub>8,6</sub>-SS-POxPPh<sub>7,9</sub>-Py, dPGS<sub>8,6</sub>-SS-PCL<sub>7,9</sub>-Py, and pyrene butanol showing strong excimer formation for pyrene butanol, weak excimer for dPGS-SS-PCL-Py, and no significant excimer presence for dPGS<sub>8,6</sub>-SS-POxPPh<sub>7,9</sub>-Py (inset: dPGS<sub>8,6</sub>-SS-POxPPh<sub>7,9</sub>-Py, dPGS<sub>8,6</sub>-SS-PCL<sub>7,9</sub>-Py, and pyrene butanol under UV-light irradiation at 366 nm) (C) mechanistic illustration of the  $\pi$ - $\pi$  interaction in dPGS<sub>8,6</sub>-SS-PCL<sub>7,9</sub>-Py micelles in an aqueous solution; in dPGS<sub>8,6</sub>-SS-PCL<sub>7,9</sub>-Py, the only interaction is between the pyrene moieties showing strong excimer formation (cyan circle); (D) in dPGS<sub>8,6</sub>-SS-POxPPh<sub>7,9</sub>-Py, the phenyl rings of the side chain interact with the pyrene suppressing excimer formation (grey circle) showing no band in the fluorescence at 480 nm with no emitted light (see inset in B).



As the light scattering experiments revealed a synergistic effect of DTX loading in dPGS<sub>8,6</sub>-SS-POxPPH<sub>7,9</sub>-Py on their CMC (Fig. 6(B)), the interaction of the cargo with the polymer was studied by solid-state NMR experiments. Docetaxel's low UV-VIS activity, no fluorescence, and its disappearance in solution NMR, if incorporated in micelles, exclude these techniques to check possible  $\pi$ - $\pi$  interactions between the cargo and the polymeric material. In recent years, the use of cross-polarization solid-state <sup>13</sup>C NMR has shown great potential to gain structural insights into a drug-loaded micelle core.<sup>41–43</sup> For that, three formulations with (i) only drug; (ii) only polymer; and (iii) drug in micelles were prepared in aqueous solutions and subsequently freeze-dried. In the cross-polarization solid-state <sup>13</sup>C NMR spectrum, the signals corresponding to the aromatic carbons of DTX between 120–145 ppm were found to shift slightly in the formulation compared to free DTX, exhibiting interactions between the cargo and the polymer (see ESI,† (Fig. S35 and S36)). However, as Docetaxel is a rather complex structure, this analysis remains challenging, only enabling little insights into the drug-loaded micelle core.

## 2.5 *In vitro* stability: serum–protein interaction and reductive/enzymatic degradation

After a potential administration into the bloodstream, micelles would interact with the blood's non-cellular components, leading to a biomolecular surface layer. This event is suspected as a cause of injected particles' insufficient *in vivo* stability and to lower their targeting ability.<sup>44–46</sup> In order to study the biomolecular layer and

*in vitro* stability, the micelles were incubated with Human Serum Albumin (HSA), the most abundant serum protein in humans. By DLS, the size evolution of DTX@dPGS<sub>8,6</sub>-SS-POxPPH<sub>7,9</sub>-Py micelles was monitored in 10 mg mL<sup>-1</sup> HSA in PBS at 37 °C (Fig. 8(A), red dots) over four days. To keep the viscosity of the solution low, the protein concentration was reduced from physiological concentrations of 45 mg mL<sup>-1</sup> to 10 mg mL<sup>-1</sup> to avoid distorting effects on the Brownian Motion. DTX@dPGS<sub>8,6</sub>-SS-POxPPH<sub>7,9</sub>-Py micelles without any additives in PBS at 4 °C (Fig. 8, purple squares) or 37 °C (Fig. 8, black squares) served as control (initial size for all samples 102 nm). The micelles were found to absorb no protein on their surface as the size was in line with the controls, with no significant size change over four days for all three samples ending up at 109 nm for the HSA samples, controls at 37 °C at 104 nm and 4 °C at 106 nm, respectively. Further, the light scattering intensity of serum-incubated micelles remained constant over four days, indicating stable particles in the presence of serum proteins (see ESI,† Fig. S32). These data are consistent with Isothermal titration calorimetry (ITC) experiments showing that dPGS and HSA are not interacting under physiological conditions (150 mM NaCl, 37 °C).<sup>47</sup> This observation is critical as adsorbed material would cover the dPGS units decreasing their targeting ability.

In tumor cells, the GSH level is increased to 10 mM with only micromolar contents extracellular.<sup>48</sup> So, the selective cleavage of the reductive-sensitive disulfide bridge was investigated in the presence of 10 mM GSH at 37 °C for four days (Fig. 8(B), blue triangles). Also, given the endocytosis pathway upon

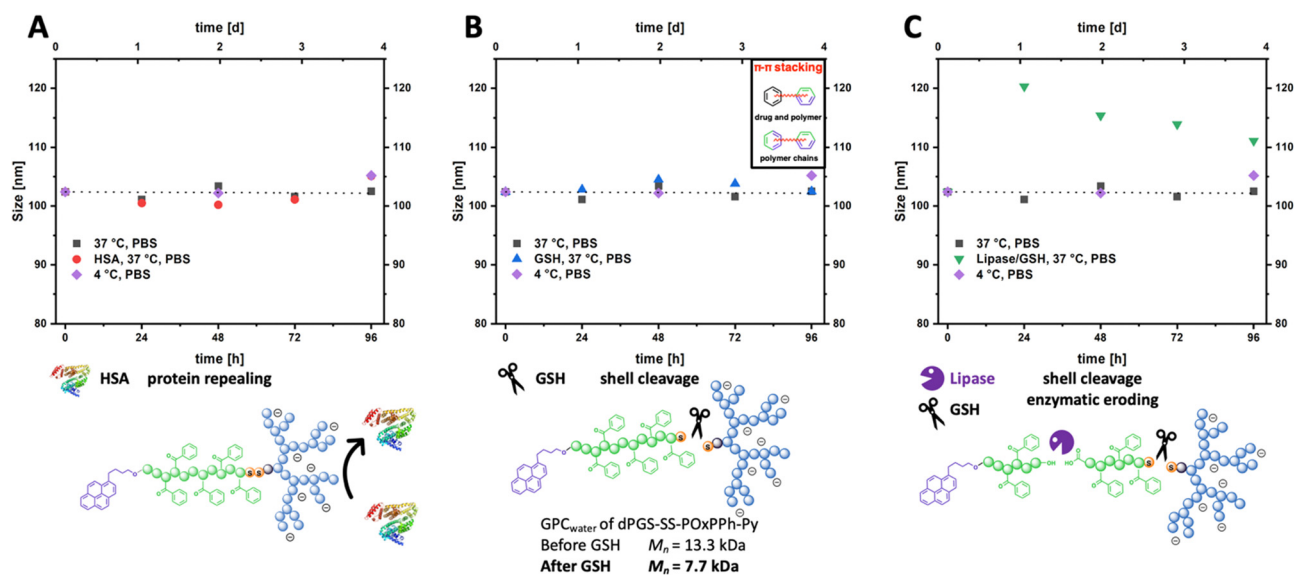


**Fig. 8** Time-dependent DLS measurements on the evolution of the size of DTX@dPGS<sub>8,6</sub>-SS-POxPPH<sub>7,9</sub>-Py in different conditions in PBS at 37 °C, pH 7.4 (black) and 4 °C, pH 7.4 (purple) as control; (A) in the presence of HSA (red); (B) GSH, pH 5.0 (blue); (C) lipase/GSH, pH 5.0 (green); for four days, revealing stable particles without additives and in the presence of serum proteins as indicated by constant sizes. GSH incubation showed no significant changes in the size and light scattering intensity, indicating the stabilizing effect of  $\pi$ - $\pi$  stacking on the aggregates. By GPC measurements, the cleavage of the disulfide by tracking the dPGS<sub>8,6</sub>-unit was confirmed. The hydrophobic POxPPH<sub>7,9</sub>-Py segment is retained on the column due to its limited water solubility. Incubation with additional lipase next to GSH caused an initial increase in the size attributed to a reordering of the degraded hydrophobic polyester polymer mediated by  $\pi$ - $\pi$  stacking. Below are schematic illustrations of the protein-reaping and degradation mechanism of dPGS<sub>8,6</sub>-SS-POxPPH<sub>7,9</sub>-Py by lipase and GSH. The lipase degrades the ester moieties in the hydrophobic segment, and the GSH cleaves the disulfide bridge, destroying the block copolymer's amphiphilic nature.



intracellular uptake, the micelles would be exposed to acidic conditions in the endosome and later lysosome; thus, pH was adjusted to acidic conditions. By DLS, no size change compared to the controls was detectable, ending at 103 nm. This can be attributed to the inter- and intramolecular  $\pi$ - $\pi$  stacking of the POxPPH-Py segments leading to intact colloids in solution. However, by GPC experiments in water, the cleavage of the disulfide bridge was proven by detecting the cleaved dPGS<sub>8.6</sub>-S-R unit (GPC:  $M_n = 7.7$  kDa, Fig. 8(B)). To break down these polymer aggregates, the enzymatic degradation of the ester-backbone was triggered by a surface-immobilized lipase (Novozyme 435) (Fig. 8(C), green triangle).<sup>49</sup> The use of immobilized lipases does not affect the light scattering intensity as it would by adding non-immobilized enzymes into the solution. In the presence of additional enzymes next to GSH, the aggregates start to swell to 120 nm in the initial first 24 h with a subsequent decrease in size after four days at 112 nm. In line, the light scattering intensity of lipase-treated micelles

constantly decreases over time, indicating the disassembly of the micelles. For a detailed discussion about the evolution of the light scattering intensity, see ESI† (Fig. S32). Based on these results, the micelles exhibited no interaction with serum proteins nor disassembly in their presence. They also revealed a prolonged degradation profile by selectively triggering the breaking points (ester, disulfide) in the amphiphilic polymer structure of dPGS<sub>8.6</sub>-SS-POxPPH<sub>7.9</sub>-Py.

## 2.6 *In vitro* cell viability, *in vitro* anti-cancer cell performance, and *in vitro* fate of dPGS-SS-micelles

As given by the mode of action, the uptake of docetaxel into the cell is essential for unleashing its anti-mitotic activity.<sup>50</sup> To visualize the fate of dPGS<sub>8.6</sub>-SS-POxPPH<sub>7.9</sub>-Py micelles *in vitro*, a fluorescence dye fluorescein isothiocyanate (FITC), was covalently attached to the hydrophilic shell leading to FITC-labelled dPGS<sub>8.6</sub>-SS-POxPPH<sub>7.9</sub>-Py. For the synthesis and characterization, see ESI.† By confocal laser scanning microscopy

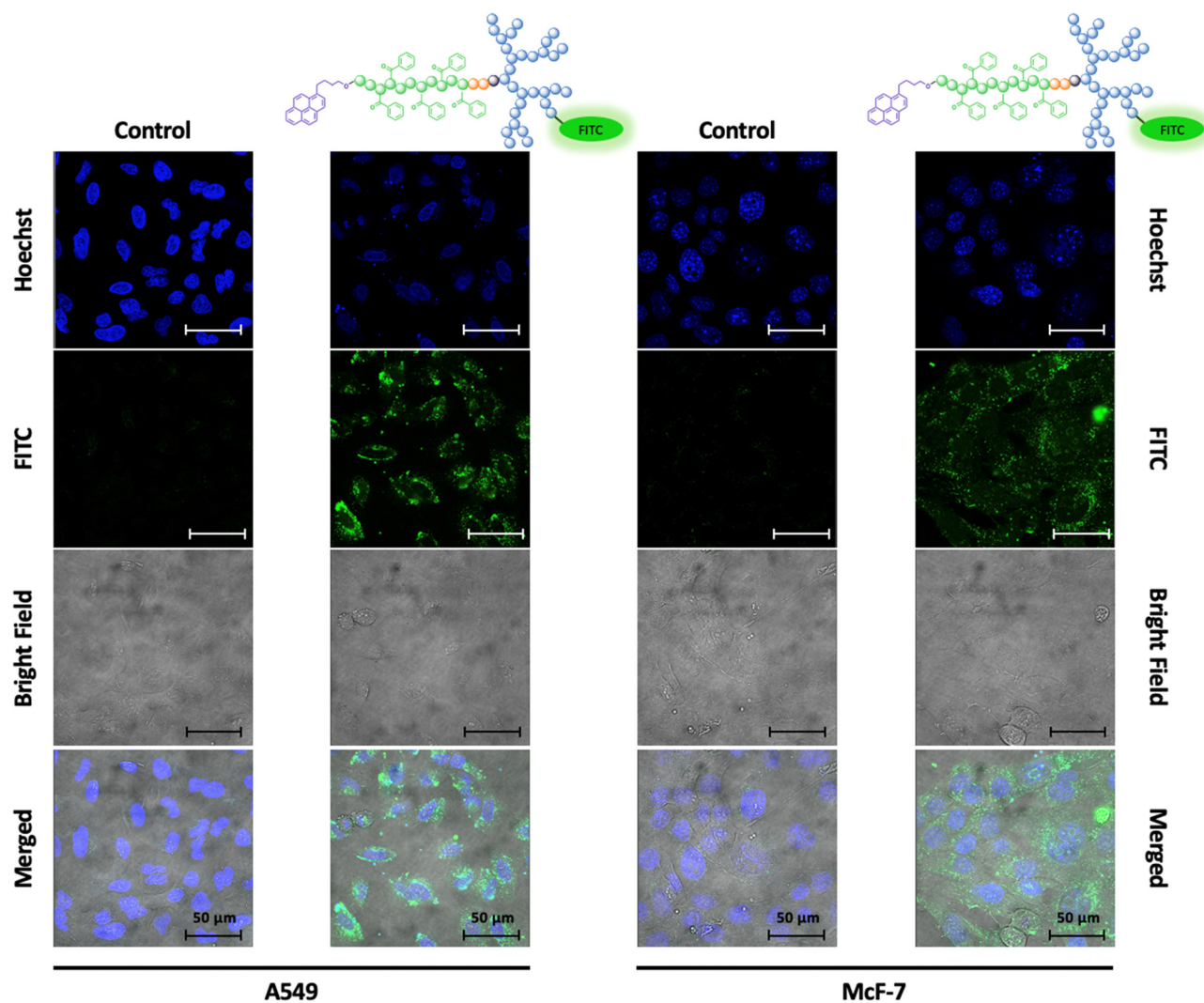


Fig. 9 Confocal laser scanning microscopy images of A549 (left) and MCF-7 (right) tumor-derived cells incubated with and without FITC-dPGS<sub>8.6</sub>-SS-POxPPH<sub>7.9</sub>-Py micelles (incubation time 24 h); the polymeric material is successfully inserted into the cell as shown by the strong fluorescence signal of the covalently attached dye; scale bar: 50  $\mu$ m, blue: Hoechst (Nuclei), green: FITC (fluorescent dye covalently attached to polymer).



(CLSM), the cellular uptake of FITC-dPGS<sub>8,6</sub>-SS-POxPPh<sub>7,9</sub>-Py was monitored after 24 h incubation time on A549 (lung cancer) and McF-7 (breast cancer) cells (Fig. 9), depicting the successful insertion of the polymeric material into the cells.

Knowing the capability of the micelle's cell insertion, the micelle's *in vitro* therapeutical performance was further studied. One of the early attempts to test drug delivery systems' effectiveness starts with evaluating their cytotoxicity. Fig. 10 displays the *in vitro* performance of empty and DTX-loaded micelles. By CCK-8 assay, the *in vitro* cell compatibility of dPGS<sub>7,8</sub>-SS-PCL<sub>7,8</sub>-Et, dPGS<sub>8,6</sub>-SS-PCL<sub>7,9</sub>-Py, and dPGS<sub>8,6</sub>-SS-POxPPh<sub>7,9</sub>-Py was tested on McF7, HeLa (cervical cancer), and A549 tumor-derived cell lines after 48 h (Fig. 10(A)–(C)). No polymer showed significant toxicity in the range of its actual CMC. Even at elevated concentrations up to 100-fold higher than the CMC, the polymers showed no influence on the cell's viability. For dPGS<sub>8,6</sub>-SS-POxPPh<sub>7,9</sub>-Py, the cell viability falls below 50% at concentrations above 300 mg L<sup>-1</sup> as tested on HeLa cells (46% cell viability, two days *in vitro*).

As the polymer dPGS<sub>8,6</sub>-SS-POxPPh<sub>7,9</sub>-Py was well-tolerated by HeLa, A549, and McF-7, the anti-tumor performance of free

DTX and DTX-loaded dPGS<sub>8,6</sub>-SS-POxPPh<sub>7,9</sub>-Py micelles on these cell lines was investigated. Fig. 10(D) and (E) shows the dose-response curve of DTX@dPGS<sub>8,6</sub>-SS-POxPPh<sub>7,9</sub>-Py and free DTX after two days *in vitro*. After two days *in vitro*, the IC<sub>50</sub> was calculated, and for free DTX, it exhibited values of 40 nM on HeLa, 43 nM on A549, and 94 nM on McF-7 cells. When incorporated in dPGS<sub>8,6</sub>-SS-POxPPh<sub>7,9</sub>-Py micelles, the DTX showed slightly increased IC<sub>50</sub> values of 69 nM on HeLa, 68 nM on A549, and 141 nM on McF-7 (Fig. 10(F)). The phenomenon of minimal increased IC<sub>50</sub> values of a polymer-supported treatment of taxane-based drugs is already known in the literature.<sup>51,52</sup> It might be attributed to the extremely high stability of the system showing slow dissociation but still proving the drug release (see Fig. 7). The  $\pi$ -electron stabilized micelles can potentially overcome common issues such as toxin overload due to their slow degradation profile while remaining highly potent *in vitro*. Further, besides the already low IC<sub>50</sub> of free DTX, its extreme hydrophobicity and off-side toxicity challenge its clinical administration; thus, drug delivery systems such as dPGS<sub>8,6</sub>-SS-POxPPh<sub>7,9</sub>-Py are essential for the successful medication of cancer patients with this class of drugs.

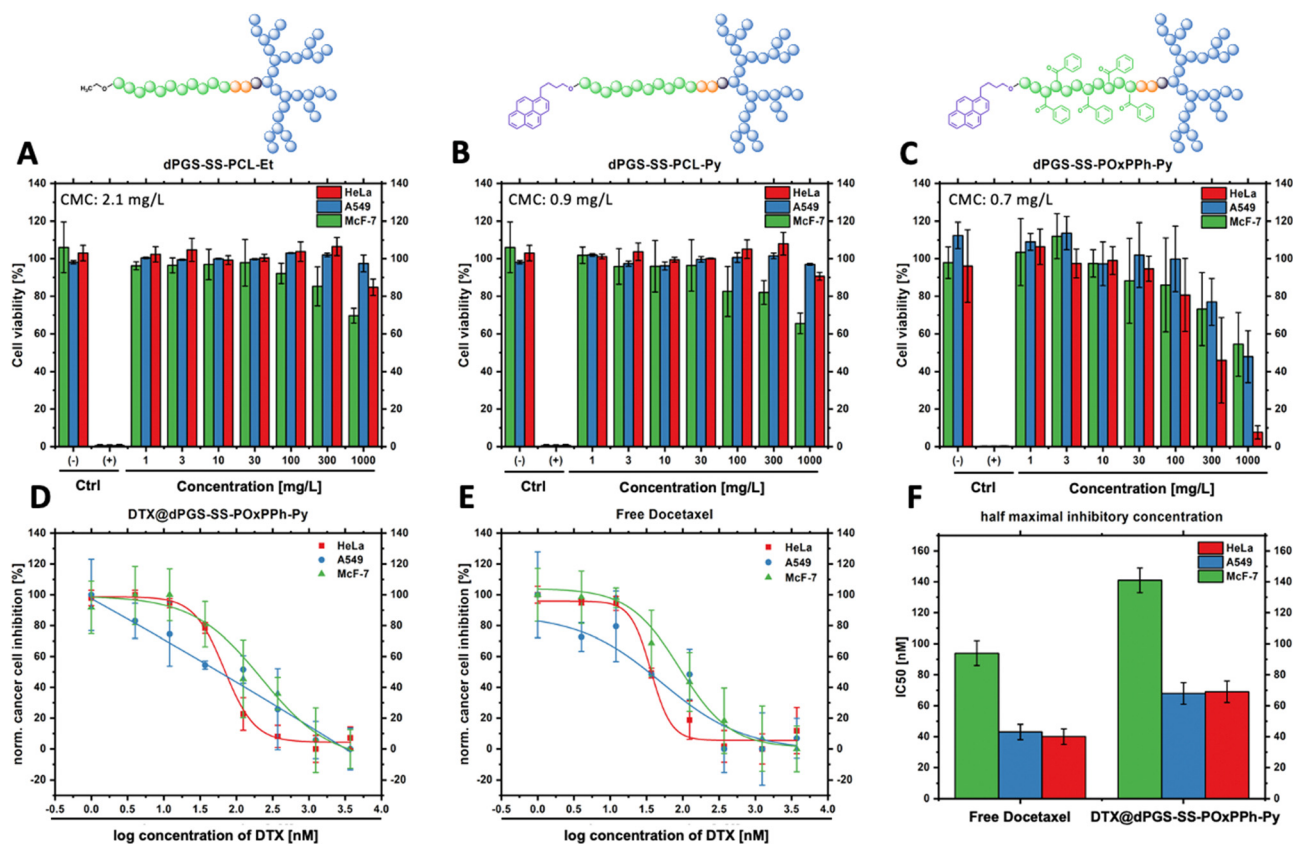


Fig. 10 *In vitro* cell compatibility studies on HeLa, A549, and McF-7 tumor-derived cell lines after 48 h incubation ( $n = 3$ , CCK-8, (-) PBS control, (+) SDS control) of (A) empty dPGS<sub>7,8</sub>-SS-PCL<sub>7,8</sub>-Et (A549 performed  $n = 2$ ) (B) empty dPGS<sub>8,6</sub>-SS-PCL<sub>7,9</sub>-Py (A549 performed  $n = 2$ ) (C) empty dPGS<sub>8,6</sub>-SS-POxPPh<sub>7,9</sub>-Py no polymer shows significant toxicity at a concentration of 100-fold higher than that of the CMC; *in vitro* dose-response curves of (D) DTX@dPGS<sub>8,6</sub>-SS-POxPPh<sub>7,9</sub>-Py (E) free docetaxel on HeLa, A549, and McF-7 cells after 48 h incubation; (F) anti-tumor performance of free Docetaxel and Docetaxel-loaded dPGS<sub>8,6</sub>-SS-POxPPh<sub>7,9</sub>-Py micelles, showing similar cancer cell inhibition (IC<sub>50</sub>) for the polymer-supported treatment and the free drug *in vitro*.



### 3. Conclusions

This work demonstrates the detailed characterization and substantial performance of  $\pi$ -electron stabilized dendritic polyglycerolsulfate amphiphilic block copolymers. The micelles show (i) very high stability in terms of extraordinarily low CMCs in the low nanomolar regime; (ii) no *in vitro* toxicity of the polymeric material; (iii) successful cell insertion shown by FITC-labelled micelles; and (iv) high efficacy in inhibiting cancer cell growth *in vitro* on several tumor-derived cell lines. Further, several spectroscopy techniques, such as UV-VIS, fluorescence, and cross-polarization solid-state  $^{13}\text{C}$  NMR, proved the presence of  $\pi$ - $\pi$  interactions in the micellar core between the polymer chains and drug molecules, majorly contributing to the high stability of the system. Thus, drug delivery micelles based on dendritic polyglycerolsulfate-cystamine-*block*-poly(4-benzoyl-1,4-oxazepan-7-one)-pyrene (dPGS-SS-POxPPh-Py) may be new alternatives for chemotherapies and will be considered for *in vivo* investigations.

### Author contributions

The manuscript was written entirely by D. B. All authors have approved the final version of the manuscript. D. B. synthesized and characterized the polymeric materials with assistance from J. H. P. The cryo-EM measurements were conducted by Dr M. D. and Dr K. L. All *in vitro* cell tests were done by E. Q. and Dr K. A. Dr M. S., Dr M. B., and Dr R. H. conceived and directed the project.

### Conflicts of interest

The authors declare no competing financial interests.

### Acknowledgements

We thank Cathleen Hudziak for conducting the GPC measurements. Marleen Selent gratefully contributed to the HPLC analysis. Eleonore Christmann-Oesterreich is acknowledged for performing the elemental analysis. The authors appreciate the access to the Core Facility BioSupraMol research facilities. Dr Andreas Schäfer significantly contributed to the solid-state NMR studies. This work was funded by the Deutsche Forschungsgemeinschaft (DFG, German Research Foundation) - 434130070 within the GRK 2662.

### References

- 1 R. L. Siegel, K. D. Miller, H. E. Fuchs and A. Jemal, *Cancer J. Clin.*, 2022, **72**, 7–33.
- 2 U. Anand, A. Dey, A. K. S. Chandel, R. Sanyal, A. Mishra, D. K. Pandey, V. De Falco, A. Upadhyay, R. Kandimalla, A. Chaudhary, J. K. Dhanjal, S. Dewanjee, J. Vallamkondu and J. M. Pérez de la Lastra, *Genes Dis.*, 2022, DOI: [10.1016/j.gendis.2022.02.007](https://doi.org/10.1016/j.gendis.2022.02.007).

- 3 L. Zhong, Y. Li, L. Xiong, W. Wang, M. Wu, T. Yuan, W. Yang, C. Tian, Z. Miao, T. Wang and S. Yang, *Signal Transduction Targeted Ther.*, 2021, **6**, 201.
- 4 H. Cabral, K. Miyata, K. Osada and K. Kataoka, *Chem. Rev.*, 2018, **118**, 6844–6892.
- 5 A. Varela-Moreira, Y. Shi, M. H. A. M. Fens, T. Lammers, W. E. Hennink and R. M. Schiffelers, *Mater. Chem. Front.*, 2017, **1**, 1485–1501.
- 6 J. Shi, P. W. Kantoff, R. Wooster and O. C. Farokhzad, *Nat. Rev. Cancer*, 2017, **17**, 20–37.
- 7 S. Zanganeh, R. Spitler, M. Erfanzadeh, A. M. Alkilany and M. Mahmoudi, *Int. J. Biochem. Cell Biol.*, 2016, **75**, 143–147.
- 8 M. Yang, E. Wu, W. Tang, J. Qian and C. Zhan, *J. Mater. Chem. B*, 2021, **9**, 6713–6727.
- 9 X. Sun, G. Wang, H. Zhang, S. Hu, X. Liu, J. Tang and Y. Shen, *ACS Nano*, 2018, **12**, 6179–6192.
- 10 J. Lu, S. C. Owen and M. S. Shoichet, *Macromolecules*, 2011, **44**, 6002–6008.
- 11 V. Mirshafiee, M. Mahmoudi, K. Lou, J. Cheng and M. L. Kraft, *Chem. Commun.*, 2013, **49**, 2557–2559.
- 12 K. A. Whitehead, J. Matthews, P. H. Chang, F. Niroui, J. R. Dorkin, M. Severgnini and D. G. Anderson, *ACS Nano*, 2012, **6**, 6922–6929.
- 13 M. Mahmoudi, *Nat. Commun.*, 2022, **13**, 49.
- 14 Y. Zhong, M. Dimde, D. Stöbener, F. Meng, C. Deng, Z. Zhong and R. Haag, *ACS Appl. Mater. Interfaces*, 2016, **8**, 27530–27538.
- 15 D. Braatz, M. Dimde, G. Ma, Y. Zhong, M. Tully, C. Grötzinger, Y. Zhang, A. Mavroskoufis, M. Schirner, Z. Zhong, M. Ballauff and R. Haag, *Biomacromolecules*, 2021, **22**, 2625–2640.
- 16 D. Braatz, M. Cherri, M. Tully, M. Dimde, G. Ma, E. Mohammadifar, F. Reisbeck, V. Ahmadi, M. Schirner and R. Haag, *Angew. Chem., Int. Ed.*, 2022, **134**, e202203942.
- 17 D. Sun, S. Zhou and W. Gao, *ACS Nano*, 2020, **14**, 12281–12290.
- 18 J. M. Metselaar and T. Lammers, *Drug Delivery Transl. Res.*, 2020, **10**, 721–725.
- 19 H. He, L. Liu, E. E. Morin, M. Liu and A. Schwendeman, *Acc. Chem. Res.*, 2019, **52**, 2445–2461.
- 20 W.-R. Zhuang, Y. Wang, P.-F. Cui, L. Xing, J. Lee, D. Kim, H.-L. Jiang and Y.-K. Oh, *J. Controlled Release*, 2019, **294**, 311–326.
- 21 Y. Masayuki, M. Mizue, Y. Noriko, O. Teruo, S. Yasuhisa, K. Kazunori and I. Shohei, *J. Controlled Release*, 1990, **11**, 269–278.
- 22 T. Hamaguchi, Y. Matsumura, M. Suzuki, K. Shimizu, R. Goda, I. Nakamura, I. Nakatomi, M. Yokoyama, K. Kataoka and T. Kakizoe, *Br. J. Cancer*, 2005, **92**, 1240–1246.
- 23 Y. Shi, M. J. van Steenberg, E. A. Teunissen, L. S. Novo, S. Gradmann, M. Baldus, C. F. van Nostrum and W. E. Hennink, *Biomacromolecules*, 2013, **14**, 1826–1837.
- 24 Y. Shi, R. van der Meel, B. Theek, E. Oude Blenke, E. H. E. Pieters, M. H. A. M. Fens, J. Ehling, R. M. Schiffelers, G. Storm, C. F. van Nostrum, T. Lammers and W. E. Hennink, *ACS Nano*, 2015, **9**, 3740–3752.



- 25 C. Liang, X. Bai, C. Qi, Q. Sun, X. Han, T. Lan, H. Zhang, X. Zheng, R. Liang, J. Jiao, Z. Zheng, J. Fang, P. Lei, Y. Wang, D. Möckel, J. M. Metselaar, G. Storm, W. E. Hennink, F. Kiessling, H. Wei, T. Lammers, Y. Shi and B. Wei, *Biomaterials*, 2021, **266**, 120432.
- 26 Z. Tu, Y. Zhong, H. Hu, D. Shao, R. Haag, M. Schirner, J. Lee, B. Sullenger and K. W. Leong, *Nat. Rev. Mater.*, 2022, **7**, 557–574.
- 27 J. Dervedde, A. Rausch, M. Weinhart, S. Enders, R. Tauber, K. Licha, M. Schirner, U. Zügel, A. von Bonin and R. Haag, *Proc. Natl. Acad. Sci. U. S. A.*, 2010, **107**, 19679–19684.
- 28 M. Weinhart, D. Gröger, S. Enders, J. Dervedde and R. Haag, *Biomacromolecules*, 2011, **12**, 2502–2511.
- 29 X. Wang and N. Hadjichristidis, *ACS Macro Lett.*, 2020, **9**, 464–470.
- 30 R. Bej, P. Dey and S. Ghosh, *Soft Matter*, 2020, **16**, 11–26.
- 31 R. C. Pratt, B. G. G. Lohmeijer, D. A. Long, R. M. Waymouth and J. L. Hedrick, *J. Am. Chem. Soc.*, 2006, **128**, 4556–4557.
- 32 B. M. Davis, J. L. Richens and P. O'Shea, *Biophys. J.*, 2011, **101**, 245–254.
- 33 S. C. Owen, D. P. Y. Chan and M. S. Shoichet, *Nano Today*, 2012, **7**, 53–65.
- 34 S. C. Kim, D. W. Kim, Y. H. Shim, J. S. Bang, H. S. Oh, S. W. Kim and M. H. Seo, *J. Controlled Release*, 2001, **72**, 191–202.
- 35 Y. Wen and J. Li, *Nat. Biomed. Eng.*, 2018, **2**, 273–274.
- 36 Y. Lu, Z. Yue, J. Xie, W. Wang, H. Zhu, E. Zhang and Z. Cao, *Nat. Biomed. Eng.*, 2018, **2**, 318–325.
- 37 C. Oerlemans, W. Bult, M. Bos, G. Storm, J. F. W. Nijssen and W. E. Hennink, *Pharm. Res.*, 2010, **27**, 2569–2589.
- 38 Y. Qiao, C. Zhan, C. Wang, X. Shi, J. Yang, X. He, E. Ji, Z. Yu, C. Yan and H. Wu, *J. Mater. Chem. B*, 2020, **8**, 8527–8535.
- 39 A. T. Haedler, H. Misslitz, C. Buehlmeier, R. Q. Albuquerque, A. Köhler and H.-W. Schmidt, *ChemPhysChem*, 2013, **14**, 1818–1829.
- 40 J. Duhamel, *Langmuir*, 2012, **28**, 6527–6538.
- 41 A.-C. Pöppler, M. Lübtow, J. Schlauersbach, J. Wiest, L. Meinel and R. Luxenhofer, *Angew. Chem., Int. Ed.*, 2019, **58**, 18540–18546.
- 42 M. Grüne, R. Luxenhofer, D. Iuga, S. P. Brown and A.-C. Pöppler, *J. Mater. Chem. B*, 2020, **8**, 6827–6836.
- 43 M. Callari, P. L. De Souza, A. Rawal and M. H. Stenzel, *Angew. Chem., Int. Ed.*, 2017, **56**, 8441–8445.
- 44 M. Farshbaf, H. Valizadeh, Y. Panahi, Y. Fatahi, M. Chen, A. Zarebkohan and H. Gao, *Int. J. Pharm.*, 2022, **614**, 121458.
- 45 T. D. Langridge and R. A. Gemeinhart, *J. Controlled Release*, 2020, **319**, 157–167.
- 46 R. Savić, T. Azzam, A. Eisenberg and D. Maysinger, *Langmuir*, 2006, **22**, 3570–3578.
- 47 Q. Ran, X. Xu, P. Dey, S. Yu, Y. Lu, J. Dzubiella, R. Haag and M. Ballauff, *J. Chem. Phys.*, 2018, **149**, 163324.
- 48 M. H. Lee, Z. Yang, C. W. Lim, Y. H. Lee, S. Dongbang, C. Kang and J. S. Kim, *Chem. Rev.*, 2013, **113**, 5071–5109.
- 49 C. Ortiz, M. L. Ferreira, O. Barbosa, J. C. S. dos Santos, R. C. Rodrigues, Á. Berenguer-Murcia, L. E. Briand and R. Fernandez-Lafuente, *Catal. Sci. Technol.*, 2019, **9**, 2380–2420.
- 50 R. S. Herbst and F. R. Khuri, *Cancer Treat. Rev.*, 2003, **29**, 407–415.
- 51 A. W. G. Alani, Y. Bae, D. A. Rao and G. S. Kwon, *Biomaterials*, 2010, **31**, 1765–1772.
- 52 A. W. Du, H. Lu and M. H. Stenzel, *Biomacromolecules*, 2015, **16**, 1470–1479.





## Supporting Information

# Dendritic Polyglycerolsulfate-SS-Poly(ester amide) Micelles for the Systemic Delivery of Docetaxel: Pushing the Limits of Stability through the Insertion of $\pi$ - $\pi$ Interactions

Daniel Braatz,<sup>a</sup> Justus H. Peter,<sup>a</sup> Mathias Dimde,<sup>a,b</sup> Elisa Quaas,<sup>a</sup> Kai Ludwig,<sup>b</sup> Katharina Achazi,<sup>a</sup> Michael Schirner,<sup>a</sup> Matthias Ballauff,<sup>\*a</sup> Rainer Haag<sup>\*a</sup>

<sup>a</sup> Institute of Chemistry and Biochemistry, Freie Universität Berlin, Berlin 14195, Germany

<sup>b</sup> Institute of Chemistry and Biochemistry, Research Center of Electron Microscopy, Freie Universität Berlin, Berlin 14195, Germany

\*Corresponding Authors

Email: mballauff@zedat.fu-berlin.de; haag@zedat.fu-berlin.de

### Graphical Abstract:

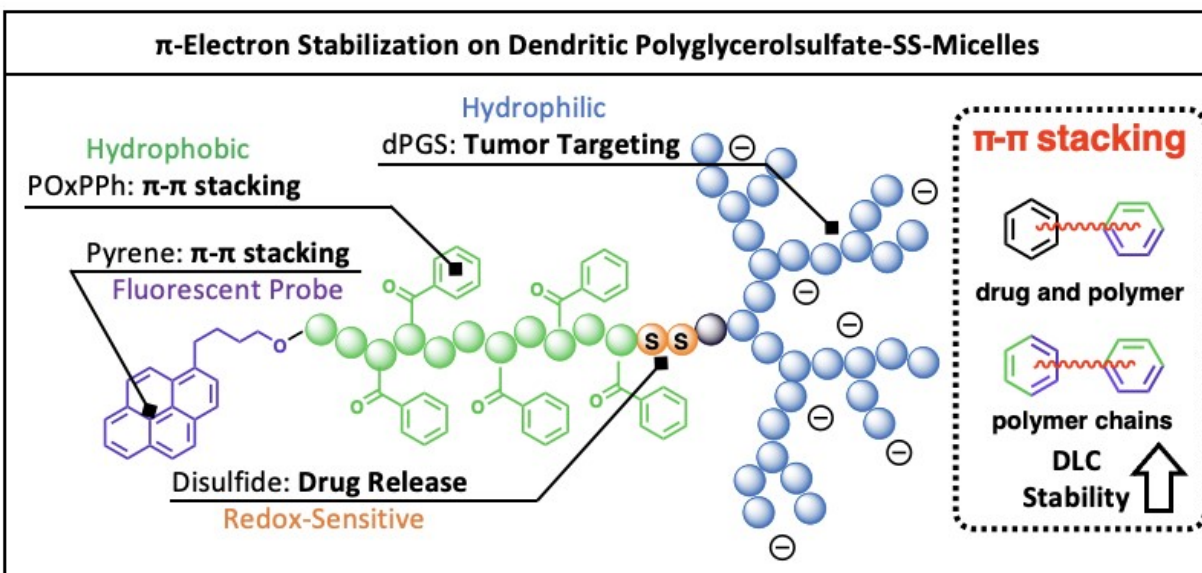


## Table of Contents

Materials and Methods .....	3
Synthesis of 4-benzoyl-1,4-oxazepan-7-one (OxPPh).....	4
Synthesis of Py-POxPPh-COOH .....	5
Synthesis of Py-PCL-COOH .....	6
Synthesis of Et-PCL-COOH.....	7
Synthesis of dPG-SS-NH <sub>2</sub> .....	8
Synthesis of dPGS-SS-POxPPh-Py .....	11
Synthesis of dPGS-SS-PCL-Py.....	15
Synthesis of dPGS-SS-PCL-Et .....	18
Synthesis of FITC-dPGS-SS-POxPPh-Py .....	20
Dynamic Light Scattering Experiments (DLS) Measurements – Size and Size Distribution .....	26
ζ-Potential Measurements.....	26
Dynamic Light Scattering (DLS) Measurements - Human Serum Albumin (HSA) Interaction with Micellar Surface.....	26
Dynamic Light Scattering (DLS) Measurements - Enzymatic Hydrolysis with Novozyme 435.....	26
Dynamic Light Scattering (DLS) Measurements - GSH- Triggered Shedding of Micelles .....	26
Dynamic Light Scattering Experiments (DLS) – Critical Micelle Concentration (CMC) .....	26
Determination of the CMC.....	27
Fabrication of Empty Micelles.....	27
Fabrication of Docetaxel-loaded Micelles .....	27
Cell Viability Tests (CCK-8 Assay, Dulbecco’s Modified Eagle’s Medium (DMEM), 48 h).....	28
Cryo-TEM measurements .....	28
Spectral studies: UV-VIS Measurements .....	28
Spectral studies: Fluorescence Measurements.....	28
CMC determinations of empty/DTX-loaded dPGS-SS-PCL-Et, dPGS-SS-PCL-Py, and dPGS-SS-POxPPh-Py .....	29
Cross-Polarization Solid-State <sup>13</sup> C NMR of free DTX, Empty dPGS-SS-POxPPh-Py, and dPGS-SS-POxPPh-Py@DTX.....	29
References .....	30

## Materials and Methods

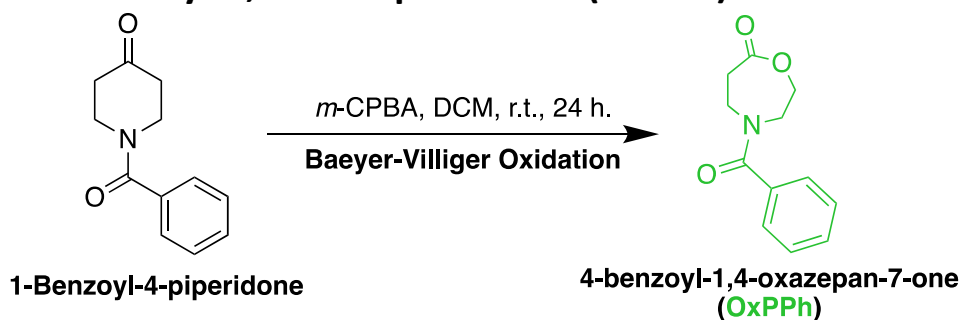
The monomers caprolactone and glycidol were purchased from Acros Organics, purified by distillation, and stored over molecular sieves. 1-Benzoyl-4-piperidone and *m*-CPBA were bought from Sigma-Aldrich. Docetaxel was ordered from MedChemExpress and stored in a freezer. Dialysis membranes were commercially available at Sigma-Aldrich. Deuterated solvents were obtained from Deutero. All the other chemicals were purchased from Sigma-Aldrich, TCI, or Acros Organics and used without purification.  $^1\text{H}$  NMR spectra and  $^1\text{H}$ -DOSY NMR spectra were recorded on a Bruker ECX 500 spectrometer operating at 500 MHz using  $\text{CDCl}_3$ ,  $\text{DMF-d}_7$ ,  $\text{CD}_3\text{OD-d}_4$ , or  $\text{D}_2\text{O}$  as a solvent. For  $^{13}\text{C}$  NMR spectra, the measurements were performed on a Bruker AVANCE700 operating at 700 MHz using  $\text{CDCl}_3$ ,  $\text{DMF-d}_7$ ,  $\text{CD}_3\text{OD-d}_4$ , or  $\text{D}_2\text{O}$  as a solvent. The chemical shifts were calibrated against the residual solvent signal.

The molecular weight and polydispersity of the polymers were determined by a Waters 1515 gel permeation chromatography (GPC) instrument equipped with two linear PLgel columns (Mixed-C) following a guard column and a differential refractive index detector. The measurements were performed using tetrahydrofuran (THF; hydrophobic segments), water (hydrophilic components), or dimethylformamide (DMF; amphiphilic segments) as the eluent at a flow rate of 1.0 mL/min at 30 °C and a series of narrow polystyrene standards (THF), Pullulan (water), and poly(methyl methacrylate) (PMMA; DMF) for the calibration of the columns.

Elemental analysis was performed with a VARIO EL III (Elementar). IR spectra were recorded with a Nicolet AVATAR 320 FT-IR 5 SXC (Thermo Fisher Scientific, Waltham, MA) with a deuterated triglycine sulfate (DTGS) detector from 4000 to 650  $\text{cm}^{-1}$ . Sample measurements were performed by dropping a solution of the compound and letting the solvent evaporate for a few seconds.

All cell experiments were conducted according to German genetic engineering laws and German biosafety guidelines in the laboratory (safety level 1). According to the manufacturer's instructions, cell viability was determined using a Cell Counting Kit (Hycultec, HY-K0301). A549, HeLa, and McF7 cells were obtained from Leibniz-Institut DSMZ - Deutsche Sammlung von Mikroorganismen und Zellkulturen GmbH and cultured in DMEM supplemented with 10% (v/v) FBS, 100 U/mL penicillin and 100  $\mu\text{g}/\text{mL}$  streptomycin. A549, HeLa, and McF7 cells were seeded in a 96-well plate at a density of  $5 \times 10^4$  cells/mL in 90  $\mu\text{l}$  DMEM Medium per well overnight at 37°C and 5%  $\text{CO}_2$ . 10  $\mu\text{l}$  of the sample (solved in deionized water) were added in serial dilutions including positive (1% SDS) and negative controls (Medium,  $\text{H}_2\text{O}$ ) and incubated for another 48 h at 37°C and 5%  $\text{CO}_2$ . For background subtraction, also wells containing no cells but only sample were used. After 48h incubation, the CCK8 solution was added (10  $\mu\text{l}/\text{well}$ ) and absorbance (450nm/650nm) was measured after approximately 3h incubation of the dye using a Tecan plate reader (Infinite pro200, TECAN-reader Tecan Group Ltd.) Measurements were performed in triplicates and repeated three times. The cell viability was calculated by setting the non-treated control to 100% and the non-cell control to 0% after subtracting the background signal using the Excel software.

## Synthesis of 4-benzoyl-1,4-oxazepan-7-one (OxPPh)



The monomer was synthesized following a slightly modified protocol.<sup>[1]</sup> Briefly, In a 250 mL round bottom flask equipped with a stir bar and a septum, 1-benzoyl-4-piperidone (4.23 g, 20.8 mmol, 1 eq.) was dissolved in 50 mL DCM. Then, *m*-CPBA (6.18 g, 30.9 mmol, 1.5 eq.) was dissolved in 70 mL of DCM and dropwise added to the stirred solution of 1-benzoyl-4-piperidone under ice-cooling. The ice bath was removed, and the mixture was stirred at room temperature for 24 hours. The solution was extracted with sodium thiosulfate, sodium bicarbonate, and sodium chloride saturated solutions (each 100 mL, 3 times). Afterward, the organic layer was collected and dried using magnesium sulfate. The solution was filtered, and the solvent was removed. Next, the received compound was purified by column chromatography on silica (pentane: ethyl acetate, 4:1). The obtained white product (1.42 g, 6.48 mmol, 31.2%) was dried under vacuum and characterized using <sup>1</sup>H NMR and mass spectrometry.

<sup>1</sup>H NMR (500 MHz, CD<sub>3</sub>OD, δ, ppm) = 7.60-7.40 (m, 5H), 4.57-4.34 (m, 2H), 4.18-3.89 (m, 2H), 3.86-3.62 (m, 2H), 3.09-2.86 (m, 2H).

MS (EI) m/z: [M]<sup>+</sup> Calculated for C<sub>12</sub>H<sub>13</sub>NO<sub>3</sub> 219.090; Found 219.087.

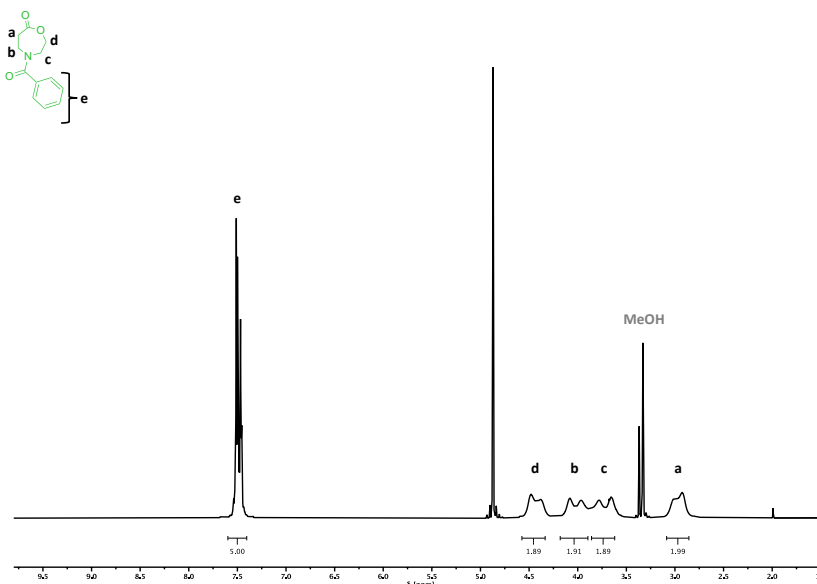
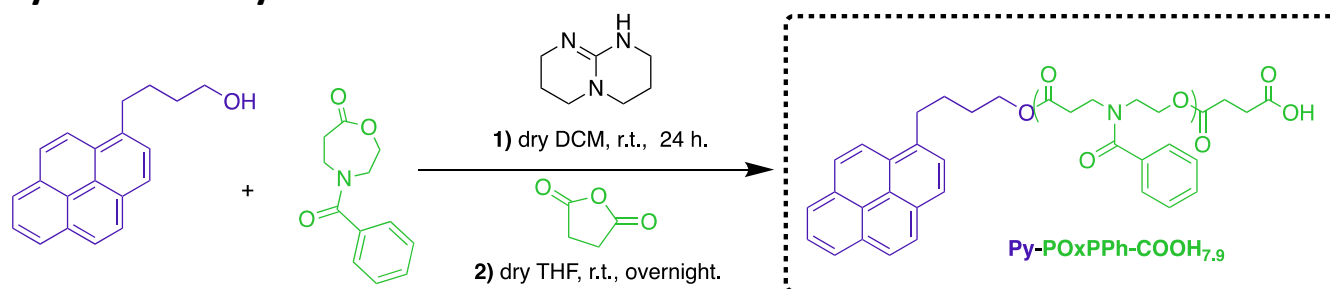


Figure S 1. <sup>1</sup>H NMR spectrum (500 MHz) of OxPPh in CD<sub>3</sub>OD.

## Synthesis of Py-POxPPh-COOH



To synthesize Py-POxPPh-COOH, in a flame-dried Schlenk flask, pyrenebutanol (38 mg, 0.14 mmol) and TBD (23 mg, 0.17 mmol) were placed, and under stirring, a 1M solution of OxPPh (3.2 mL, 3.2 mmol) in dry DCM was added (1M). The reaction solution was stirred for 24 hours at room temperature. The reaction was quenched with a 0.5M solution of succinic anhydride (0.68 mL, 0.34 mmol) in dry THF. After 24 hours at room temperature, the solution was concentrated, and the product was purified by precipitation into cold methanol three times. The product was obtained as a white crystalline substance (711.6 mg). For characterization, <sup>1</sup>H and <sup>13</sup>C NMR, and GPC were performed.

<sup>1</sup>H NMR (500 MHz, CDCl<sub>3</sub>, δ, ppm) = 8.23-7.84 (m, 9H), 7.60-7.08 (m, 182H), 4.44-3.94 (m, 73H), 3.84-3.42 (m, 145H), 2.85-2.34 (m, 4H, 74H).

**Table S 1.** Organocatalytic Ring-Opening Polymerization of OxPPh mediated by TBD.

Monomer (M)	Catalyst (C)	[M] <sub>0</sub> /[Pyrenebutanol] <sub>0</sub> /[C] <sub>0</sub>	Time [h]	conv. <sup>NMR</sup> (%)	M <sub>n</sub> <sup>theo.</sup> (kDa)	M <sub>n</sub> <sup>NMR</sup> (kDa)	M <sub>n</sub> <sup>GPC, THF</sup> (kDa)	D
OxPPh	TBD	36/1/1.2	24	99.4	8	7.9	3.9	1.3

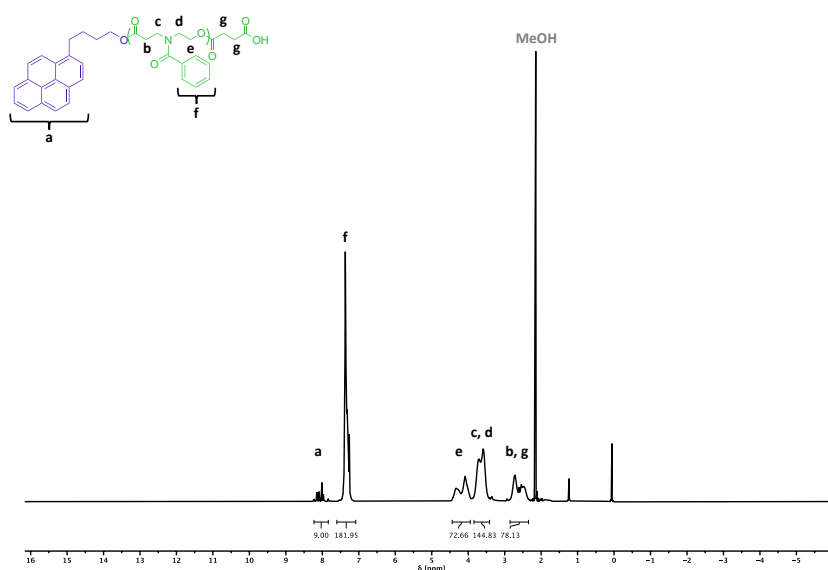


**Figure S 2.** <sup>1</sup>H NMR spectrum (500 MHz) of Py-POxPPh-COOH in CDCl<sub>3</sub>.

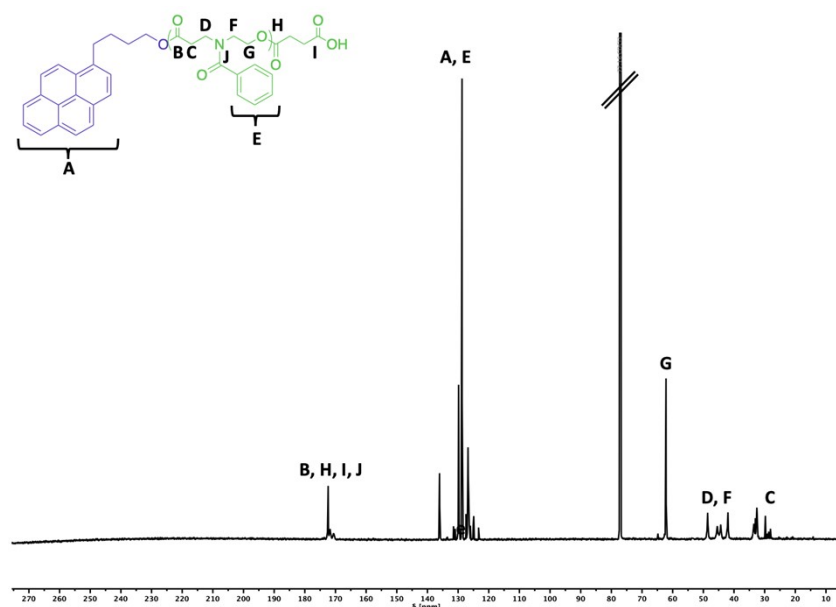
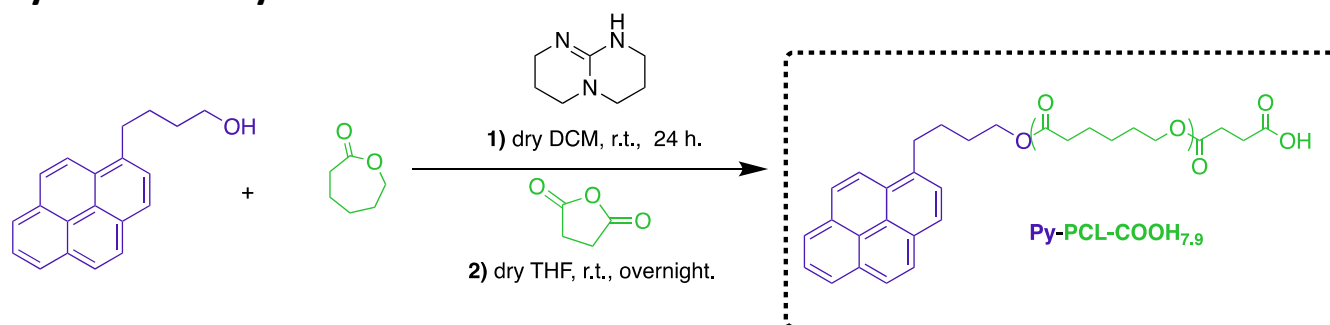


**Figure S 3.**  $^{13}\text{C}$  NMR spectrum (700 MHz) of Py-PO $_x$ PPh-COOH in  $\text{CDCl}_3$ .

## Synthesis of Py-PCL-COOH



To synthesize Py-PCL-COOH, in a flame-dried Schlenk flask, pyrenebutanol (38 mg, 0.14 mmol) and TBD (23 mg, 0.17 mmol) were placed, and under stirring, CL (8.8 mL, 8.8 mmol) was added (plus dry DCM 8.8 mL). The reaction solution was stirred for 24 hours at room temperature. The reaction was quenched with a 0.5M solution of succinic anhydride (0.68 mL, 0.34 mmol) in dry THF. After 24 hours at room temperature, the solution was concentrated, and the product was purified by precipitation into cold methanol three times. The product was obtained as a white crystalline substance (711.6 mg). For characterization,  $^1\text{H}$  and  $^{13}\text{C}$  NMR, and GPC were performed.

$^1\text{H}$  NMR (500 MHz,  $\text{CDCl}_3$ ,  $\delta$ , ppm) = 8.21-7.82 (m, 9H), 4.22-3.87 (m, 138H), 2.55-2.47 (m, 4H), 2.39-2.18 (m, 138H), 1.78-1.47 (m, 280H), 1.45-1.25 (m, 137H).

**Table S 2.** Organocatalytic Ring-Opening Polymerization of Caprolactone mediated by TBD.

Monomer (M)	Catalyst (C)	$[\text{M}]_0/[\text{Pyrenebutanol}]_0/[\text{C}]_0$	Time [h]	conv. <sup>NMR</sup> (%)	$M_n^{\text{theo.}}$ (kDa)	$M_n^{\text{NMR}}$ (kDa)	$M_n^{\text{GPC, THF}}$ (kDa)	$\bar{D}$
Caprolactone	TBD	70/1/1.2	24	99.3	8	7.9	6.9	1.1

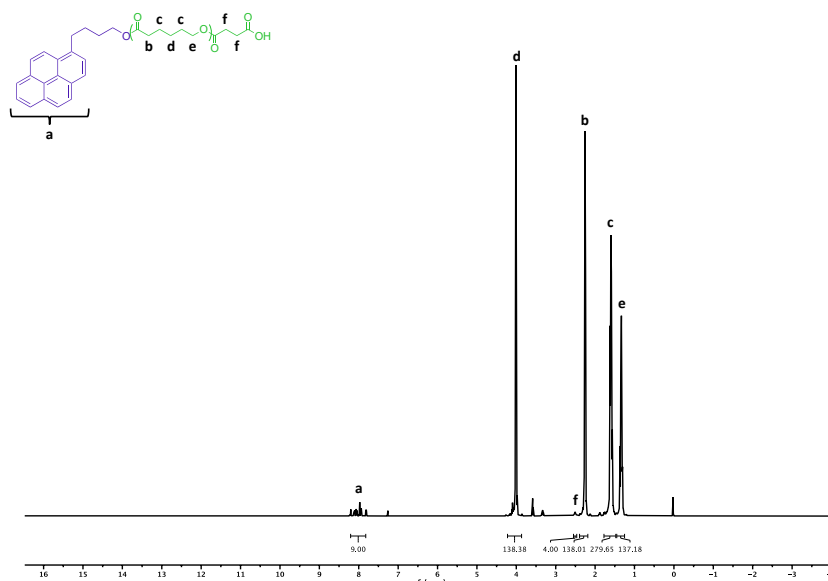


Figure S 4.  $^1\text{H}$  NMR spectrum (500 MHz) of Py-PCL-COOH in  $\text{CDCl}_3$ .

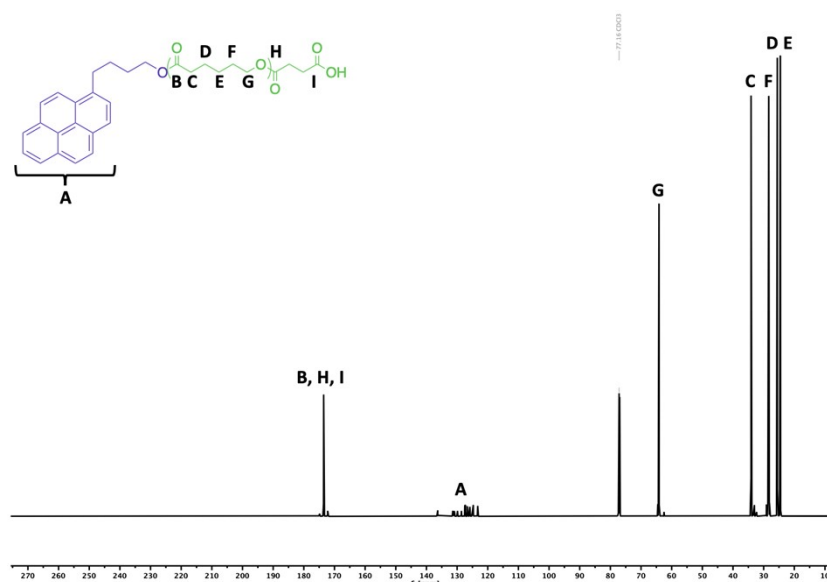
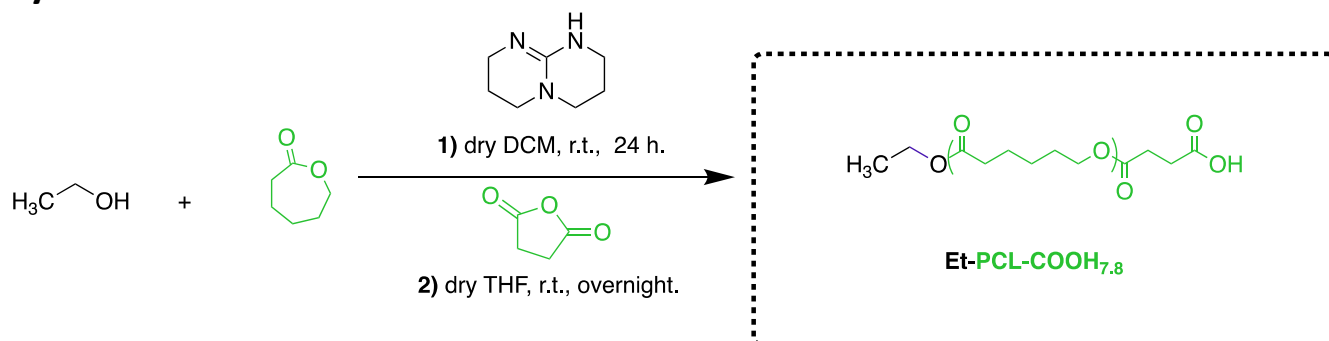


Figure S 5.  $^{13}\text{C}$  NMR spectrum (500 MHz) of Py-PCL-COOH in  $\text{CDCl}_3$ .

## Synthesis of Et-PCL-COOH



The synthesis,  $^1\text{H}$  NMR, and GPC characterization of Et-PCL-COOH are described in more detail elsewhere.<sup>[2]</sup> In brief, in a flame-dried Schlenk flask, freshly distilled caprolactone (15 g) was placed. To the flask, dry DCM was added to obtain a 1M solution. Then, the initiator dry ethanol and the catalyst

TBD (1.2 eq.) were added. The reaction was stirred at room temperature for 24 hours. Then, succinic anhydride (4 eq., dry THF, 0.5M) was added, and the reaction was further stirred for 24 hours at room temperature. Then, the solvent was removed under vacuum. The polymer was purified by precipitation from acetone in cold methanol three times. The obtained white polymers were dried under vacuum and further characterized by  $^1\text{H}$  and  $^{13}\text{C}$  NMR, and GPC.

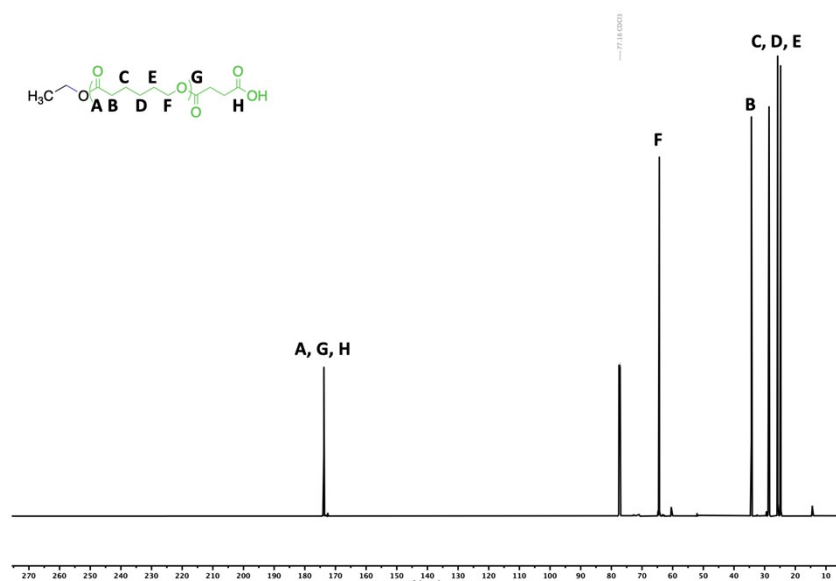
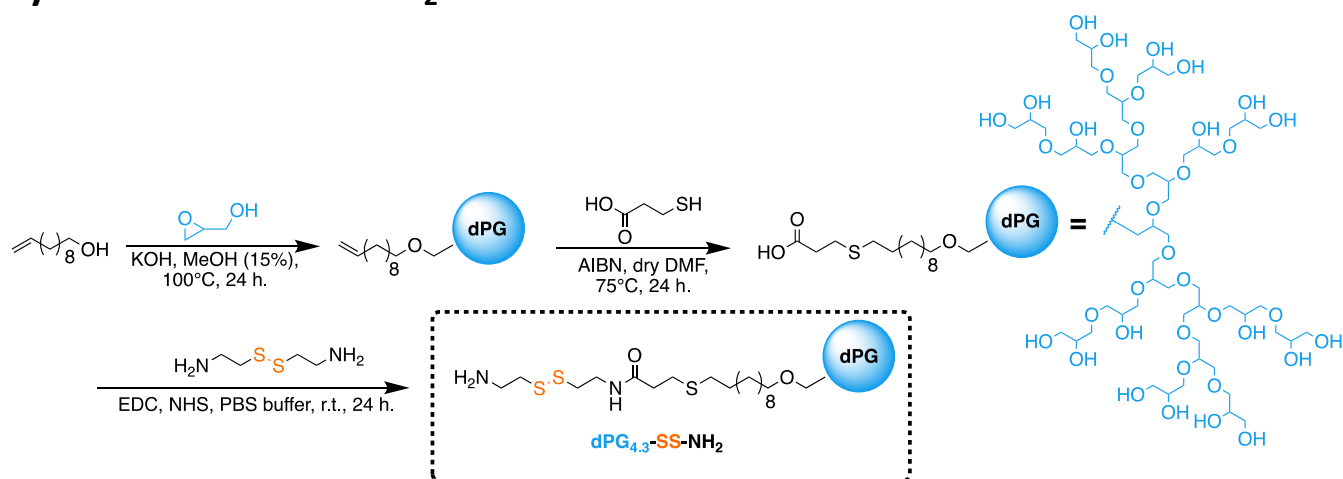


Figure S 6.  $^{13}\text{C}$  NMR spectrum (700 MHz) of Et-PCL-COOH in  $\text{CDCl}_3$ .

## Synthesis of dPG-SS-NH<sub>2</sub>



The synthesis of dPG-SS-NH<sub>2</sub> was performed according to an already published protocol.<sup>[2]</sup> In short, the reaction was performed in a synthesis reactor (HiTEC). To synthesize dPG-SS-NH<sub>2</sub>, 10-undecenol (20.66 g, 0.12 mmol) was loaded into the reactor flask. *In situ* potassium methoxide (KOH 0.31 g, 5 mL MeOH, MeOK, 15% deprotonation) was formed and dried at 60 °C under vacuum. The reactor was filled with an argon atmosphere, heated to 100 °C, and freshly distilled glycidol (200 g, 2.7 mmol) was added over a period of 24 h. After 26 h, the reaction temperature was reduced to 75 °C, and subsequently dry DMF (600 mL), mercaptopropionic acid (29.50 g, 278.0 mmol), and azobisisobutyronitrile (AIBN; 4.56 g, 27.8 mmol) were added to the reaction. The reaction was stirred for 4 h at a constant temperature of 75 °C. The crude product was purified by precipitation in acetone with subsequent tangential flow filtration (TFF) dialysis (Sartocon Slice 200 Stainless Steel Holder) in water/ethanol 10:1 (MWCO: 1 kDa) for 3 days. The solvent was removed under reduced pressure, and after lyophilization (Alpha 3-4 LSC basic), a yellow viscous polymer was obtained. In a Flask, cystamine (7.41 g, 32.9 mmol) was placed, and phosphate-Braatz *et. al*



buffered saline (PBS) buffer (1 L, pH 7.4, 100 mM) was added until the cystamine was dissolved. At the same time, dPG-COOH (25 g, 6.6 mmol) was dissolved in 2-(N-morpholino) ethanesulfonic acid (MES)-buffer (500 mL, pH 5.0, 50 mM). Next, EDC\*HCL (6.31 g, 32.9 mmol) and NHS (3.8 g, 32.9 mmol) were added. At room temperature, the reaction solution was stirred for 30 min, and then the cystamine solution was slowly added. The reaction was stirred over 16 h, and the product was purified by precipitation into cold acetone. Then the product was further purified by TFF dialysis in water for 3 days (MWCO: 1 kDa) and then lyophilized. A yellow, oily polymer (16.8 g) was obtained. The obtained product was characterized by  $^1\text{H}$  and  $^{13}\text{C}$  NMR, IR, and GPC.

$^1\text{H}$  NMR (500 MHz,  $\text{CD}_3\text{OD}$ ,  $\delta$ , ppm) = 4.02-3.36 (m, 288H), 3.03-2.32 (m, 12H), 1.65-1.50 (m, 4H), 1.46-1.25 (m, 14H).

FTIR ( $\nu$ ,  $\text{cm}^{-1}$ ) = 1647 (C=O, sec. amide)

**Table S 3.** Anionic Polymerization of Glycidol initiated by 10-undecenol.

Monomer (M)	Catalyst (C)	$[\text{M}]_0/[\text{10-undecenol}]_0/[\text{C}]_0$	Time [h]	$M_n^{\text{theo.}}$ (kDa)	$M_n^{\text{NMR}}$ (kDa)	$M_n^{\text{GPC, water}}$ (kDa)	$\mathcal{D}$
Glycidol	MeOK	22.5/1/0.15	24	4	4.3	4.4	1.5

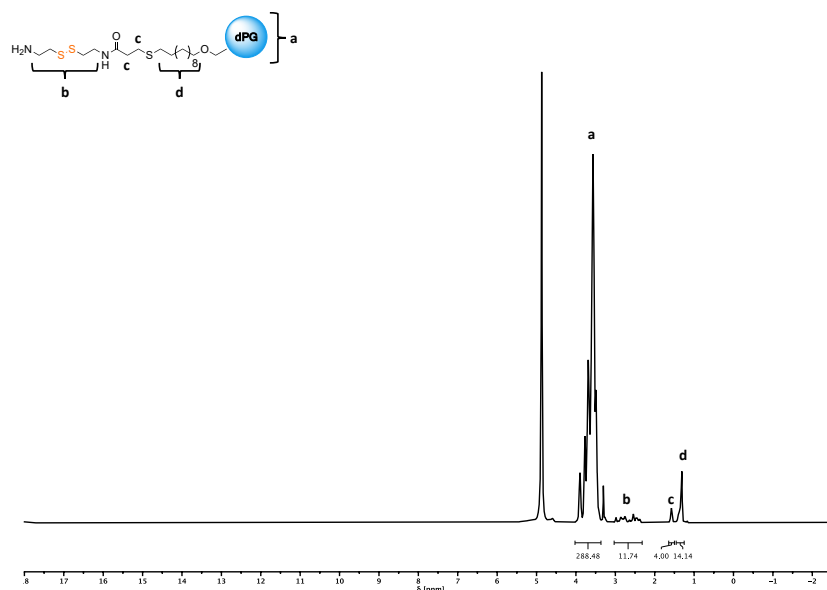


**Figure S 7.**  $^1\text{H}$  NMR spectrum (500 MHz) of dPG-SS- $\text{NH}_2$  in  $\text{CD}_3\text{OD}$ .

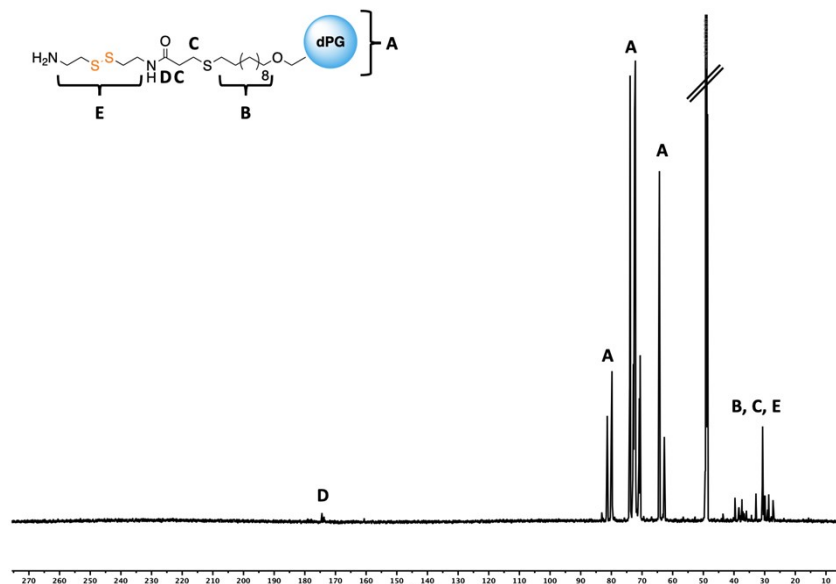


**Figure S 8.**  $^{13}\text{C}$  NMR (700 MHz) of dPG-SS-NH<sub>2</sub> in CD<sub>3</sub>OD.

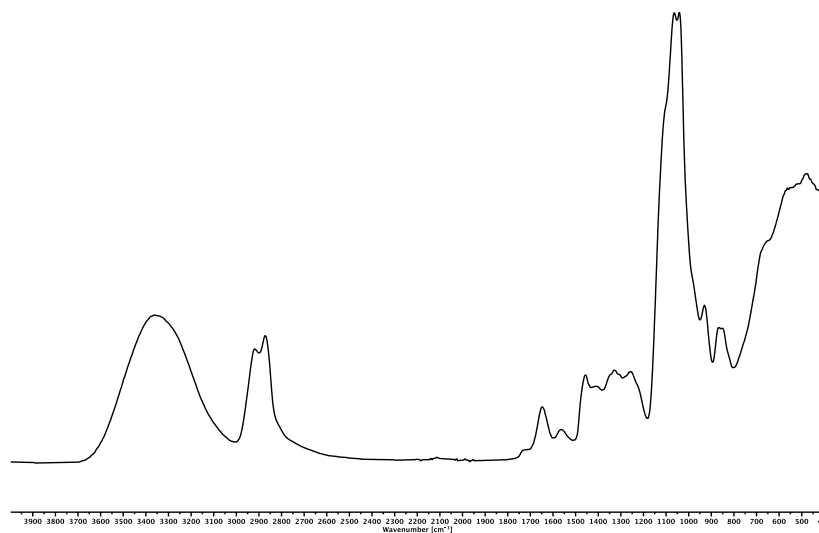
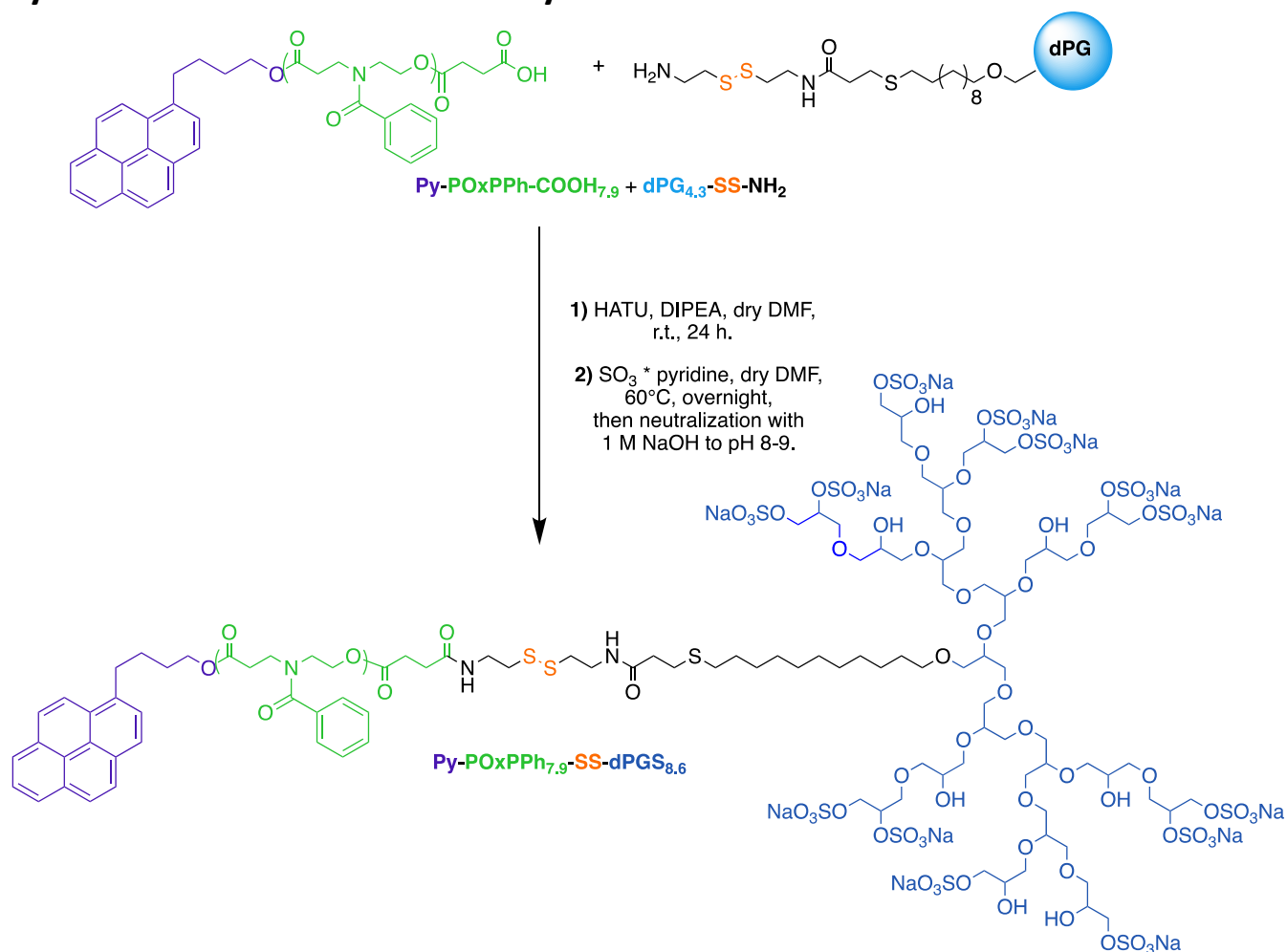


**Figure S 9.** FTIR spectrum of dPG-SS-NH<sub>2</sub>.

## Synthesis of dPGS-SS-POxPPh-Py



First, the hydrophobic block, Py-POxPPh-COOH, and the hydrophilic block, dPG-SS-NH<sub>2</sub>, were coupled using an amide coupling protocol. In a flame-dried Schlenk-flask Py-POxPPh-COOH (0.50 g, 0.065 mmol), HATU (0.06 g, 0.15 mmol), and DIPEA (0.02 g, 0.03 mL, 0.17 mmol) were added. The reactants were dissolved in 5 mL of dry DMF. The acid was then activated under stirring at room temperature for 2 hours. Then, dPG-SS-NH<sub>2</sub> (0.30 g, 0.075 mmol) was dissolved in 5 mL of dry DMF and was slowly added to the solution. The reaction was stirred at room temperature overnight. For purification and separation of uncoupled polymer chains, the crude product was dialyzed against methanol for 3 days (MWCO 3.5 kDa). Then, the methanol was changed to water. The product was obtained after lyophilization (453 mg). For characterization, <sup>1</sup>H NMR and DOSY NMR were performed.

Next, the dPG-SS-POxPPh-Py (400 mg) was dissolved in 5 mL of dry DMF and heated to 60°C. SO<sub>3</sub>\*pyridine (2.15 g, 13.48 mmol) dissolved in 10 mL was added over 5 hours to this solution. The solution was further stirred overnight at 60°C. Then, the solution was quenched by adding 1M NaOH until a pH of 8 was reached. The amphiphilic copolymer was dialyzed against brine with an ever-decreasing salt content over a period of 5 days. After lyophilization, a yellow, crystalline polymer was obtained (650 mg). The product was characterized by <sup>1</sup>H and <sup>13</sup>C NMR, GPC, elemental analysis, and FTIR. Degree of Sulfation (EA): 87%.

<sup>1</sup>H NMR<sub>before sulfation</sub> (500 MHz, DMF-d<sub>7</sub>, δ, ppm) = 8.49-8.12 (m, 9H), 7.62-7.26 (m, 177H), 4.98-4.51 (m, 76H), 4.42-4.04 (m, 70H), 3.82-3.45 (m, 582H), 2.89-2.58 (m, 75H+DMF), 1.60-1.53 (m, 5H), 1.41-1.28 (m, 19H).

GPC<sub>after sulfation</sub> (H<sub>2</sub>O) =  $M_w$ : 1.33 kg/mol;  $\bar{D}$ : 2.00  
 FTIR ( $\nu$ , cm<sup>-1</sup>) = 1732 (C=O, ester); 1631 (C=O, tert. amide)

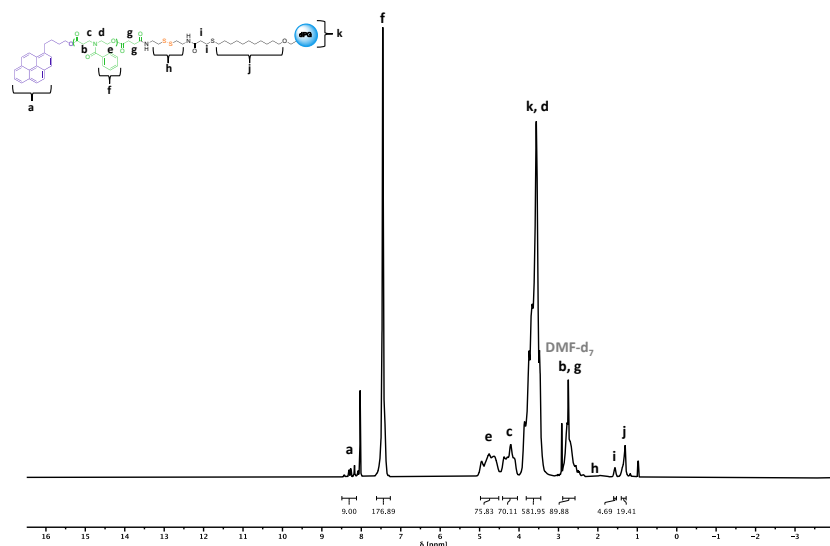


Figure S 10. <sup>1</sup>H NMR spectrum (500 MHz) of dPG-SS-POxPPh-Py in DMF-d<sub>7</sub>.

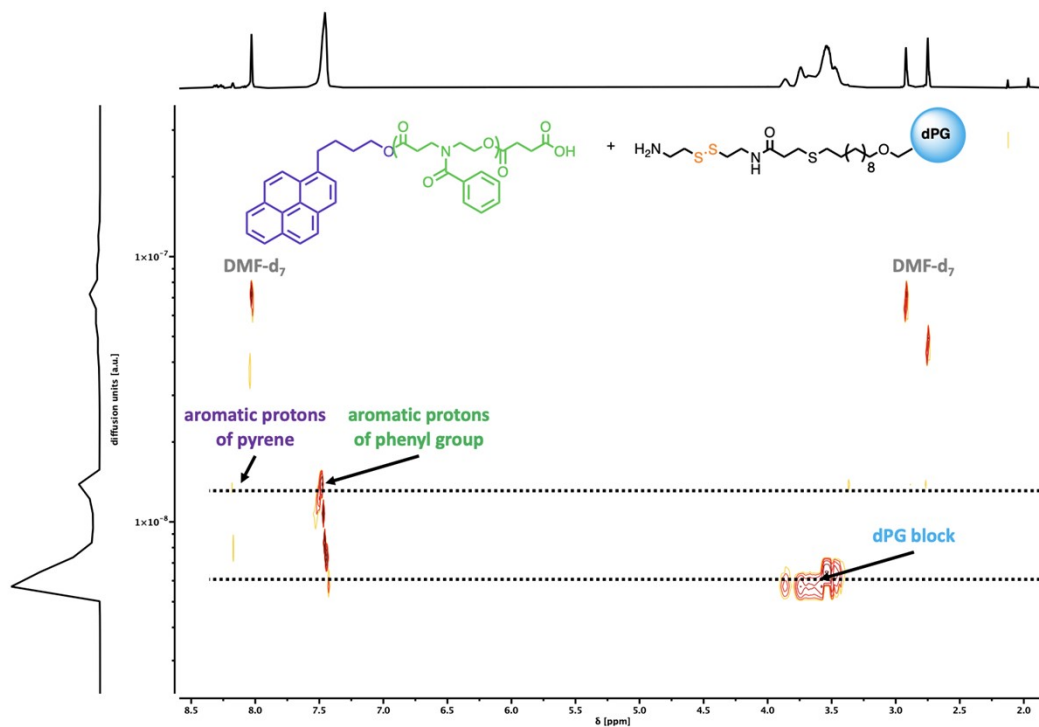


Figure S 11. <sup>1</sup>H-derived DOSY NMR spectrum (500 MHz) of non-coupled Py-POxPPh-COOH and dPG-SS-NH<sub>2</sub> in DMF-d<sub>7</sub> showing two distinguished diffusion species.

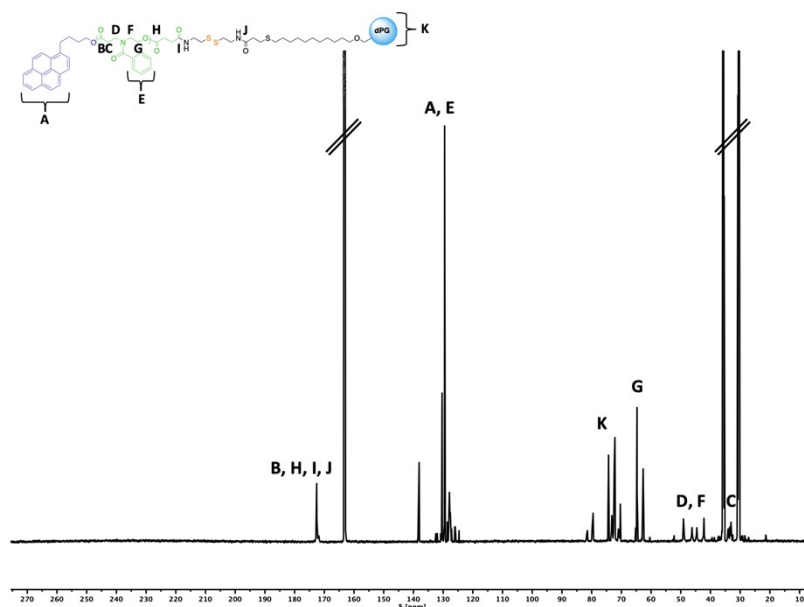


Figure S 12.  $^{13}\text{C}$  NMR (700 MHz) of dPG-SS-POxPPh-Py in  $\text{DMF-d}_7$ .

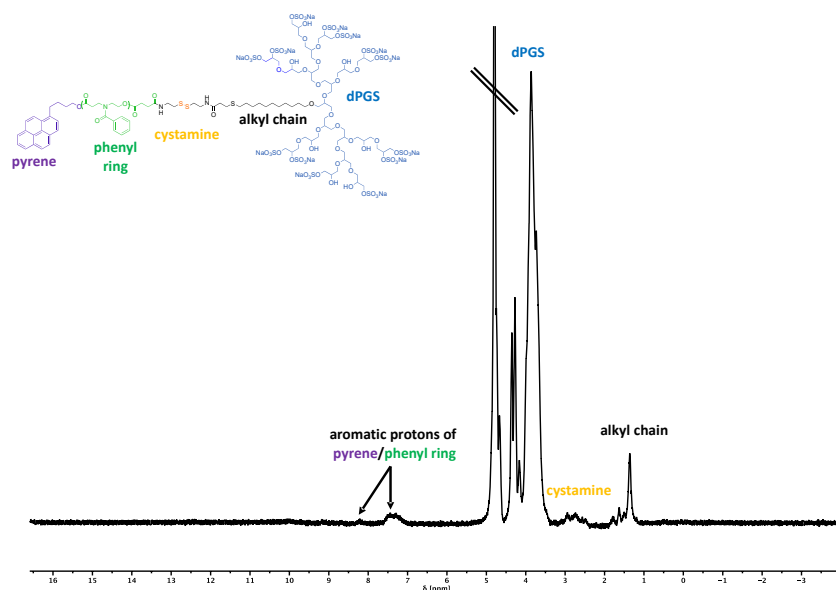
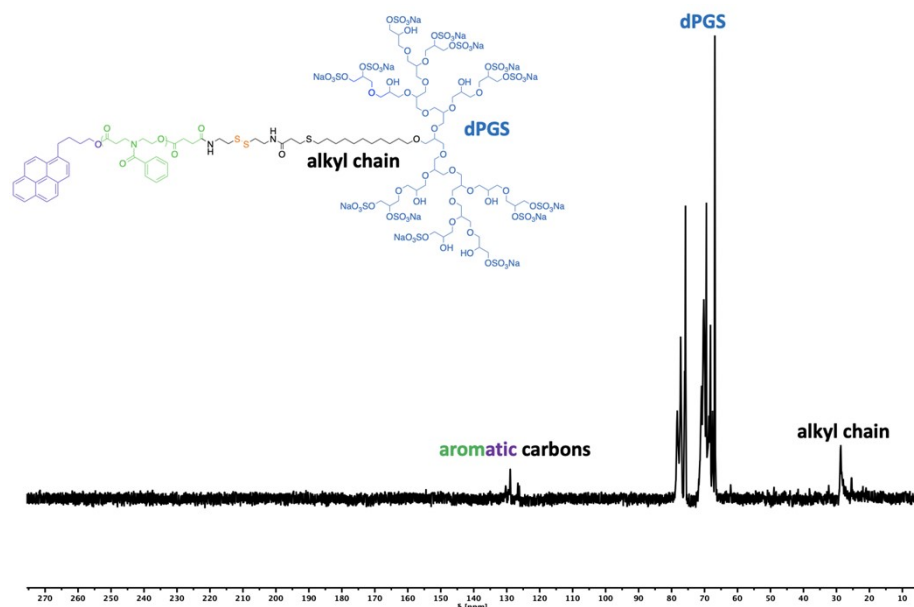
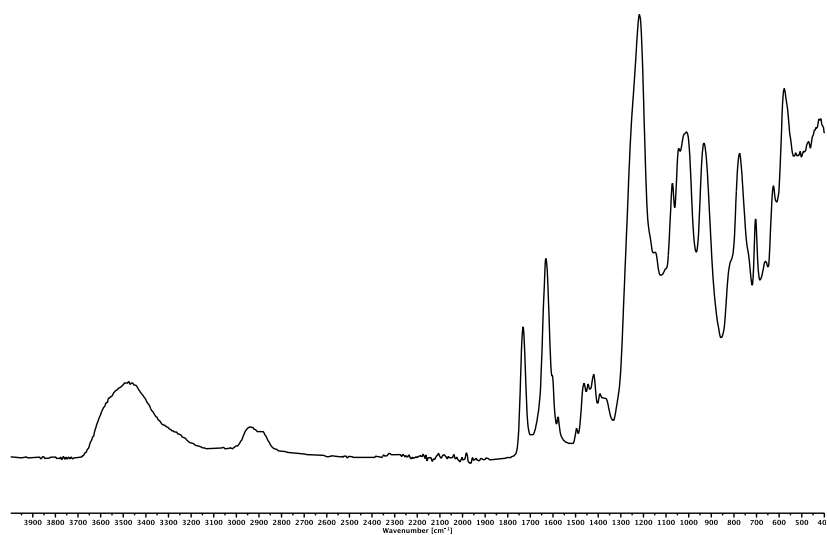


Figure S 13.  $^1\text{H}$  NMR spectrum (500 MHz) of dPGs-SS-POxPPh-Py in  $\text{D}_2\text{O}$ .

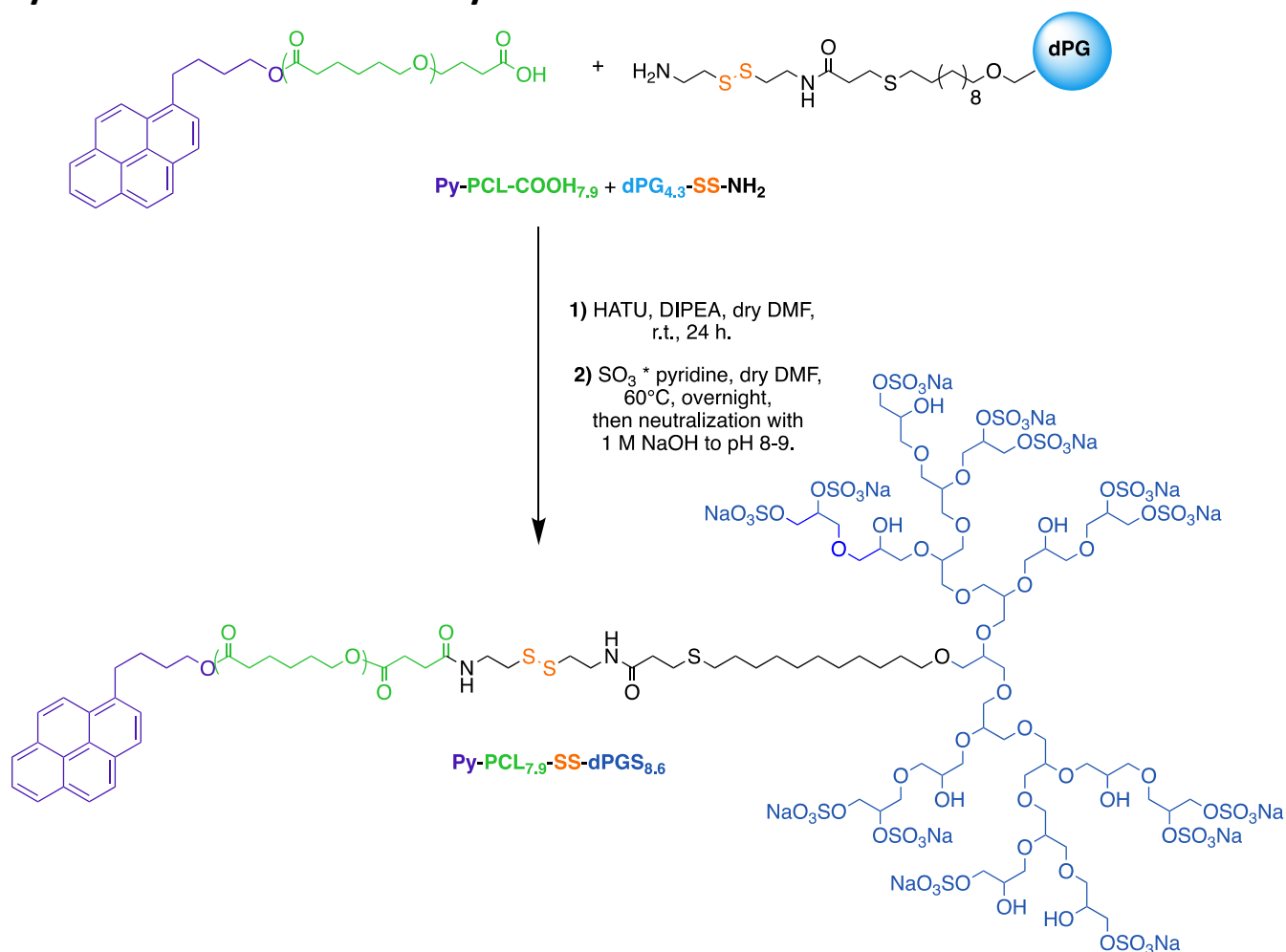


**Figure S 14.**  $^{13}\text{C}$  NMR spectrum (700 MHz) of dPGS-SS-POxPPh-Py in  $\text{D}_2\text{O}$ .



**Figure S 15.** FTIR spectrum of dPGS-SS-POxPPh-Py.

## Synthesis of dPGS-SS-PCL-Py



First, the hydrophobic block, Py-PCL-COOH, and the hydrophilic block, dPG-SS-NH<sub>2</sub>, were coupling using an amide coupling protocol. In a flame-dried Schlenk-flask Py-PCL-COOH (0.32 g, 0.040 mmol), HATU (0.04 g, 0.09 mmol), and DIPEA (0.01 g, 0.02 mL, 0.10 mmol) were added. The reactants were dissolved in 5 mL of dry DMF. The acid was then activated under stirring at room temperature for 2 hours. Then, dPG-SS-NH<sub>2</sub> (0.19 g, 0.047 mmol) was dissolved in 5 mL of dry DMF and was slowly added to the solution. The reaction was stirred at room temperature overnight. For purification and separation of uncoupled polymer chains, the crude product was dialyzed against methanol for 3 days (MWCO 3.5 kDa). Then, the methanol was changed to water. The product was obtained after lyophilization (426 mg). For characterization, <sup>1</sup>H NMR was performed.

Next, the dPG-SS-PCL-Py (400 mg) was dissolved in 5 mL of dry DMF and heated to 60°C. SO<sub>3</sub>\*pyridine (2.15 g, 13.48 mmol) dissolved in 10 mL was added over 5 hours to this solution. The solution was further stirred overnight at 60°C. Then, the solution was quenched by adding 1M NaOH until a pH of 8 was reached. The amphiphilic copolymer was dialyzed against brine with an ever-decreasing salt content over a period of 5 days. After lyophilization, a yellow, crystalline polymer was obtained (480 mg). The product was characterized by <sup>1</sup>H and <sup>13</sup>C NMR, GPC, elemental analysis, and FTIR. Degree of Sulfation (EA): 84%.

<sup>1</sup>H NMR<sub>before sulfation</sub> (500 MHz, DMF-d<sub>7</sub>, δ, ppm) = 8.43-8.11 (m, 9H), 4.27-3.97 (m, 117H), 3.90-3.42 (m, 196H), 2.64-2.53 (m, 4H), 2.49-2.22 (m, 227H), 1.78-1.52 (m, 229H), 1.48-1.28 (m, 123H).

GPC<sub>after sulfation</sub> (H<sub>2</sub>O) = *M<sub>w</sub>*: 1.24 kg/mol; *D*: 1.93

FTIR (ν, cm<sup>-1</sup>) = 1723 (C=O, ester); 1643 (C=O, sec. amide)

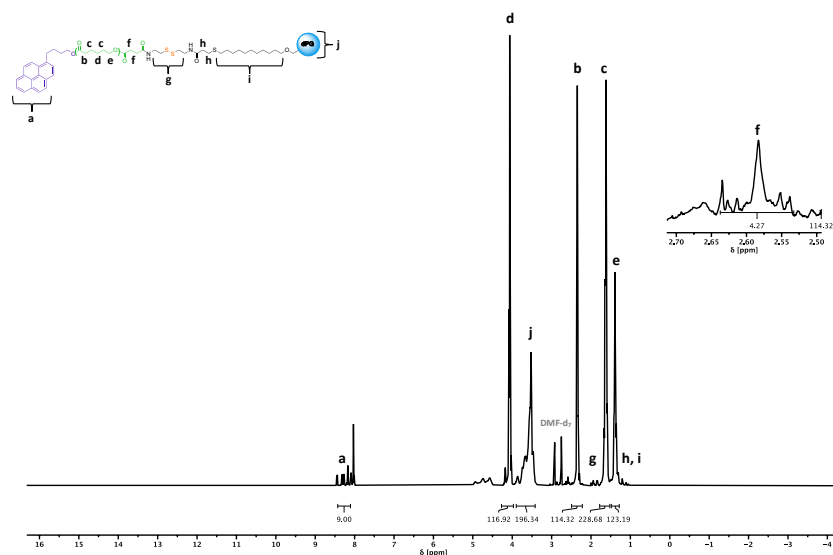


Figure S 16.  $^1\text{H}$  NMR spectrum (500 MHz) of dPG-SS-PCL-Py in  $\text{DMF-d}_7$ .

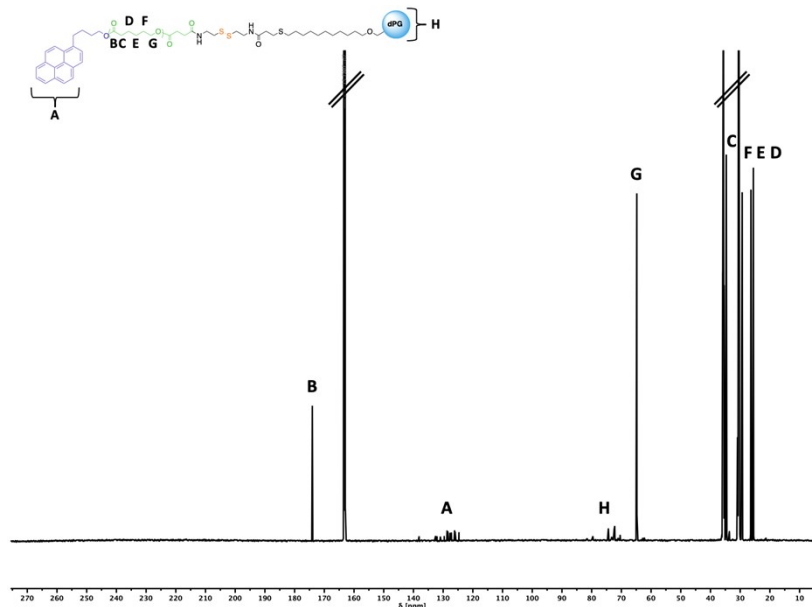


Figure S 17.  $^{13}\text{C}$  NMR (700 MHz) of dPG-SS-PCL-Py in  $\text{DMF-d}_7$ .



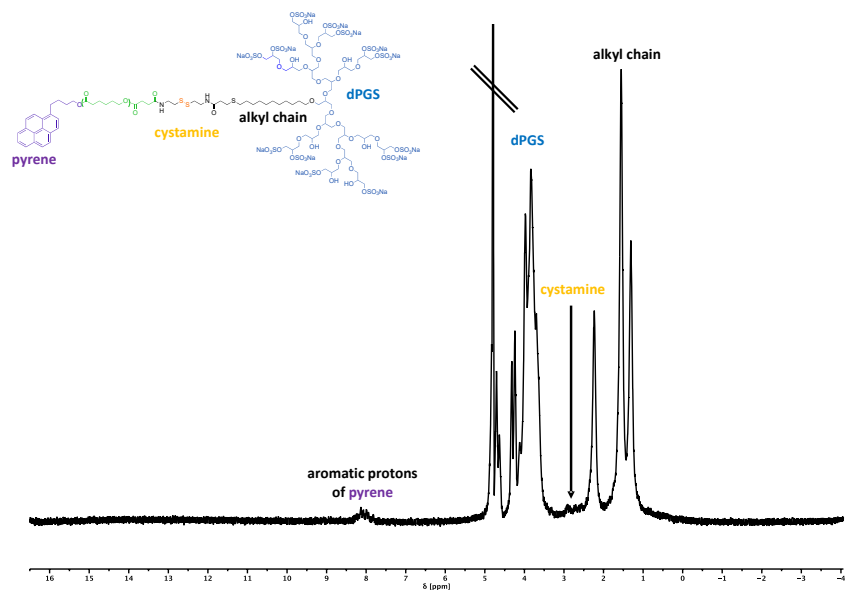


Figure S 18. <sup>1</sup>H NMR spectrum (500 MHz) of dPGS-SS-PCL-Py in D<sub>2</sub>O.

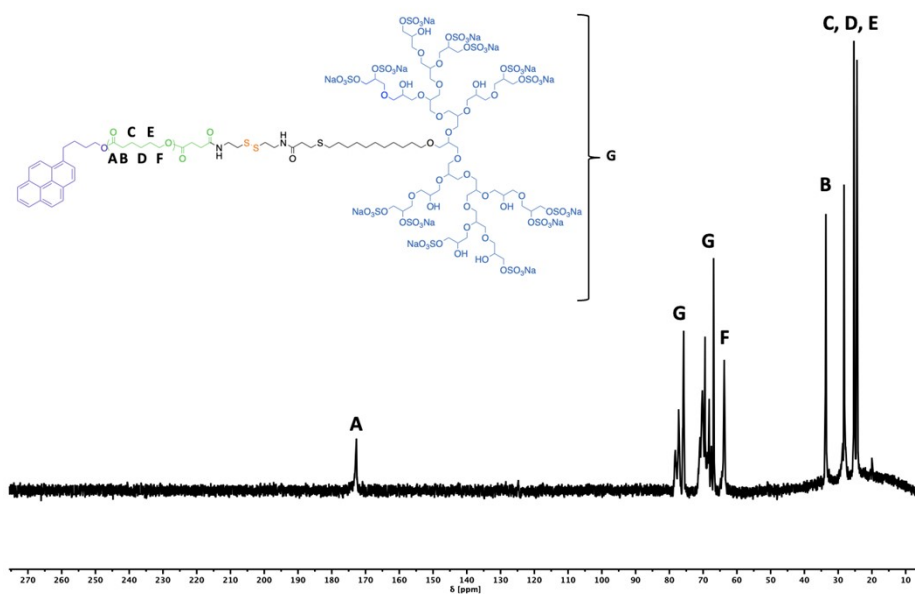


Figure S 19. <sup>13</sup>C NMR spectrum (700 MHz) of dPGS-SS-PCL-Py in D<sub>2</sub>O.

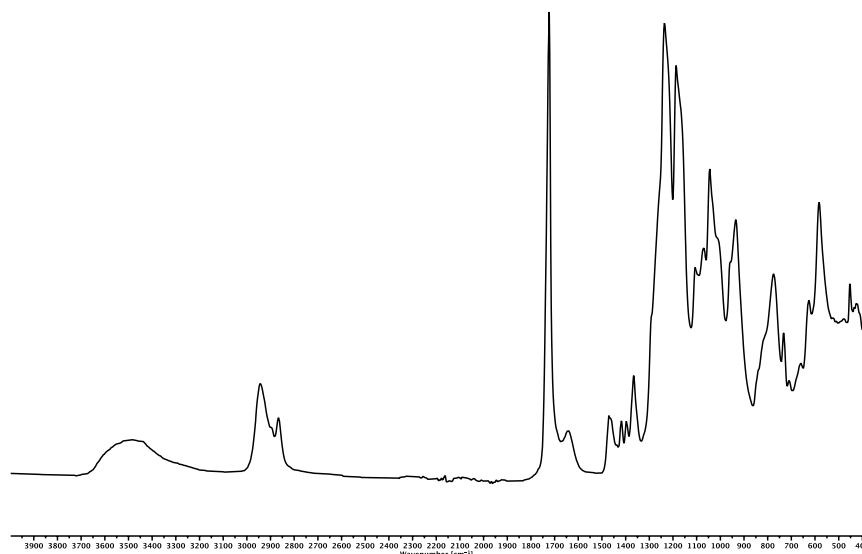
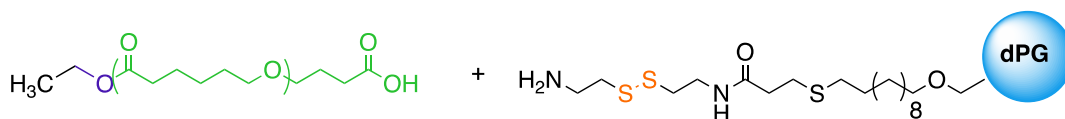


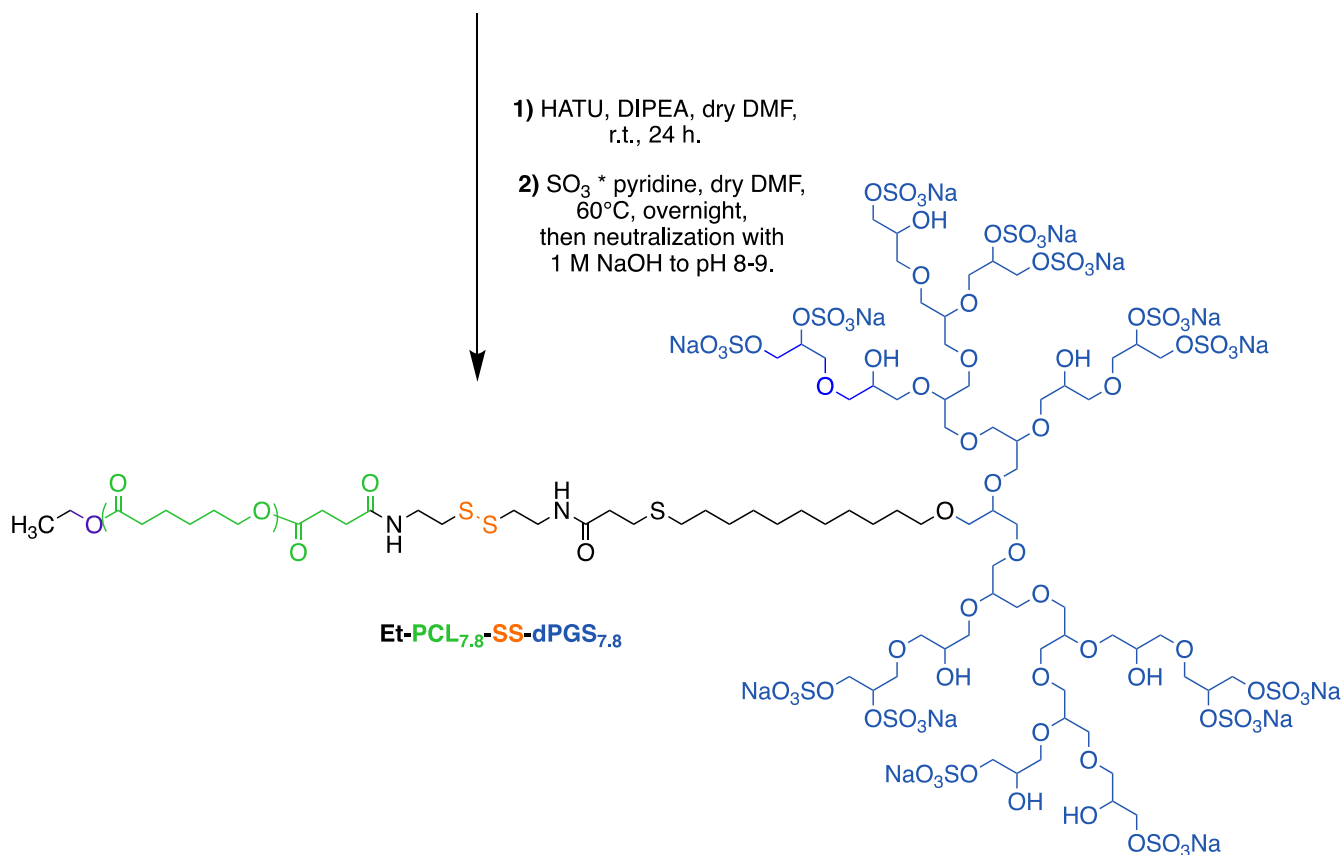
Figure S 20. FTIR spectrum of dPGS-SS-PCL-Py.

## Synthesis of dPGS-SS-PCL-Et



1) HATU, DIPEA, dry DMF,  
r.t., 24 h.

2) SO<sub>3</sub> \* pyridine, dry DMF,  
60°C, overnight,  
then neutralization with  
1 M NaOH to pH 8-9.



The synthesis, <sup>1</sup>H NMR, GPC, and EA analysis are described elsewhere in more detail.<sup>[2]</sup>

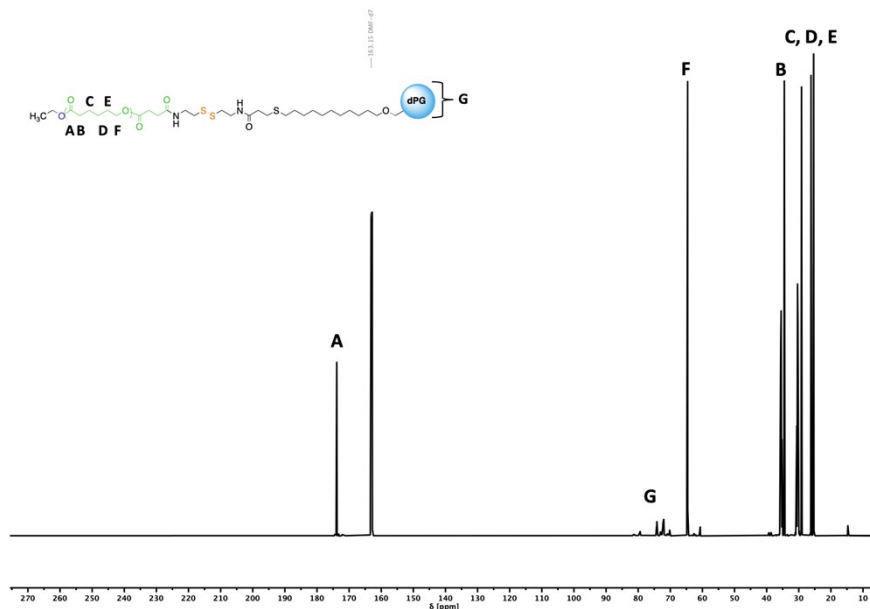


Figure S 21.  $^{13}\text{C}$  NMR (700 MHz) of dPG-SS-PCL-Et in  $\text{DMF-d}_7$ .

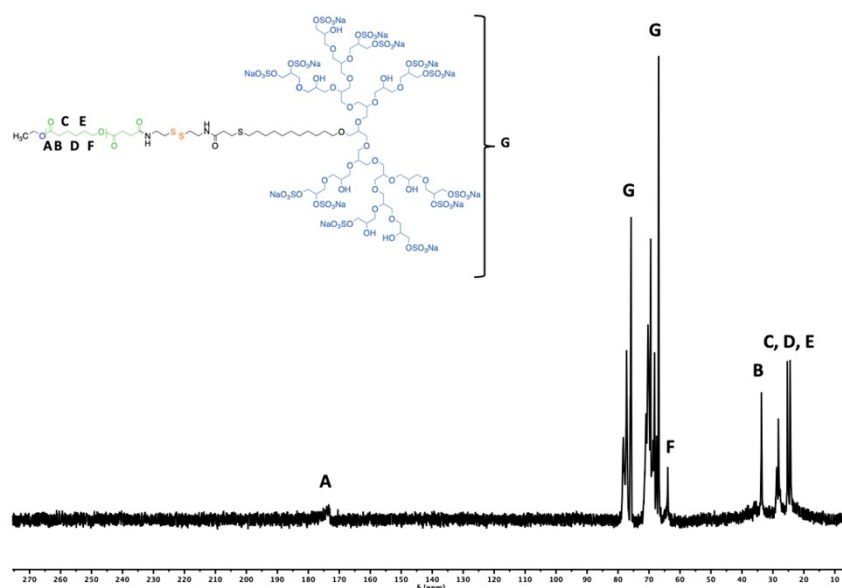


Figure S 22.  $^{13}\text{C}$  NMR (700 MHz) of dPGS-SS-PCL-Et in  $\text{D}_2\text{O}$ .

FTIR ( $\nu$ ,  $\text{cm}^{-1}$ ) = 1725 (C=O, ester); 1643 (C=O, sec. amide)

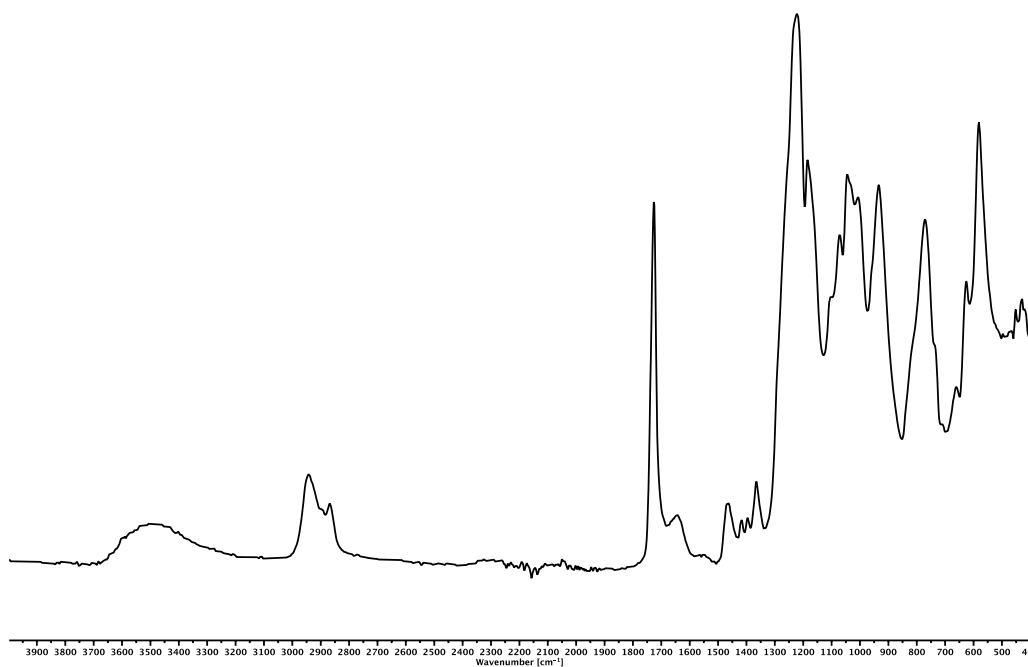
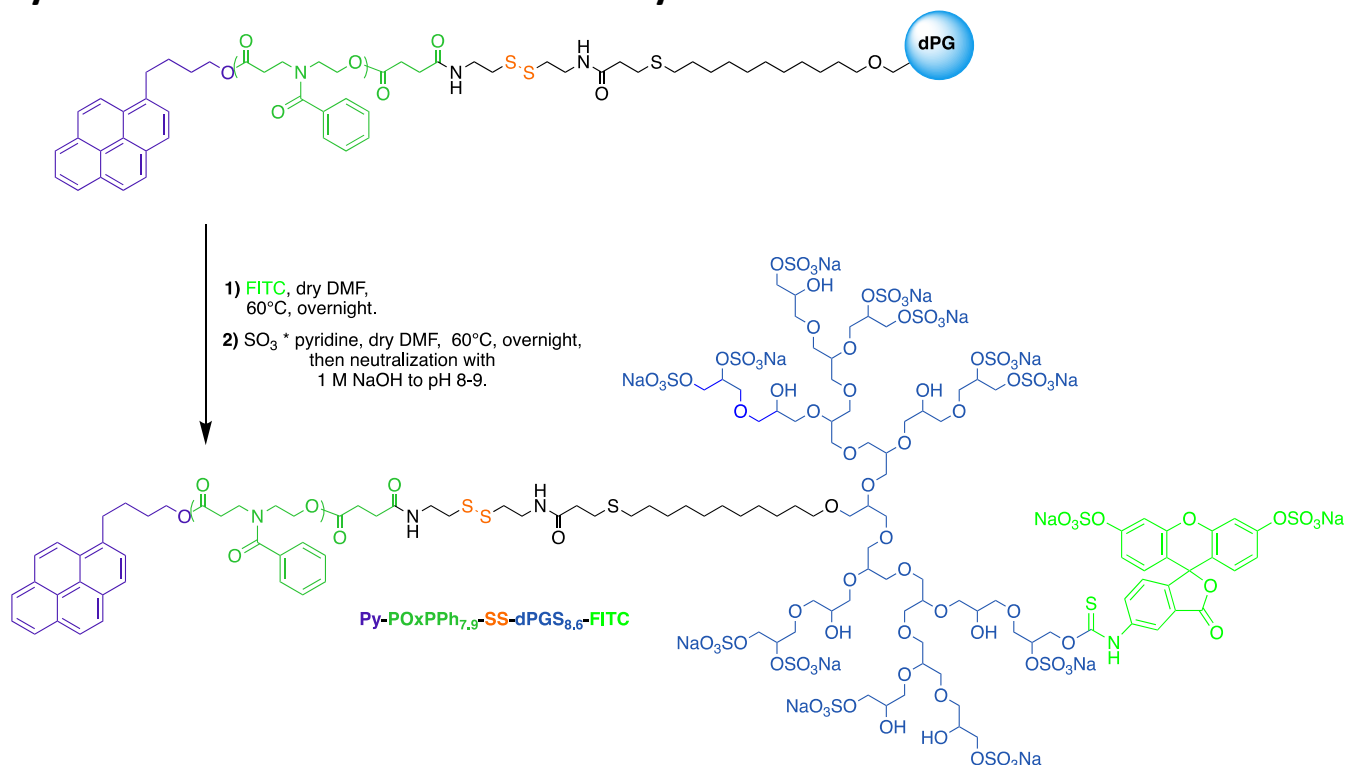


Figure S 23. FTIR spectrum of dPGS-SS-PCL-Et.

## Synthesis of FITC-dPGS-SS-POxPPh-Py



FITC-labeling of the copolymer, FITC (0.018 g, 0.045 mmol), and dPG-SS-POxPPh-Py (150 mg) were dissolved in 5 mL of dry DMF. The solution was heated to 60°C and stirred overnight in the dark. Next, slowly added SO<sub>3</sub>\*pyridine (0.35 g, 2.22 mmol) dissolved in 10 mL of dry DMF. After further stirring at 60°C overnight, the solution was quenched by adding 1M NaOH until a pH of 8 was reached. The labeled polymer was dialyzed against brine with an ever-decreasing salt content over a period of 5 days. The solution was concentrated, and free dye was removed with an SEC Sephadex G-25 column, where the

yellow band of the labeled polymer was collected. After lyophilization, the polymer obtained was a yellow powder (252 mg).  $^1\text{H}$  NMR and UV spectroscopy characterized the product. Degree of Sulfation (EA): 84%.

According to the calibration curve, the coupling efficiency of the FITC-labeling was 30% (6.72  $\mu\text{g}/\text{mL}$  (17  $\mu\text{M}$ ) of FITC in 1 mg/ml of copolymer solutions).

FTIR ( $\nu$ ,  $\text{cm}^{-1}$ ) = 1734 (C=O, ester); 1633 (C=O, tert. amide)

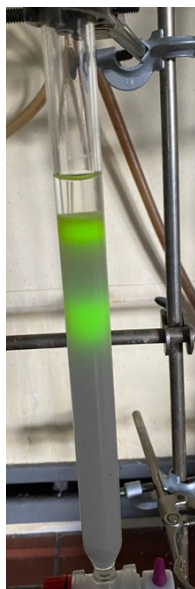


**Figure S 24.** Picture of the Sephadex G-25 column of FITC-dPGS-SS-POxPPh-Py showing free dye on top of the column; the polymer ran as a sharp band and was collected. The sample was irradiated by UV light at 366 nm).

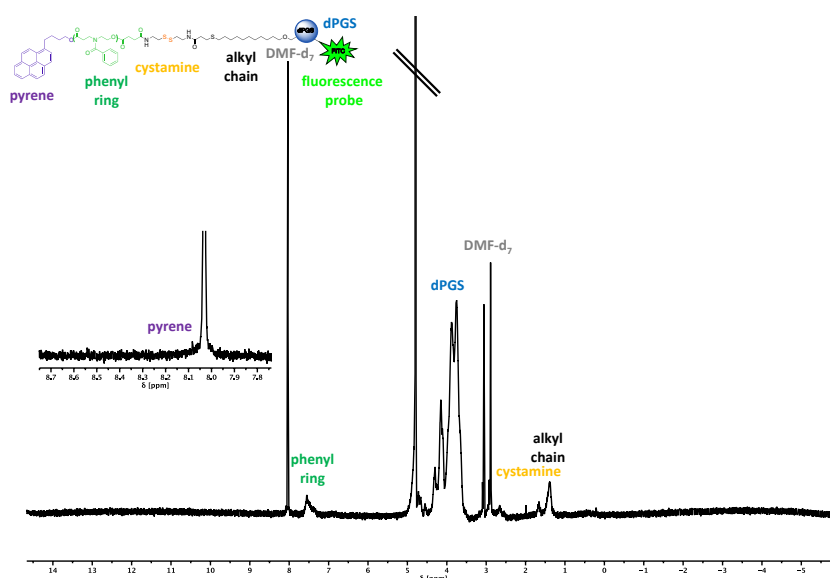


**Figure S 25.**  $^1\text{H}$  NMR spectrum (500 MHz) of FITC-dPGS-SS-POxPPh-Py in  $\text{DMF-d}_7:\text{D}_2\text{O}$  1:1.

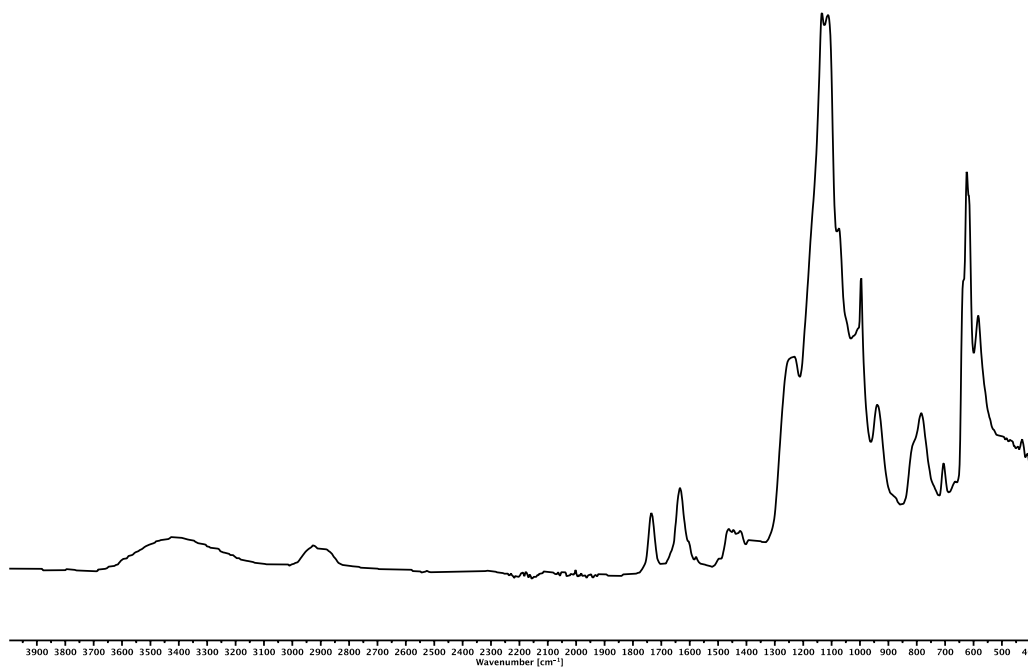


**Figure S 26.** FTIR spectrum of FITC-dPGS-SS-POxPPh-Py.

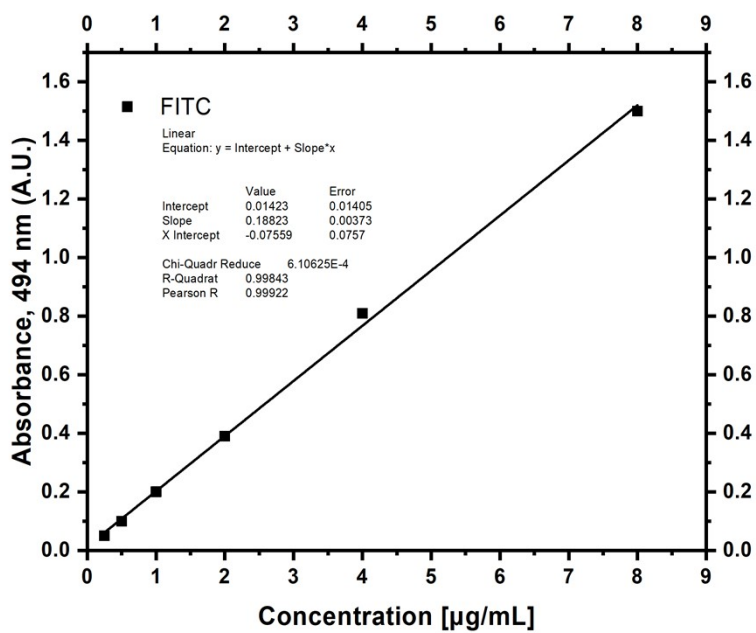


**Figure S 27.** UV-VIS Calibration curve of FITC in PBS using different concentrations of the dye.

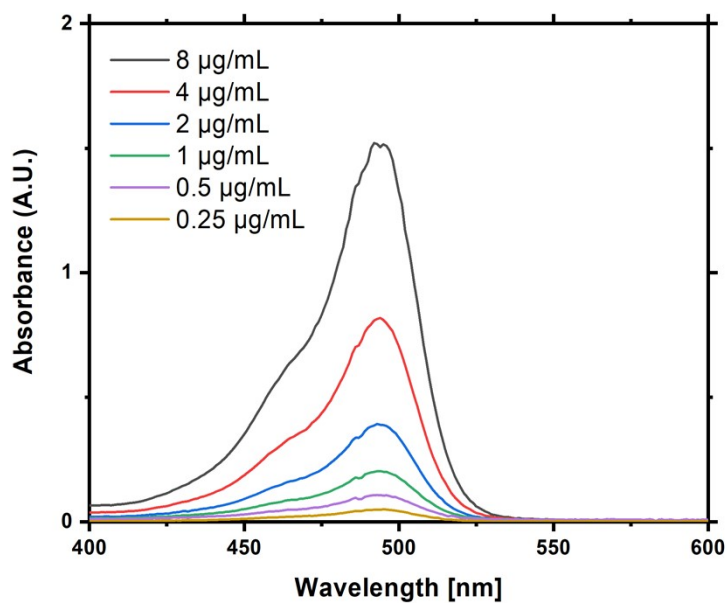


**Figure S 28.** UV-VIS calibration curve of FITC in PBS using different concentrations of the dye.

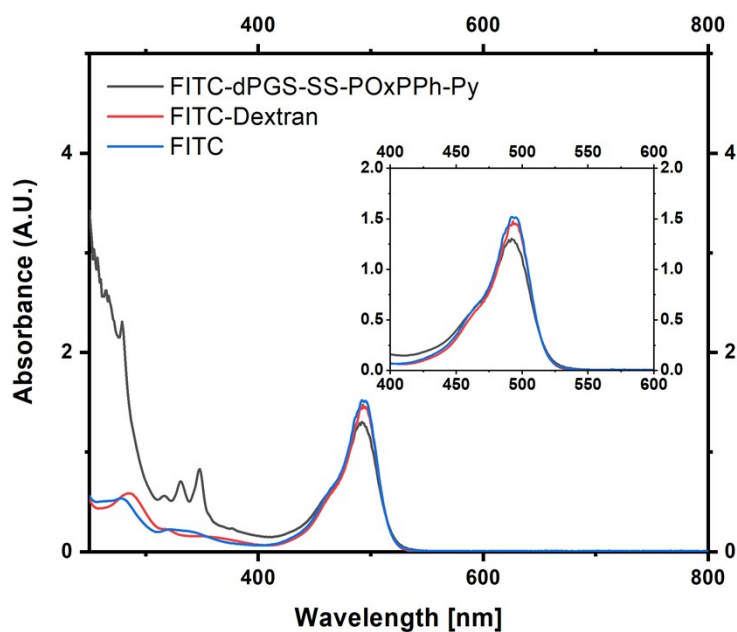


**Figure S 29.** UV-VIS spectra of FITC-labeled dPGS-SS-POxPPh-Py, FITC-labeled Dextran as control, and free FITC in PBS at 37 °C.

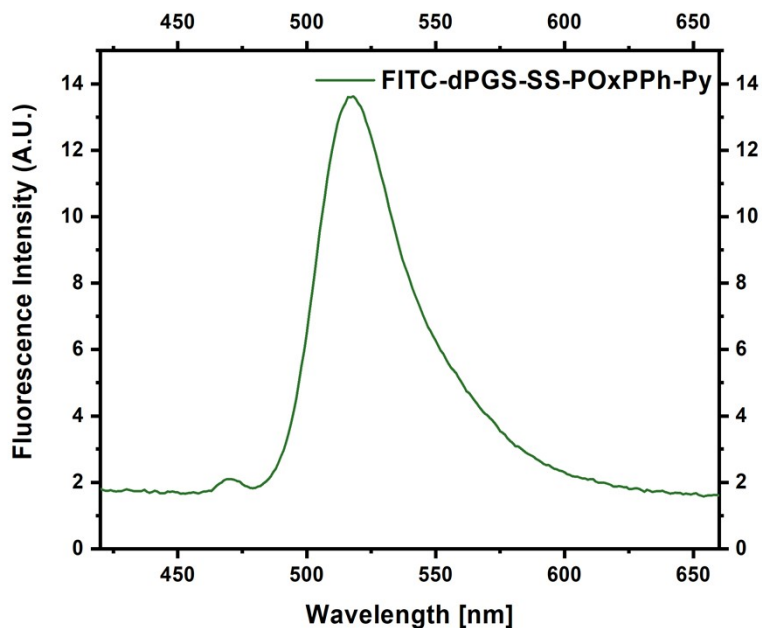


**Figure S 30.** Fluorescence spectrum of FITC-dPGS-SS-POxPPh-Py ( $\lambda_{ex}$  405 nm) in PBS at 37 °C at 65  $\mu\text{g/mL}$ .

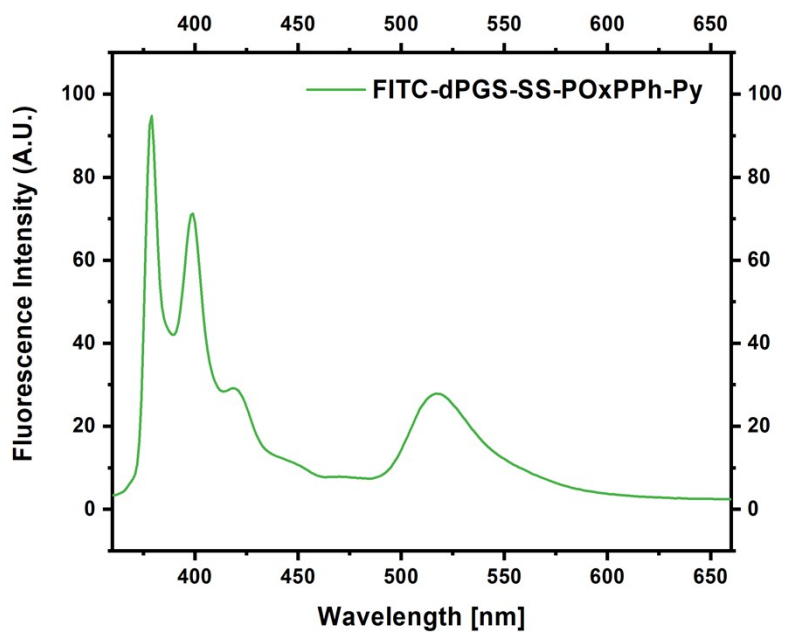


**Figure S 31.** Fluorescence spectrum of FITC-dPGS-SS-POxPPh-Py ( $\lambda_{ex}$  350 nm) in PBS at 37 °C at 65  $\mu\text{g/mL}$ .



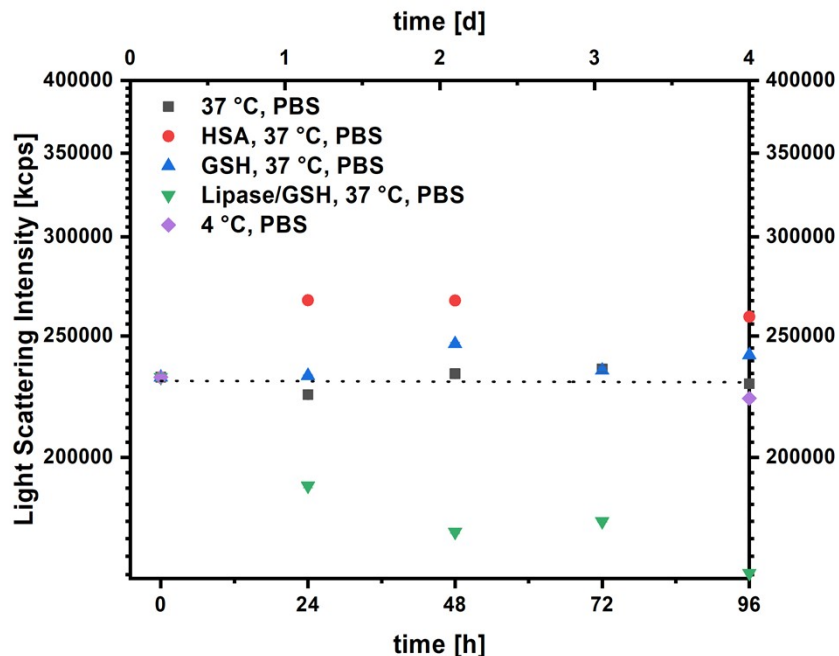


**Figure S 32.** Time-dependent DLS measurements on the evolution of the light scattering intensity of DTX@dPGS-SS-POxPPh-Py in different conditions: in PBS at 37 °C, pH 7.4 (black), and 4 °C, pH 7.4 (purple) as control; in the presence of HSA (red); GSH, pH 5.0 (blue); Lipase/GSH (green); according to  $I_{SLS} \sim C_{polymer}$  the light scattering intensity allows the determination of the concentration of scattering species in solution; as for the controls, constant intensities were detected, the particle's concentration was stable over 4 days; also for HSA, the intensity kept constant (notably, the initial increase is due to the addition of light scattering protein); GSH addition does not influence the concentration with no breakdown of the aggregates, however, by enzymatic degradation (lipase), the light scattering intensity drops constantly displaying the decrease of scattering species (disruption of micelles).

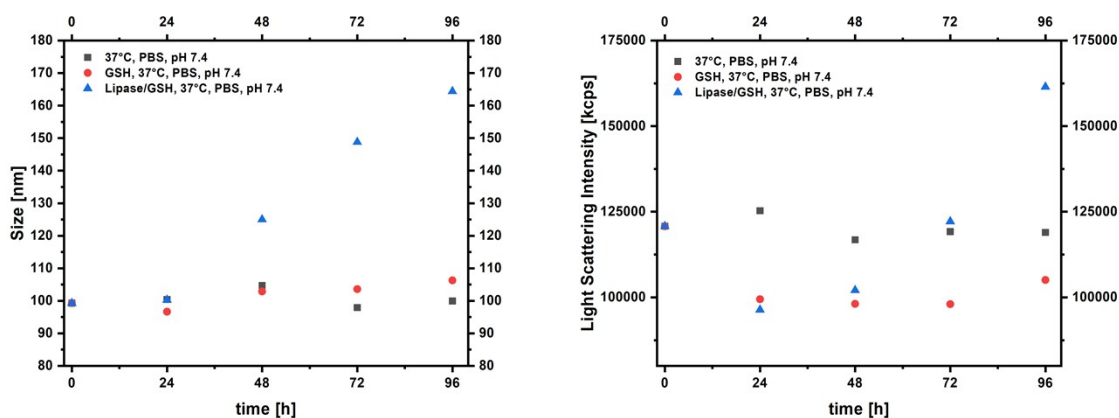


**Figure S 33.** Time-dependent DLS measurements on the evolution of the size (left) and the light scattering intensity (right) of DTX@dPGS-SS-POxPPh-Py in different conditions: in PBS at 37 °C, pH 7.4 (black, as control); in the presence of GSH, pH 7.4 (red); Lipase/GSH, pH 7.4 (blue). For the control sample, the size and light scattering intensity remained constant over 4 days; for GSH, pH 7.4, an initial decrease of the light scattering intensity was detected; however, after one day, it also remained constant, the size remained constant over 4 days; For Lipase/GSH, after an initial light scattering intensity decrease, the

*size and light scattering intensity have shown to increase, indicating swelling of the micelles upon enzymatic/reductive degradation.*

## **Dynamic Light Scattering Experiments (DLS) Measurements – Size and Size Distribution**

The size and size distribution of the micelles was investigated by DLS measurements as described above. In short, the micelles were measured at a fixed concentration of 1 mg/mL at 37 °C. A series of three measurements were performed to check the reproducibility of the experiments.

## **ζ-Potential Measurements**

The ζ-potential of the samples was measured using a Malvern Zetasizer Ultra (Malvern Instruments Limited, U.K.) in folded capillary cells (Malvern Analytics) at a constant temperature of 25 °C in 10 mM PB buffer solution at a fixed concentration of 1 mg/mL. The samples were calibrated for 2 min before the measurement was performed.

## **Dynamic Light Scattering (DLS) Measurements - Human Serum Albumin (HSA) Interaction with Micellar Surface**

First, the micelle was formed in PBS using the method described above. Next, the micellar solution got incubated with HSA with a fixed protein concentration of 10 mg/mL. The samples were incubated at 37 °C for various periods, and then, their size and distribution were measured as described above.

## **Dynamic Light Scattering (DLS) Measurements - Enzymatic Hydrolysis with Novozyme 435**

The micelles were incubated with 200 wt % Novozyme 435 concerning the polymer amount. For example, 1 mL of 1 mg/mL micelles solution in PBS was set with 2 mg of Novozyme and shaken at 37 °C for a predetermined time interval. The micelle integrity was investigated by DLS as described above.

## **Dynamic Light Scattering (DLS) Measurements - GSH- Triggered Shedding of Micelles**

In the case of GSH samples, the micelle was first formed using the described method above and then incubated in a solution containing 10 mM GSH with the same buffer. The samples were incubated at 37 °C for various periods, and then, their size and distribution were measured as described above.

## **Dynamic Light Scattering Experiments (DLS) – Critical Micelle Concentration (CMC)**

The CMC was investigated following an established protocol.<sup>[2]</sup> The critical micelle concentration (CMC) was determined by measuring the light scattering intensity using a Malvern Zetasizer Ultra (Malvern Instruments Limited, U.K.) equipped with a 10 mW He–Ne laser operating at a wavelength of 632.8 nm. The scattered light was detected using the backscattering setting at an angle of 173° (NIBS, noninvasive backscatter). The measurements were carried out in 12 mm square glass cuvettes (Hellma Analytics) at a constant temperature of 37 °C, respectively. In the case of sizes at 37°C, the samples were incubated for at least 2 h at 37 °C. All samples were calibrated for 2 min before the experiment was performed. Briefly, the light scattering intensity was measured at various concentrations ranging from 0.015 µg/mL up to 1000 µg/mL starting from a 1 mg/mL stock solution by serial dilution with the respective buffer

solution at 25 °C. A series of three measurements were performed to check the reproducibility of the experiments.

## Determination of the CMC

The CMC was determined following an established protocol.<sup>[2]</sup> The CMC was determined by the use of the DLS technique, and aqueous polymer solutions were prepared in respective buffer solutions. The concentration was not higher than 20-folds of the CMC to hinder any interaggregates of the micelles. The light scattering intensity (in kcps) was plotted against the concentration (in mg/L). A linear trend could be observed as the intensity of scattered light is proportional to the number of scattering particles. The linear behavior was no longer detected when the concentration was too high, indicating interaggregation occurred, and these concentrations were neglected. Subsequently, the light scattering intensity (in kcps) was plotted against the concentration (in mg/L) to determine the CMC where both axes were scaled logarithmically. Again, as the intensity of scattered light is proportional to scattering particles, a sharp increase in scattering intensity can be understood that amphiphilic unimers start forming aggregates. This point can be considered as CMC. Also, the derived count rate was approximated as a horizontal line when under-reaching the CMC since scattering is predominantly from the buffer system and can be correlated to be constant.

## Fabrication of Empty Micelles

5 mg of the respective polymer were suspended in 500 µL of acetone (HPLC grade). Next, 100 µL of the separate buffer, e.g., PBS or PB buffer, was added, and the sample was placed in an ultrasonic bath until a turbid solution without precipitation was obtained. This solution was slowly added to a stirred solution of the same buffer (4.90 mL) as used in the step before. Finally, the acetone was removed under vacuum. MilliQ again adjusted the volume to a final volume of 5 mL ( $c_{\text{polymer}} = 1 \text{ mg/mL}$ ). In all cases, clear solutions without precipitation were obtained. As described above, the formed micelles were analyzed in terms of their size, stability, size distribution, and ζ-Potential. The prepared micelles were stored at 4°C in the fridge.

## Fabrication of Docetaxel-loaded Micelles

1 mg of Docetaxel and 5 mg of the respective polymer were suspended in 500 µL of acetone (HPLC grade). Next, 100 µL of the buffer, e.g., PBS or PB buffer, was added, and the sample was placed in an ultrasonic bath until a turbid solution without precipitation was obtained. This solution was slowly added to a stirred solution of the same buffer (4.90 mL) as used in the step before. Finally, the acetone was removed under vacuum. MilliQ again adjusted the volume to a final volume of 5 mL ( $c_{\text{polymer}} = 1 \text{ mg/mL}$ ). To remove the non-encapsulated drug, the solution was passed through a 0.2 µm RC syringe filter. In all cases, clear solutions without precipitation were obtained. As described above, the formed micelles were analyzed in terms of their size, stability, size distribution, and ζ-Potential. The prepared micelles were stored at 4°C in the fridge. For the detection of the drug-loading content of Docetaxel, the micelle formulations were freeze-dried, and the dry powder was resuspended in 70:30 Acetonitrile/water. The DTX concentration was then detected by HPLC analysis (83 bar, UV detection: 227 nm). The standard curve was prepared by serial dilution of a 1 mg/mL stock solution of DTX ranging from 250 µg/mL to 16 µg/mL Acetonitrile/water 70:30. The Drug Loading Efficiency (DLE%) and Drug Loading Capacity (DLC in wt%) were calculated accordingly:

$$DLC\% = \frac{\text{Weight of DTX in Nanoformulation}}{\text{Weight of Sample}} \times 100\%$$

$$DLE\% = \frac{\text{Weight of DTX in Nanoformulation}}{\text{Weight of total DTX added}}$$

## **Cell Viability Tests (CCK-8 Assay, Dulbecco's Modified Eagle's Medium (DMEM), 48 h).**

Cells were seeded in a transparent 96-well plate with a density of 10 000 cells per well and cultured for 24 h. The medium (DMEM) was removed and replaced with a medium containing micelle (empty or loaded), followed by 48 h of incubation. Subsequently, 10  $\mu$ L of premixed Cell Counting Kit-8 (CCK-8) solution (Dojindo Molecular Technologies, Inc., Rockville), containing the proprietary WST-8 tetrazolium salt, was added to each well. Viable cells reduce this salt to a formazan dye whose absorbance can be measured in the medium. The absorbance was measured at 450 nm using a Tecan Infinite 200 Pro microplate reader after 2 h. Three independent experimental runs with triplicates were performed (n = 3).

## **Cryo-TEM measurements**

Perforated carbon film-covered microscopical 200 mesh grids (R1/4 batch of Quantifoil, MicroTools GmbH, Jena, Germany) were cleaned with chloroform and hydrophilized by 60 s glow discharging at 10 mA in a Safematic CCU-010 device (safematic GmbH, Zizers, Switzerland). Subsequently, 4  $\mu$ l aliquots of the sample solution were applied to the grids. The samples were vitrified by automatic blotting and plunged to freezing with an FEI Vitrobot Mark IV (Thermo Fisher Scientific Inc., Waltham, Massachusetts, USA) using liquid ethane as a cryogen. The vitrified specimens were transferred to the autoloader of an FEI TALOS ARCTICA electron microscope (Thermo Fisher Scientific Inc., Waltham, Massachusetts, USA). This microscope is equipped with a high-brightness field-emission gun (XFEG) operated at an acceleration voltage of 200 kV. Micrographs were acquired on an FEI Falcon 3 direct electron detector (Thermo Fisher Scientific Inc., Waltham, Massachusetts, USA) using a 100  $\mu$ m objective aperture.

## **Spectral studies: UV-VIS Measurements**

For UV-VIS measurements, the samples were prepared as described above. The samples were measured using an Agilent Cary 8454 in 12 mm square glass cuvettes (Hellma Analytics) at a constant temperature of 37  $^{\circ}$ C. Before every measurement, a background measurement was performed. All samples were calibrated for 2 minutes at 37  $^{\circ}$ C.

## **Spectral studies: Fluorescence Measurements**

For fluorescence measurements, the samples were prepared as described above. The samples were measured using a JASCO FP-6500 spectrometer in 12 mm square glass cuvettes (Hellma Analytics) at a constant temperature of 37  $^{\circ}$ C. Before every measurement, a background measurement was performed. All samples were calibrated for 2 minutes at 37  $^{\circ}$ C. For pyrene detection, the samples were excited at a wavelength of  $\lambda_{ex} = 350$  nm. For FITC detection, the samples were excited at a wavelength of  $\lambda_{ex} = 480$  nm.

## CMC determinations of empty/DTX-loaded dPGS-SS-PCL-Et, dPGS-SS-PCL-Py, and dPGS-SS-POxPPh-Py

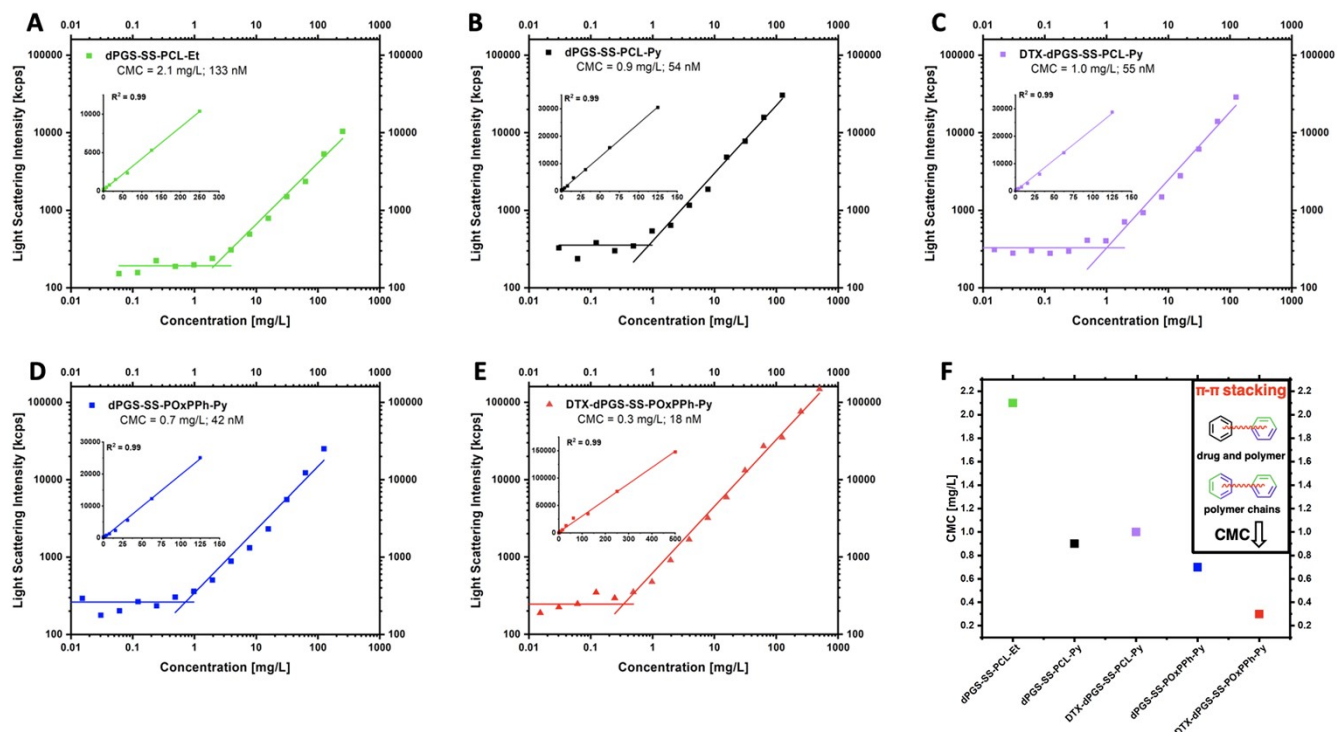


**Figure S 34.** CMC determinations of (A) dPGS-SS-PCL-Et (B) dPGS-SS-PCL-Py (C) DTX-dPGS-SS-PCL-Py (D) dPGS-SS-POxPPh-Py (E) DTX-dPGS-SS-POxPPh-Py; in PBS at 37 °C by a light scattering experiment with different concentrations (inset: linear dependencies of the count rate and concentration;  $R^2 = 0.99$ ) (F) influence of the  $\pi$ -electron density on the CMC;  $\pi$ - $\pi$  interactions significantly decrease the CMC.

## Cross-Polarization Solid-State $^{13}\text{C}$ NMR of free DTX, Empty dPGS-SS-POxPPh-Py, and dPGS-SS-POxPPh-Py@DTX

The  $^{13}\text{C}$  CP solid-state measurements were conducted at 8.8 T using a JEOL ECZ600 spectrometer operating at 600 MHz proton resonance. The samples were freshly prepared in aqueous solutions as described above, followed by lyophilization to obtain dry powders. The powders were mortared, and 30 mg of the respective sample was loaded onto the MAS rotors (diameter: 3.2 mm). All chemical shifts are reported relative to Adamantane ( $^{13}\text{C}$ ) as an external reference.

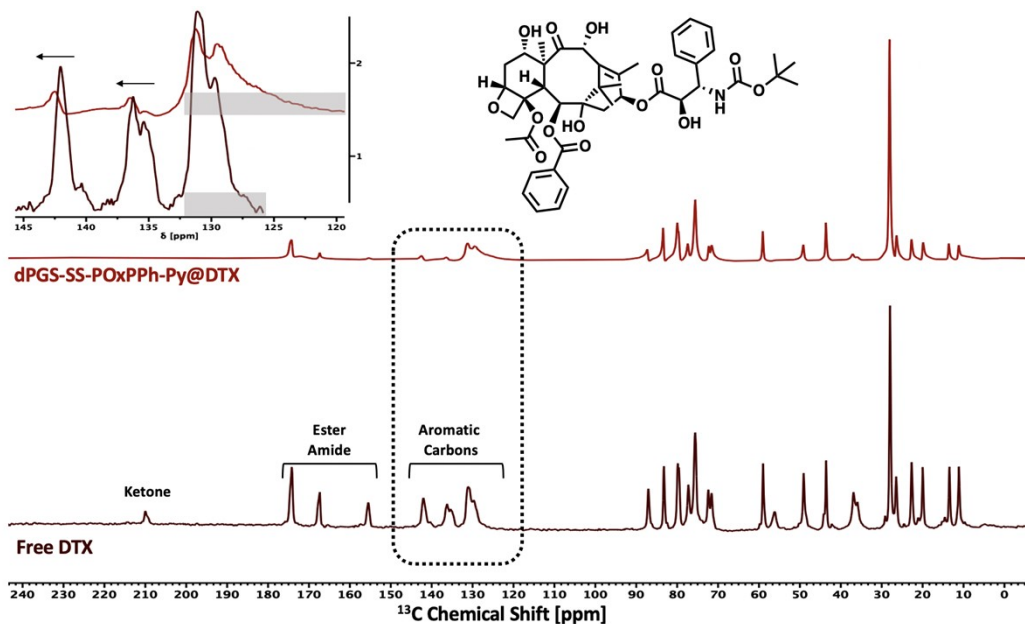


**Figure S 35.** Solid-State  $^{13}\text{C}$  CP NMR spectra of free DTX (below, dark red), and  $\text{dPGS-SS-POxPPh-Py@DTX}$  formulation (above, light red). An enlarged section from the stacked spectra shows the aromatic carbons of DTX as they appear mainly to be affected by the interaction with the polymer. A general trend of broader (grey areas) and slightly shifted signals (indicated by arrows to the left) in the formulation compared to the free drug can be found.

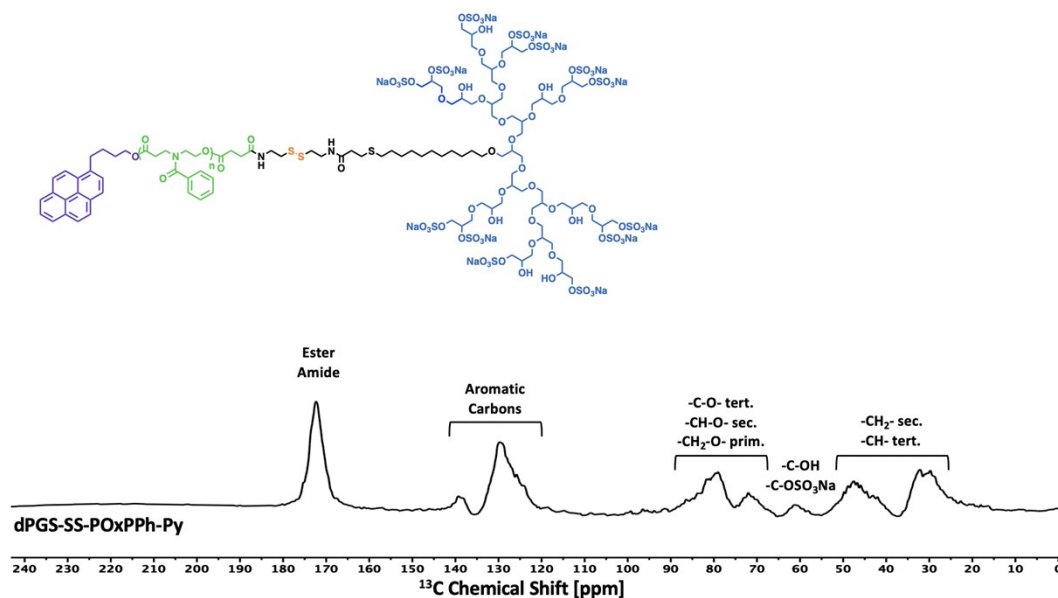


**Figure S 36.** Solid-State  $^{13}\text{C}$  CP spectrum of empty  $\text{dPGS-SS-POxPPh-Py}$ .

## References

- [1] X. Wang, N. Hadjichristidis, *ACS Macro Letters* **2020**, *9*, 464-470.
- [2] D. Braatz, M. Dimde, G. Ma, Y. Zhong, M. Tully, C. Grötzinger, Y. Zhang, A. Mavroskoufis, M. Schirner, Z. Zhong, M. Ballauff, R. Haag, *Biomacromolecules* **2021**, *22*, 2625-2640.

## 5 Conclusion and Outlook

This thesis aimed to investigate dendritic polyglycerolsulfate as a replacement for PEG in the construction of targeted drug delivery systems. For the design, functional amphiphilic block copolymer micelles were desired with defined molecular weight ratios between the hydrophilic and the hydrophobic segments. Additionally, this work investigated the influence on the stability dictated by the core-forming polymer's nature by employing different cohesive forces to the core segment, including hydrophobic and  $\pi$ - $\pi$  interactions. To our understanding, a low CMC is an indispensable criterium for the clinical application of self-assembled systems; thus, the goal was to obtain highly stable drug-delivery micelles that resist high dilution in the patient's bloodstream. The *in vitro* cell compatibility, *in vivo* therapeutic efficacy, safety, and biodistribution were investigated in suitable cell and animal models as a final proof of concept.

In the first project, well-defined dPGS-SS-PCL/PLA/PLGA amphiphilic block copolymers were prepared by organo-catalyst-mediated ROP of the respective monomers caprolactone, lactide, and lactide/glycolide forming the hydrophobic block; aROP of glycidol followed by amide coupling of cysteamine gave the hydrophilic segment (dPG-SS-NH<sub>2</sub>). Finally, amide coupling of these blocks and subsequential sulfation acquired the functional amphiphilic block copolymers with defined molecular weight ratios. The morphology, size, surface charge, and, most importantly, their stabilities were systematically analyzed using cryo-EM and light scattering techniques. The spherical particles showed monodispersed size distributions in the 81–187 nm range, strong negative charges between –52 and –41 mV, and low critical micelle concentrations (CMCs) of up to 1.13–3.58 mg/L (134–527 nM). As the model drug, Sunitinib was chosen, which could be successfully encapsulated in the carriers, finding drug-loading efficiencies of 38 to 83% (8–17 wt%). The selective drug release was proven in both *in vitro* and *in vivo* studies. The serum protein interaction and stability in the presence of HSA, the most abundant serum protein, was studied by light scattering and fast protein liquid chromatography (FPLC), revealing neither interaction nor disassembly of the carriers (serum stability 24 h: 94%). Compared to the nonsulfated dPG-SS-PCL-Et micelles, their sulfated analogs enabled the substantial accumulation of the carrier systems in the cancerous tissue (tumor and metastasis) in an HT-29 tumor-bearing mice. The detection of the fluorophore in the cancerous tissue after even seven days upon administration points to a prolonged release profile of these carriers, suggesting that the micelles could serve as a kind of depot for the drug. The sustained release profile was also indicated by *in vitro* drug release experiments simulating the environment of cancer cells by adding glutathione (GSH) and enzymes (surface-immobilized lipase), showing 85% drug release after four days with low leaching of only 20%. For testing the therapeutic efficacy and safety of the dPGS-SS-PCL-Et micelles, an

HeLa-tumor-bearing mice model was established, and the mice were treated with (i) PBS serving as control; (ii) free Sunitinib which was applied daily in the first 12 days in concentrations of 40 mg/kg for each injection (twelve injections each  $c_{\text{Sunitinib}} = 40 \text{ mg/kg} = 480 \text{ mg/kg}$ ; 1 equiv.); and (iii) dPGS-SS-micelle-encapsulated Sunitinib was administered on days 1, 4, 7, 10, and 13 with a reduced drug concentration of 10 mg/kg for each injection (five injections each  $c_{\text{Sunitinib}} = 10 \text{ mg/kg} = 50 \text{ mg/kg}$ ; 0.1 equiv.). After 40 days, no tumor growth inhibition was detected for PBS, resulting in a tumor size of  $947 \text{ mm}^3$  from an initial size of  $71 \text{ mm}^3$  (total growth rate: 1,333%). Free Sunitinib inhibited the tumor growth as the size after 40 days was  $421 \text{ mm}^3$  (total growth rate: 592%). However, for the micelle-supported treatment with a 10-fold lower drug dosage, the total growth rate was successfully decreased to 523%, final size:  $372 \text{ mm}^3$ ). Also, the prolonged release profile was observed, as the tumor growth was suppressed until day 30, or 17 days after the last injection. Further, neither the administration of PBS nor free Sunitinib had adverse effects on the body weight or the tissue of the mice's organs, such as the heart or liver, and so did the dPGS-SS-micelles therapy. Thus, dPGS could successfully enhance the therapeutic potential with no adverse side effects to the organism.

In the second project, the hydrophobic segment was changed to recently published poly(ester amide)s, so-called N-Acylated-1,4-oxazepan-7-ones (OxP), enabling the straightforward preparation of polymers with a tailored number of aromatic moieties in their sidechain. This modification aimed to answer whether the stability of the systems from project 1 can be further increased to boost their therapeutic potential. For this, the intrinsic targetability of dendritic polyglycerolsulfate toward cancerous tissue was combined with  $\pi$ -electron stabilization, which has already proven its great potential in clinically tested candidates. To understand the influence of  $\pi$ -electron-rich domains on stability, a library of three different amphiphilic block copolymers with varying  $\pi$ -electron density was designed, including (i) with no  $\pi$ -electrons (dPGS-SS-PCL-Et); (ii) with  $\pi$ -electrons located on the chain end (dPGS-SS-PCL-Py); and (iii) with  $\pi$ -electron distributed along the hydrophobic polymer block (dPGS-SS-POxPPh-Py). Again, the morphology, size, and surface charge were systematically analyzed using cryo-EM and light scattering techniques. The spherical particles showed monodispersed size distributions in the 81–129 nm range, with strong negative charges between  $-44$  and  $-34 \text{ mV}$ . Quantitatively light scattering experiments show extremely low critical micelle concentrations (CMCs) of up to 0.3–2.1 mg/L (18–133 nM), which is 55-fold lower than conventional block copolymer micelles. Additional studies by UV-VIS, Fluorescence, and solid-state  $^{13}\text{C}$  Cross-Polarization NMR proved the presence of  $\pi$ - $\pi$  interactions in the aromatic micellar core between the polymer chains and the cargo, pointing to a substantial contribution of these noncovalent interactions to the system's high stability. Also, the micelles are stable under



physiological conditions with no blood serum protein absorption on their surface after four days. The precise *in vitro* degradation by reductive and enzymatic cleavage is analyzed using light scattering and gel permeation chromatography (GPC) experiments. The high potency of inhibiting cancer cell growth by the DTX-formulations on different tumor-derived cell lines also points to the selective drug release in cancerous tissue, revealing half-maximal inhibitory concentrations ( $IC_{50}$ ) efficiently reduced to 68 nM. Confocal laser scanning microscopy (CLSM) monitored the successful cell insertion of the micelles by fluoresceine-labeled FITC-dPGS-SS-POxPPh-Py. All in all, this study allows more profound insights into the conception of drug delivery systems, starting at their synthesis, continuing with the systematic screening of their stability, understanding their molecular self-assembly, and finally, *in vitro* performance regarding cellular uptake, cell tolerability, and cancer growth inhibition. Further, it demonstrates that implementing  $\pi$ -electron rich domains into self-assembled dPGS-SS-polymeric micelles holds great potential as drug delivery platforms.

This thesis has emphasized the potential of dPGS-SS-micelles for being a key figure in replacing PEG-containing carriers in drug delivery applications. The sulfation of the amphiphilic block copolymer scaffold had a tendinous impact on the biodistribution and has resulted in selective accumulation of the dPGS-micellar systems in the cancerous tissue with no accumulation in healthy tissue. Further, for the dPGS-SS-micelle-supported treatment, the required drug dosage to inhibit the tumor growth was efficiently reduced by 10-fold compared to administrating the free drug, minimizing undesired side effects on the worn-out patients. By employing  $\pi$ - $\pi$  interactions to the micellar core, the stability was increased to CMCs in the range of 0.3 mg/mL, 55-fold lower than that of conventional micellar systems.

For future investigations, it is crucial to understand the underlying cancer-targeting mechanism of dPGS-functionalized systems. Several techniques, such as isothermal titration calorimetry (ITC) or microscale thermophoresis (MST), have already been established for comparable systems, enabling the detection of intermolecular interactions of the polymer with another (bio)macromolecule of interest. Also, the immunogenicity and antigenicity of dPGS systems have yet to be studied; for PEG, anti-PEG IgG and IgM antibodies are the main antagonists for the immune response. After the worldwide vaccination campaign to defeat the COVID-19 pandemic, this problem will certainly become even more prominent. To answer this question, enzyme-linked immunosorbent assay (ELISA) or surface plasmon resonance (SPR) experiments should be performed to detect possible interactions of these antibodies with the polymer. All these experiments must be conducted concerning the physiological conditions in the bloodstream and the cancer cell environment.

Regarding the polymer design, the installment of chemical crosslinking to the core and the drug should be considered, as these systems can completely overcome leaching events or disassembly in the bloodstream. Another critical aspect tackles the availability and supply of these drug delivery systems. Again, the COVID-19 pandemic revealed another bottleneck: the challenges of cold chain supplies. Therefore, the freeze-drying process of these medications must be studied to ensure a constant and cost-effective supply. The knowledge of already market-authorized lyophilized nanoformulations can most likely be exploited for dPGS-SS-micelles; core-crosslinking also has shown to be beneficial in the free-drying process.<sup>[198]</sup>

## 6 Zusammenfassung

Das Ziel dieser Arbeit war es, dendritisches Polyglycerolsulfat als Ersatz für PEG bei der Konstruktion zielgerichteter Arzneimittelabgabesysteme zu untersuchen. Für das Design wurden verschiedene funktionelle amphiphile Blockcopolymermicellen, mit jeweils wohl definierten Molekulargewichtsverhältnissen zwischen den hydrophilen und den hydrophoben Segmenten, synthetisiert. Darüber hinaus wurde in dieser Arbeit der Einfluss des kernbildenden Polymers auf die Stabilität untersucht, indem verschiedene Kohäsionskräfte in das Kernsegment eingebettet wurden, darunter waren sowohl hydrophobe als auch  $\pi$ - $\pi$ -Wechselwirkungen. Unserem Verständnis nach ist eine niedrige kritische Micellenkonzentrationen (engl. CMC) ein unverzichtbares Kriterium für die klinische Anwendung von selbstorganisierten Systemen. Aus diesem Grund war es das Ziel, stabile Mizellen für die Medikamentenabgabe zu erhalten, die einer hohen Verdünnung im Blutkreislauf des Patienten standhalten. Die *in vitro* Zellkompatibilität, die *in vivo* Therapiewirksamkeit, die Pharmakodynamik (engl. Safety) und die Biodistribution wurden in geeigneten Zell- und Tiermodellen untersucht, um einen endgültigen Konzeptnachweis zu erbringen.

Im ersten Projekt wurden wohldefinierte amphiphile dPGS-SS-PCL/PLA/PLGA-Blockcopolymerere durch Organokatalysator-vermittelte Ringöffnende Polymerisation (engl. ROP) der jeweiligen Monomere Caprolacton, Lactid und Lactid/Glycolid hergestellt, die jeweils den hydrophoben Block bildeten. Anionische Ringöffnende Polymerisation (engl. aROP) von Glycidol, gefolgt von einer Amidkopplung von Cysteamin, ergab das hydrophile Segment (dPG-SS-NH<sub>2</sub>). Die Amidkopplung dieser beiden Blöcke und die anschließende Sulfatierung ergaben schlussendlich die funktionellen amphiphilen Blockcopolymerere mit definierten Molekulargewichtsverhältnissen. Die Micellen wurden hinsichtlich ihrer Morphologie, Größe, Oberflächenladung und vor allem ihrer Stabilität systematisch mit Hilfe von Kryo-EM und Lichtstreuungstechniken untersucht. Die sphärischen Partikel wiesen monodisperse Größenverteilungen im Bereich von 81-187 nm, starke negative Ladungen zwischen -52 und -41 mV und niedrige kritische Micellenkonzentrationen (engl. CMC) von bis zu 1,13-3,58 mg/L (134-527 nM) auf. Als Modellarzneimittel wurde Sunitinib ausgewählt, das erfolgreich in die Träger eingekapselt werden konnte, wobei eine Beladungseffizienz von 38 bis 83 % (8-17 Gew.-%) erreicht wurde. Die selektive Wirkstofffreisetzung wurde sowohl in *in vitro* als auch in *in vivo* Studien nachgewiesen. Die Interaktion und Stabilität der Wirkstoffträgersysteme in Anwesenheit von HSA, dem häufigsten Serumprotein, wurde mittels Lichtstreuung und schneller Protein-Flüssigkeitschromatographie (engl. FPLC) untersucht, wobei weder eine Interaktion mit dem Protein noch das Auseinanderfallen der Wirkstoffträger festgestellt wurde.

(Serumstabilität 24 h: 94 %). Im Vergleich zu den nicht sulfatierten dPG-SS-PCL-Et Micellen ergaben ihre sulfatierten Analoga eine beträchtliche Anreicherung der Trägersysteme im Krebsgewebe (Tumor und Metastase) von Mäusen, die einen HT-29-Tumor trugen. Der Nachweis des Fluorophors im Krebsgewebe deutete sogar noch sieben Tage nach der Verabreichung auf ein verlängertes Freisetzungsprofil dieser Trägersysteme hin, was wiederum darauf hinwies, dass die Micellen als eine Art Depot für den Wirkstoff dienen könnten. Das verlängerte Freisetzungsprofil wurde auch durch *in vitro* Experimente, welche auf die gezielte Wirkstofffreisetzung abzielten, nachgewiesen. Bei diesen Experimenten wurde die Umgebung von Krebszellen durch die Zugabe von Glutathion (GSH) und Enzymen (oberflächenimmobilisierte Lipase) simuliert. Dabei wurde eine Wirkstofffreisetzung von 85 % nach vier Tagen bei einem geringen Wirkstoffverlust von nur 20 % beobachtet. Um die therapeutische Wirksamkeit und Verträglichkeit der dPGS-SS-PCL-Et Micellen zu testen, wurde ein HeLa-Tumor-tragendes Mausmodell etabliert, und die Mäuse wurden mit folgenden Therapien behandelt: (i) PBS diente als Kontrolle; (ii) freies Sunitinib, das in den ersten zwölf Tagen täglich in einer Konzentration von 40 mg/kg mit jeder Injektion verabreicht wurde (zwölf Injektionen je  $c_{\text{Sunitinib}} = 40 \text{ mg/kg} = 480 \text{ mg/kg}$ ; 1 Äquiv. ); und (iii) dPGS-SS-Micelle verkapseltes Sunitinib wurde an den Tagen 1, 4, 7, 10 und 13 mit einer reduzierten Wirkstoffkonzentration von 10 mg/kg bei jeder Injektion verabreicht (fünf Injektionen je  $c_{\text{Sunitinib}} = 10 \text{ mg/kg} = 50 \text{ mg/kg}$ ; 0,1 Äquiv.). Nach 40 Tagen wurde durch die Injektion von PBS keine Hemmung des Tumorwachstums festgestellt, was zu einer finalen Tumorgroße von 947 mm<sup>3</sup> bei einer Ausgangsgröße von 71 mm<sup>3</sup> führte (Gesamtwachstumsrate: 1.333 %). Freies Sunitinib hingegen hemmte das Tumorwachstum, da die Größe nach 40 Tagen 421 mm<sup>3</sup> betrug (Gesamtwachstumsrate: 592 %). Bei der micellengestützten Behandlung mit einer 10-fach geringeren Wirkstoffdosis wurde die Gesamtwachstumsrate erfolgreich auf 523 % gesenkt (Endgröße: 372 mm<sup>3</sup>). Außerdem wurde ebenfalls das verlängerte Freisetzungsprofil beobachtet, da das Tumorwachstum bis zum 30. Tag, also 17 Tage nach der letzten Injektion, unterdrückt wurde. Darüber hinaus hatte weder die Verabreichung von PBS noch von freiem Sunitinib nachteilige Auswirkungen auf das Körpergewicht oder das Gewebe der Mäuseorgane wie Herz oder Leber. Diese Beobachtung trifft ebenfalls auf die dPGS-SS-Micellen Therapie zu. Somit konnte dPGS das therapeutische Potenzial erfolgreich und ohne nachteilige Nebenwirkungen für den Organismus steigern.

Im zweiten Projekt wurde das hydrophobe Segment durch kürzlich publizierte Poly(esteramide), so genannte N-acylierte 1,4-Oxazepan-7-one (OxP), ersetzt. Dies soll die Herstellung von Polymeren mit einer maßgeschneiderten Anzahl aromatischer Einheiten in der Seitenkette ermöglichen. Mit dieser Modifikation sollte untersucht werden, ob die Stabilität der Systeme aus Projekt 1 weiter erhöht werden kann, um ihr therapeutisches Potenzial zu

steigern. Zu diesem Zweck wurde die intrinsische Eigenschaft von dendritischem Polyglycerolsulfat sich in Krebsgewebe anzureichern, mit der  $\pi$ -Elektronenstabilisierung kombiniert, wobei Letzteres bereits sein Potenzial bei klinisch getesteten Wirkstoffträgern unter Beweis stellen konnte. Um den Einfluss von  $\pi$ -Elektronen-reichen Domänen auf die Stabilität zu verstehen, wurde eine Bibliothek von drei verschiedenen amphiphilen Blockcopolymeren mit unterschiedlicher  $\pi$ -Elektronendichte entwickelt, darunter waren (i) ohne  $\pi$ -Elektronen (dPGS-SS-PCL-Et); (ii) mit  $\pi$ -Elektronen am Kettenende (dPGS-SS-PCL-Py); und (iii) mit  $\pi$ -Elektronen, die entlang des hydrophoben Polymerblocks verteilt sind (dPGS-SS-POxPPh-Py). Auch hier wurden die Morphologie, die Größe und die Oberflächenladung systematisch mit Kryo-EM und Lichtstreuungstechniken analysiert. Die sphärischen Partikel zeigten monodisperse Größenverteilungen im Bereich von 81-129 nm mit starken negativen Ladungen zwischen -44 und -34 mV. Quantitative Lichtstreuungsexperimente zeigten niedrige kritische Micellenkonzentrationen (engl. CMC) von bis zu 0,3-2,1 mg/L (18-133 nM), was 55-mal niedriger ist als die CMC von herkömmlichen Blockcopolymermicellen. Zusätzliche Untersuchungen mittels UV-VIS, Fluoreszenz und Festkörper  $^{13}\text{C}$ -Kreuzpolarisations-NMR bewiesen das Vorhandensein von  $\pi$ - $\pi$ -Wechselwirkungen zwischen den Polymerketten und des Wirkstoffes im aromatischen Micellenkern. Diese nicht-kovalenten Wechselwirkungen tragen einen erheblichen Anteil zu der hohen Stabilität dieses Systems bei. Außerdem wurde festgestellt, dass die Mizellen unter physiologischen Bedingungen stabil sind und dass nach vier Tagen kein Blutserumproteine auf ihrer Oberfläche absorbiert wurden. Der gezielte *in vitro* Abbau der Micellen durch reduktive und enzymatische Spaltung wird mit Hilfe von Lichtstreuungs- und Gelpermeationschromatographie-Experimenten (engl. GPC) analysiert. Die hohe Wirksamkeit der DTX-Formulierungen zur Hemmung des Krebszellwachstums bei verschiedenen Tumorzelllinien deutet ebenfalls auf die selektive Freisetzung des Wirkstoffes im Krebsgewebe hin, wobei die halbmaximale Hemmkonzentration (engl.  $IC_{50}$ ) effizient auf 68 nM reduziert wurde. Mit Hilfe der konfokalen Laser-Scanning-Mikroskopie (engl. CLSM) wurde die erfolgreiche Einlagerung der Micellen in die Krebszellen durch Fluorescein-markiertes FITC-dPGS-SS-POxPPh-Py untersucht. Zusammenfassend ermöglicht diese Studie tiefere Einblicke in die Konzeption von Wirkstofftransportsystemen, angefangen bei ihrer Synthese, der systematischen Untersuchung ihrer Stabilität und das Verständnis ihrer molekularen Selbstorganisation bis hin zu *in vitro* Studien hinsichtlich ihrer Zellaufnahme, Zellverträglichkeit und Hemmung des Krebswachstums. Außerdem wird gezeigt, dass die Implementierung von  $\pi$ -Elektronen-reichen Domänen in selbstorganisierten dPGS-SS-Polymermicellen großes Potenzial für die Verabreichung von Arzneimitteln hat.

Diese Arbeit hat das Potenzial von dPGS-SS-Micellen als Alternative zu PEG-haltigen Wirkstoffträgersystemen für die Verabreichung von Medikamenten zu dienen hervorgehoben. Die Sulfatierung des amphiphilen Blockcopolymer-Gerüsts hatte einen entscheidenden Einfluss auf die Verteilung der Systeme im Körper und führte zu einer selektiven Anreicherung der dPGS-SS-Micellensysteme im Krebsgewebe, ohne eine Anreicherung im gesunden Gewebe zu verursachen. Darüber hinaus wurde bei der dPGS-SS-Micellen gestützten Behandlung, die zur Hemmung des Tumorwachstums erforderliche Medikamentendosis im Vergleich zur Verabreichung des freien Medikaments um das 10-fache reduziert, wodurch unerwünschte Nebenwirkungen bei den Patienten minimiert werden können. Durch den Einsatz von  $\pi$ - $\pi$ -Wechselwirkungen im micellaren Kern konnte eine Stabilität im Hinblick auf die CMC von bis zu 0,3 mg/ml erreicht werden, was 55-mal niedriger ist als die CMC von herkömmlichen micellaren Systemen.

Für künftige Untersuchungen ist es von entscheidender Bedeutung, den zugrundeliegenden Mechanismus von dPGS-funktionalisierten Systemen zu verstehen, welcher die gezielte Anreicherung der Systeme im Krebsgewebe bewirkt. Für vergleichbare Systeme wurden bereits mehrere Techniken wie die isotherme Titrationskalorimetrie (engl. ITC) oder die mikroskalige Thermophorese (engl. MST) entwickelt, mit denen sich intermolekulare Wechselwirkungen eines Polymers mit einem anderen (Bio-)Makromolekül von Interesse untersuchen lassen. Auch die Immunogenität und Antigenität von dPGS-Systemen muss noch weiter im Detail untersucht werden. Bei PEG sind Anti-PEG-IgG- und IgM-Antikörper die wichtigsten Antagonisten für die Immunantwort. Nach der weltweiten Impfkampagne zur Bekämpfung der COVID-19-Pandemie wird dieses Problem sicherlich noch stärker in den Vordergrund treten. Zur Beantwortung dieser Frage sollten Experimente mit Enzymimmunoassays (engl. ELISA) oder Oberflächenplasmonenresonanz (engl. SPR) durchgeführt werden, um mögliche Wechselwirkungen dieser Antikörper mit dem Polymer zu untersuchen. Alle diese Experimente müssen in Hinsicht auf die physiologischen Bedingungen im Blutkreislauf und in der Umgebung des Krebsgewebes durchgeführt werden.

Bei der Gestaltung des Polymers sollte die chemische Vernetzung des Kerns und die Einbettung des Arzneimittels in dieses Netzwerk in Betracht gezogen werden, da diese Systeme den ungewünschten Wirkstoffverlust oder das Auseinanderfallen in der Blutbahn vollständig verhindern können. Ein weiterer kritischer Aspekt ist die Verfügbarkeit und Bereitstellung dieser Medikamentenverabreichungssysteme. Auch hier hat die COVID-19-Pandemie einen weiteren Engpass offenbart: die Herausforderungen der Kühlkettenversorgung. Daher muss ein Gefriertrocknungsverfahren für diese Medikamente entwickelt und untersucht werden, damit eine konstante und kostengünstige Versorgung gewährleistet werden kann. Das Wissen von bereits zugelassene gefriergetrockneten

Nanoformulierungen kann höchstwahrscheinlich für dPGS-SS-Micellen genutzt werden; die Kernvernetzung hat sich auch beim Gefriertrocknungsprozess als vorteilhaft erwiesen.<sup>[198]</sup>

## 7 References

- [1] R. L. Siegel, K. D. Miller, N. S. Wagle, A. Jemal, *Ca-Cancer J. Clin.* **2023**, *73*, 17-48.
- [2] N. Kamaly, B. Yameen, J. Wu, O. C. Farokhzad, *Chem. Rev.* **2016**, *116*, 2602-2663.
- [3] a) H. Cabral, K. Miyata, K. Osada, K. Kataoka, *Chem. Rev.* **2018**, *118*, 6844-6892; b) D. Hwang, J. D. Ramsey, A. V. Kabanov, *Adv. Drug Delivery Rev.* **2020**, *156*, 80-118.
- [4] X. Fan, Z. Li, X. J. Loh, *Polym. Chem.* **2016**, *7*, 5898-5919.
- [5] J. F. Scheerstra, A. C. Wauters, J. Tel, L. K. E. A. Abdelmohsen, J. C. M. van Hest, *Mater. Today Adv.* **2022**, *13*, 100203.
- [6] K. Strebhardt, A. Ullrich, *Nat. Rev. Cancer* **2008**, *8*, 473-480.
- [7] H. Ringsdorf, *Journal of Polymer Science: Polymer Symposia* **1975**, *51*, 135-153.
- [8] a) J. Lu, S. C. Owen, M. S. Shoichet, *Macromolecules* **2011**, *44*, 6002-6008; b) A. K. Barui, J. Y. Oh, B. Jana, C. Kim, J.-H. Ryu, *Adv. Ther.* **2020**, *3*, 1900124.
- [9] H. He, L. Liu, E. E. Morin, M. Liu, A. Schwendeman, *Acc. Chem. Res.* **2019**, *52*, 2445-2461.
- [10] P. Mi, K. Miyata, K. Kataoka, H. Cabral, *Adv. Ther.* **2021**, *4*, 2000159.
- [11] F. Rodríguez, P. Caruana, N. De la Fuente, P. Español, M. Gámez, J. Balart, E. Llurba, R. Rovira, R. Ruiz, C. Martín-Lorente, J. L. Corchero, M. V. Céspedes, *Biomolecules* **2022**, *12*, 784.
- [12] N. d'Avanzo, C. Celia, A. Barone, M. Carafa, L. Di Marzio, H. A. Santos, M. Fresta, *Adv. Ther.* **2020**, *3*, 1900170.
- [13] S. Zalba, T. L. M. ten Hagen, C. Burgui, M. J. Garrido, *J. Controlled Release* **2022**, *351*, 22-36.
- [14] a) Y. Cai, J. Qi, Y. Lu, H. He, W. Wu, *Adv. Drug Delivery Rev.* **2022**, *188*, 114463; b) X. Sun, G. Wang, H. Zhang, S. Hu, X. Liu, J. Tang, Y. Shen, *ACS Nano* **2018**, *12*, 6179-6192.
- [15] X. Yao, C. Qi, C. Sun, F. Huo, X. Jiang, *Nano Today* **2023**, *48*, 101738.
- [16] D. Braatz, J. H. Peter, M. Dimde, E. Quaas, K. Ludwig, K. Achazi, M. Schirner, M. Ballauff, R. Haag, *J. Mater. Chem. B* **2023**, *11*, 3797-3807.
- [17] Y. Barenholz, *J. Controlled Release* **2012**, *160*, 117-134.
- [18] W. J. Gradishar, *Expert Opin. Pharmacother.* **2006**, *7*, 1041-1053.
- [19] J. Gallego-Jara, G. Lozano-Terol, R. A. Sola-Martínez, M. Cánovas-Díaz, T. de Diego Puente, *Molecules* **2020**, *25*, 5986.
- [20] K. A. Whitehead, J. Matthews, P. H. Chang, F. Niroui, J. R. Dorkin, M. Severgnini, D. G. Anderson, *ACS Nano* **2012**, *6*, 6922-6929.
- [21] P. F. Zipfel, C. Skerka, *Mol. Immunol.* **2022**, *150*, 90-98.
- [22] L. Houdaihed, J. C. Evans, C. Allen, *Mol. Pharmaceutics* **2017**, *14*, 2503-2517.



- [23] L. I. Atanase, *Polymers* **2021**, *13*, 477.
- [24] S. C. Owen, D. P. Y. Chan, M. S. Shoichet, *Nano Today* **2012**, *7*, 53-65.
- [25] M. Ghezzi, S. Pescina, C. Padula, P. Santi, E. Del Favero, L. Cantù, S. Nicoli, *J. Controlled Release* **2021**, *332*, 312-336.
- [26] B. M. Davis, J. L. Richens, P. O'Shea, *Biophys. J.* **2011**, *101*, 245-254.
- [27] H.-j. Hsu, Y. Han, M. Cheong, P. Král, S. Hong, *Nanomedicine: Nanotechnology, Biology and Medicine* **2018**, *14*, 1879-1889.
- [28] L. Glavas, P. Olsén, K. Odelius, A.-C. Albertsson, *Biomacromolecules* **2013**, *14*, 4150-4156.
- [29] Y. Shi, T. Lammers, G. Storm, W. E. Hennink, *Macromol. Biosci.* **2017**, *17*, 1600160.
- [30] J. Wang, W. Mao, L. L. Lock, J. Tang, M. Sui, W. Sun, H. Cui, D. Xu, Y. Shen, *ACS Nano* **2015**, *9*, 7195-7206.
- [31] A. E. Nel, L. Mädler, D. Velegol, T. Xia, E. M. V. Hoek, P. Somasundaran, F. Klaessig, V. Castranova, M. Thompson, *Nat. Mater.* **2009**, *8*, 543-557.
- [32] W. Richtering, I. Alberg, R. Zentel, *Small* **2020**, *16*, 2002162.
- [33] a) K. Achazi, R. Haag, M. Ballauff, J. Dervede, J. N. Kizhakkedathu, D. Maysinger, G. Multhaupt, *Angew. Chem., Int. Ed.* **2021**, *60*, 3882-3904; b) Q. Wei, T. Becherer, S. Angioletti-Uberti, J. Dzubiella, C. Wischke, A. T. Neffe, A. Lendlein, M. Ballauff, R. Haag, *Angew. Chem., Int. Ed.* **2014**, *53*, 8004-8031.
- [34] a) N. Bertrand, P. Grenier, M. Mahmoudi, E. M. Lima, E. A. Appel, F. Dormont, J.-M. Lim, R. Karnik, R. Langer, O. C. Farokhzad, *Nat. Commun.* **2017**, *8*, 777; b) S. Behzadi, V. Serpooshan, R. Sakhtianchi, B. Müller, K. Landfester, D. Crespy, M. Mahmoudi, *Colloids Surf., B* **2014**, *123*, 143-149; c) S. Tenzer, D. Docter, J. Kuharev, A. Musyanovych, V. Fetz, R. Hecht, F. Schlenk, D. Fischer, K. Kiouptsi, C. Reinhardt, K. Landfester, H. Schild, M. Maskos, S. K. Knauer, R. H. Stauber, *Nat. Nanotechnol.* **2013**, *8*, 772-781.
- [35] J. M. Harris, R. B. Chess, *Nat. Rev. Drug Discovery* **2003**, *2*, 214-221.
- [36] J. Herzberger, K. Niederer, H. Pohlitz, J. Seiwert, M. Worm, F. R. Wurm, H. Frey, *Chem. Rev.* **2016**, *116*, 2170-2243.
- [37] D. Braatz, M. Cherri, M. Tully, M. Dimde, G. Ma, E. Mohammadifar, F. Reisbeck, V. Ahmadi, M. Schirner, R. Haag, *Angew. Chem., Int. Ed.* **2022**, *61*, e202203942.
- [38] A. Thomas, S. S. Müller, H. Frey, *Biomacromolecules* **2014**, *15*, 1935-1954.
- [39] B.-M. Chen, T.-L. Cheng, S. R. Roffler, *ACS Nano* **2021**, *15*, 14022-14048.
- [40] J. McCallen, J. Prybylski, Q. Yang, S. K. Lai, *ACS Biomater. Sci. Eng.* **2017**, *3*, 1605-1615.
- [41] P. H. Kierstead, H. Okochi, V. J. Venditto, T. C. Chuong, S. Kivimae, J. M. J. Fréchet, F. C. Szoka, *J. Controlled Release* **2015**, *213*, 1-9.

- [42] K. Shiraishi, M. Hamano, H. Ma, K. Kawano, Y. Maitani, T. Aoshi, K. J. Ishii, M. Yokoyama, *J. Controlled Release* **2013**, *165*, 183-190.
- [43] K. Shiraishi, K. Kawano, Y. Maitani, T. Aoshi, K. J. Ishii, Y. Sanada, S. Mochizuki, K. Sakurai, M. Yokoyama, *J. Controlled Release* **2016**, *234*, 59-67.
- [44] P. J. Flory, *J. Am. Chem. Soc.* **1952**, *74*, 2718-2723.
- [45] S. R. Sandler, F. R. Berg, *J. Polym. Sci., Part A-1: Polym. Chem.* **1966**, *4*, 1253-1259.
- [46] A. Dworak, W. Walach, B. Trzebicka, *Macromol. Chem. Phys.* **1995**, *196*, 1963-1970.
- [47] R. Tokar, P. Kubisa, S. Penczek, A. Dworak, *Macromolecules* **1994**, *27*, 320-322.
- [48] A. Sunder, R. Hanselmann, H. Frey, R. Mülhaupt, *Macromolecules* **1999**, *32*, 4240-4246.
- [49] C. Tonhauser, C. Schüll, C. Dingels, H. Frey, *ACS Macro Lett.* **2012**, *1*, 1094-1097.
- [50] R. A. Shenoi, J. K. Narayanannair, J. L. Hamilton, B. F. L. Lai, S. Horte, R. K. Kainthan, J. P. Varghese, K. G. Rajeev, M. Manoharan, J. N. Kizhakkedathu, *J. Am. Chem. Soc.* **2012**, *134*, 14945-14957.
- [51] E. Mohammadifar, F. Zabihi, Z. Tu, S. Hedtrich, A. Nemat Kharat, M. Adeli, R. Haag, *Polym. Chem.* **2017**, *8*, 7375-7383.
- [52] R. A. Shenoi, I. Chafeeva, B. F. L. Lai, S. Horte, J. N. Kizhakkedathu, *J. Polym. Sci., Part A: Polym. Chem.* **2015**, *53*, 2104-2115.
- [53] a) S. Abbina, S. Vappala, P. Kumar, E. M. J. Siren, C. C. La, U. Abbasi, D. E. Brooks, J. N. Kizhakkedathu, *J. Mater. Chem. B* **2017**, *5*, 9249-9277; b) D. Wilms, S.-E. Stiriba, H. Frey, *Acc. Chem. Res.* **2010**, *43*, 129-141; c) M. Calderón, M. A. Quadir, S. K. Sharma, R. Haag, *Adv. Mater.* **2010**, *22*, 190-218.
- [54] T. Tsuruta, S. Inoue, H. Koenuma, *Angew. Makromol. Chem.* **1968**, *112*, 58-65.
- [55] C. Billouard, S. Carlotti, P. Desbois, A. Deffieux, *Macromolecules* **2004**, *37*, 4038-4043.
- [56] M. Gervais, A. Labbé, S. Carlotti, A. Deffieux, *Macromolecules* **2009**, *42*, 2395-2400.
- [57] M. Imran ul-haq, B. F. L. Lai, R. Chapanian, J. N. Kizhakkedathu, *Biomaterials* **2012**, *33*, 9135-9147.
- [58] P. Pouyan, M. Cherri, R. Haag, *Polymers* **2022**, *14*, 2684.
- [59] H. Türk, R. Haag, S. Alban, *Bioconjugate Chem.* **2004**, *15*, 162-167.
- [60] N. Rades, K. Licha, R. Haag, *Polymers* **2018**, *10*, 595.
- [61] A. Sousa-Herves, P. Würfel, N. Wegner, J. Khandare, K. Licha, R. Haag, P. Welker, M. Calderón, *Nanoscale* **2015**, *7*, 3923-3932.
- [62] M. Cherri, M. Ferraro, E. Mohammadifar, E. Quaas, K. Achazi, K. Ludwig, C. Grötzinger, M. Schirner, R. Haag, *ACS Biomater. Sci. Eng.* **2021**, *7*, 2569-2579.
- [63] Y. Zhong, M. Dimde, D. Stöbener, F. Meng, C. Deng, Z. Zhong, R. Haag, *ACS Appl. Mater. Interfaces* **2016**, *8*, 27530-27538.

- [64] J. Dervede, A. Rausch, M. Weinhart, S. Enders, R. Tauber, K. Licha, M. Schirner, U. Zügel, A. von Bonin, R. Haag, *PNAS* **2010**, *107*, 19679-19684.
- [65] S. Kumari, M. Arora, J. Singh, S. S. Chauhan, S. Kumar, A. Chopra, *3 Biotech* **2021**, *11*, 38.
- [66] M. Weinhart, D. Gröger, S. Enders, J. Dervede, R. Haag, *Biomacromolecules* **2011**, *12*, 2502-2511.
- [67] Q. Ran, X. Xu, P. Dey, S. Yu, Y. Lu, J. Dzubiella, R. Haag, M. Ballauff, *J. Chem. Phys.* **2018**, *149*, 163324.
- [68] a) Y. Yan, K. T. Gause, M. M. J. Kamphuis, C.-S. Ang, N. M. O'Brien-Simpson, J. C. Lenzo, E. C. Reynolds, E. C. Nice, F. Caruso, *ACS Nano* **2013**, *7*, 10960-10970; b) M. P. Monopoli, D. Walczyk, A. Campbell, G. Elia, I. Lynch, F. Baldelli Bombelli, K. A. Dawson, *J. Am. Chem. Soc.* **2011**, *133*, 2525-2534.
- [69] C. Fasting, C. A. Schalley, M. Weber, O. Seitz, S. Hecht, B. Koksich, J. Dervede, C. Graf, E.-W. Knapp, R. Haag, *Angew. Chem., Int. Ed.* **2012**, *51*, 10472-10498.
- [70] N. Zhang, P. R. Wardwell, R. A. Bader, *Pharmaceutics* **2013**, *5*, 329-352.
- [71] D. L. Rabenstein, *Nat. Prod. Rep.* **2002**, *19*, 312-331.
- [72] S.-N. Ma, Z.-X. Mao, Y. Wu, M.-X. Liang, D.-D. Wang, X. Chen, P.-a. Chang, W. Zhang, J.-H. Tang, *Cell Adhes. Migr.* **2020**, *14*, 118-128.
- [73] F. Z. Dahmani, H. Yang, J. Zhou, J. Yao, T. Zhang, Q. Zhang, *Eur. J. Pharm. Sci.* **2012**, *47*, 179-189.
- [74] G. Mattheolabakis, L. Milane, A. Singh, M. M. Amiji, *J. Drug Targeting* **2015**, *23*, 605-618.
- [75] H.-J. Cho, I.-S. Yoon, H. Y. Yoon, H. Koo, Y.-J. Jin, S.-H. Ko, J.-S. Shim, K. Kim, I. C. Kwon, D.-D. Kim, *Biomaterials* **2012**, *33*, 1190-1200.
- [76] M. Swierczewska, H. S. Han, K. Kim, J. H. Park, S. Lee, *Adv. Drug Delivery Rev.* **2016**, *99*, 70-84.
- [77] D. A. Tomalia, D. P. Sheetz, *J. Polym. Sci., Part A-1: Polym. Chem.* **1966**, *4*, 2253-2265.
- [78] R. Konradi, B. Pidhatika, A. Mühlebach, M. Textor, *Langmuir* **2008**, *24*, 613-616.
- [79] S. Jana, M. Uchman, *Prog. Polym. Sci.* **2020**, *106*, 101252.
- [80] R. Luxenhofer, A. Schulz, C. Roques, S. Li, T. K. Bronich, E. V. Batrakova, R. Jordan, A. V. Kabanov, *Biomaterials* **2010**, *31*, 4972-4979.
- [81] L.-Y. Qiu, L. Yan, L. Zhang, Y.-M. Jin, Q.-H. Zhao, *Int. J. Pharm.* **2013**, *456*, 315-324.
- [82] N. E. Göppert, M. Kleinsteuber, C. Weber, U. S. Schubert, *Macromolecules* **2020**, *53*, 10837-10846.
- [83] C.-H. Wang, K.-R. Fan, G.-H. Hsiue, *Biomaterials* **2005**, *26*, 2803-2811.

- [84] H. P. C. Van Kuringen, J. Lenoir, E. Adriaens, J. Bender, B. G. De Geest, R. Hoogenboom, *Macromol. Biosci.* **2012**, *12*, 1114-1123.
- [85] Y. Ikada, H. Tsuji, *Macromol. Rapid Commun.* **2000**, *21*, 117-132.
- [86] B. D. Ulery, L. S. Nair, C. T. Laurencin, *J. Polym. Sci., Part B: Polym. Phys.* **2011**, *49*, 832-864.
- [87] A. Göpferich, *Biomaterials* **1996**, *17*, 103-114.
- [88] L. N. Woodard, M. A. Grunlan, *ACS Macro Lett.* **2018**, *7*, 976-982.
- [89] A. Stjern Dahl, A. Finne-Wistrand, A. C. Albertsson, C. M. Bäckesjö, U. Lindgren, *J. Biomed. Mater. Res., Part A* **2008**, *87A*, 1086-1091.
- [90] F. Nederberg, E. F. Connor, M. Möller, T. Glauser, J. L. Hedrick, *Angew. Chem., Int. Ed.* **2001**, *40*, 2712-2715.
- [91] A. P. Dove, *ACS Macro Lett.* **2012**, *1*, 1409-1412.
- [92] G. Becker, F. R. Wurm, *Chem. Soc. Rev.* **2018**, *47*, 7739-7782.
- [93] J. Li, R. M. Stayshich, T. Y. Meyer, *J. Am. Chem. Soc.* **2011**, *133*, 6910-6913.
- [94] H. Qian, A. R. Wohl, J. T. Crow, C. W. Macosko, T. R. Hoyer, *Macromolecules* **2011**, *44*, 7132-7140.
- [95] P. Alexandridis, T. Alan Hatton, *Colloids Surf., A* **1995**, *96*, 1-46.
- [96] A. V. Kabanov, E. V. Batrakova, V. Y. Alakhov, *J. Controlled Release* **2002**, *82*, 189-212.
- [97] A. Venne, S. Li, R. Mandeville, A. Kabanov, V. Alakhov, *Cancer Res.* **1996**, *56*, 3626-3629.
- [98] J. C. Sachdev, M. Jahanzeb, *Clin. Breast Cancer* **2016**, *16*, 73-81.
- [99] S. Danson, D. Ferry, V. Alakhov, J. Margison, D. Kerr, D. Jowle, M. Brampton, G. Halbert, M. Ranson, *Br. J. Cancer* **2004**, *90*, 2085-2091.
- [100] E. Peggion, M. Terbojevich, A. Cosani, C. Colombini, *J. Am. Chem. Soc.* **1966**, *88*, 3630-3632.
- [101] M. Yokoyama, S. Inoue, K. Kataoka, N. Yui, T. Okano, Y. Sakurai, *Angew. Makromol. Chem.* **1989**, *190*, 2041-2054.
- [102] H. Cabral, K. Kataoka, *J. Controlled Release* **2014**, *190*, 465-476.
- [103] Y. Bae, S. Fukushima, A. Harada, K. Kataoka, *Angew. Chem., Int. Ed.* **2003**, *42*, 4640-4643.
- [104] F. Koizumi, M. Kitagawa, T. Negishi, T. Onda, S.-i. Matsumoto, T. Hamaguchi, Y. Matsumura, *Cancer Res.* **2006**, *66*, 10048-10056.
- [105] M. Harada, I. Bobe, H. Saito, N. Shibata, R. Tanaka, T. Hayashi, Y. Kato, *Cancer Sci.* **2011**, *102*, 192-199.
- [106] T. Bus, A. Traeger, U. S. Schubert, *J. Mater. Chem. B* **2018**, *6*, 6904-6918.

- [107] T. Hamaguchi, Y. Matsumura, M. Suzuki, K. Shimizu, R. Goda, I. Nakamura, I. Nakatomi, M. Yokoyama, K. Kataoka, T. Kakizoe, *Br. J. Cancer* **2005**, *92*, 1240-1246.
- [108] Y. Fujiwara, H. Mukai, T. Saeki, J. Ro, Y.-C. Lin, S. E. Nagai, K. S. Lee, J. Watanabe, S. Ohtani, S. B. Kim, K. Kuroi, K. Tsugawa, Y. Tokuda, H. Iwata, Y. H. Park, Y. Yang, Y. Nambu, *Br. J. Cancer* **2019**, *120*, 475-480.
- [109] H. S. Oberoi, N. V. Nukolova, A. V. Kabanov, T. K. Bronich, *Adv. Drug Delivery Rev.* **2013**, *65*, 1667-1685.
- [110] N. Nishiyama, S. Okazaki, H. Cabral, M. Miyamoto, Y. Kato, Y. Sugiyama, K. Nishio, Y. Matsumura, K. Kataoka, *Cancer Res.* **2003**, *63*, 8977-8983.
- [111] H. Cabral, N. Nishiyama, S. Okazaki, H. Koyama, K. Kataoka, *J. Controlled Release* **2005**, *101*, 223-232.
- [112] N. Nishiyama, M. Yokoyama, T. Aoyagi, T. Okano, Y. Sakurai, K. Kataoka, *Langmuir* **1999**, *15*, 377-383.
- [113] J. Kopeček, P. Kopečková, *Adv. Drug Delivery Rev.* **2010**, *62*, 122-149.
- [114] P. Chytil, L. Kostka, T. Etrych, *J. Pers. Med.* **2021**, *11*, 115.
- [115] C. Li, S. Wallace, *Adv. Drug Delivery Rev.* **2008**, *60*, 886-898.
- [116] Y. Shi, M. J. van Steenbergen, E. A. Teunissen, L. s. Novo, S. Gradmann, M. Baldus, C. F. van Nostrum, W. E. Hennink, *Biomacromolecules* **2013**, *14*, 1826-1837.
- [117] Y. Shi, R. van der Meel, B. Theek, E. Oude Blenke, E. H. E. Pieters, M. H. A. M. Fens, J. Ehling, R. M. Schiffelers, G. Storm, C. F. van Nostrum, T. Lammers, W. E. Hennink, *ACS Nano* **2015**, *9*, 3740-3752.
- [118] C. Liang, X. Bai, C. Qi, Q. Sun, X. Han, T. Lan, H. Zhang, X. Zheng, R. Liang, J. Jiao, Z. Zheng, J. Fang, P. Lei, Y. Wang, D. Möckel, J. M. Metselaar, G. Storm, W. E. Hennink, F. Kiessling, H. Wei, T. Lammers, Y. Shi, B. Wei, *Biomaterials* **2021**, *266*, 120432.
- [119] A. A. Shalmani, Z. Ahmed, M. Sheybanifard, A. Wang, M. Weiler, E. M. Buhl, G. Klinkenberg, R. Schmid, W. Hennink, F. Kiessling, J. M. Metselaar, T. Lammers, Q. Peña, Y. Shi, *Biomacromolecules* **2023**.
- [120] S. Fujishige, K. Kubota, I. Ando, *J. Phys. Chem.* **1989**, *93*, 3311-3313.
- [121] O. Soga, C. F. van Nostrum, A. Ramzi, T. Visser, F. Soulimani, P. M. Frederik, P. H. H. Bomans, W. E. Hennink, *Langmuir* **2004**, *20*, 9388-9395.
- [122] D. Neradovic, M. J. van Steenbergen, L. Vansteelant, Y. J. Meijer, C. F. van Nostrum, W. E. Hennink, *Macromolecules* **2003**, *36*, 7491-7498.
- [123] O. Soga, C. F. van Nostrum, M. Fens, C. J. F. Rijcken, R. M. Schiffelers, G. Storm, W. E. Hennink, *J. Controlled Release* **2005**, *103*, 341-353.

- [124] M. Talelli, M. Iman, A. K. Varkouhi, C. J. F. Rijcken, R. M. Schiffelers, T. Etrych, K. Ulbrich, C. F. van Nostrum, T. Lammers, G. Storm, W. E. Hennink, *Biomaterials* **2010**, *31*, 7797-7804.
- [125] M. Talelli, M. Barz, C. J. F. Rijcken, F. Kiessling, W. E. Hennink, T. Lammers, *Nano Today* **2015**, *10*, 93-117.
- [126] C. J. F. Rijcken, F. De Lorenzi, I. Biancacci, R. G. J. M. Hanssen, M. Thewissen, Q. Hu, F. Atrafi, R. M. J. Liskamp, R. H. J. Mathijssen, I. H. C. Miedema, C. W. Menke - van der Houven van Oordt, G. A. M. S. van Dongen, D. J. Vugts, M. Timmers, W. E. Hennink, T. Lammers, *Adv. Drug Delivery Rev.* **2022**, *191*, 114613.
- [127] T. Lorson, M. M. Lübtow, E. Wegener, M. S. Haider, S. Borova, D. Nahm, R. Jordan, M. Sokolski-Papkov, A. V. Kabanov, R. Luxenhofer, *Biomaterials* **2018**, *178*, 204-280.
- [128] R. Luxenhofer, G. Sahay, A. Schulz, D. Alakhova, T. K. Bronich, R. Jordan, A. V. Kabanov, *J. Controlled Release* **2011**, *153*, 73-82.
- [129] A. Schulz, S. Jaksch, R. Schubel, E. Wegener, Z. Di, Y. Han, A. Meister, J. Kressler, A. V. Kabanov, R. Luxenhofer, C. M. Papadakis, R. Jordan, *ACS Nano* **2014**, *8*, 2686-2696.
- [130] L. Hahn, M. M. Lübtow, T. Lorson, F. Schmitt, A. Appelt-Menzel, R. Schobert, R. Luxenhofer, *Biomacromolecules* **2018**, *19*, 3119-3128.
- [131] C. Lim, J. D. Ramsey, D. Hwang, S. C. M. Teixeira, C.-D. Poon, J. D. Strauss, E. P. Rosen, M. Sokolsky-Papkov, A. V. Kabanov, *Small* **2022**, *18*, 2103552.
- [132] a) W. Zhang, R. Taheri-Ledari, F. Ganjali, S. S. Mirmohammadi, F. S. Qazi, M. Saeidirad, A. KashtiAray, S. Zarei-Shokat, Y. Tian, A. Maleki, *RSC Adv.* **2023**, *13*, 80-114; b) M. H. Stenzel, *Angew. Chem., Int. Ed.* **2021**, *60*, 2202-2206.
- [133] X. Wang, N. Hadjichristidis, *Macromolecules* **2020**, *53*, 223-232.
- [134] X. Wang, Z. Zhang, N. Hadjichristidis, *Prog. Polym. Sci.* **2023**, *136*, 101634.
- [135] S. Iqbal, Y. Qu, Z. Dong, J. Zhao, A. Rauf Khan, S. Rehman, Z. Zhao, *Eur. Polym. J.* **2020**, *141*, 110097.
- [136] X. Wang, N. Hadjichristidis, *ACS Macro Lett.* **2020**, *9*, 464-470.
- [137] K. Matsumoto, T. Yamamoto, R. Kamata, H. Maeda, *J. Biochem.* **1984**, *96*, 739-749.
- [138] H. Maeda, H. Nakamura, J. Fang, *Adv. Drug Delivery Rev.* **2013**, *65*, 71-79.
- [139] a) J. W. Nichols, Y. H. Bae, *J. Controlled Release* **2014**, *190*, 451-464; b) F. Danhier, *J. Controlled Release* **2016**, *244*, 108-121.
- [140] W. Gu, F. Meng, R. Haag, Z. Zhong, *J. Controlled Release* **2021**, *329*, 676-695.
- [141] L. Taiariol, C. Chaix, C. Farre, E. Moreau, *Chem. Rev.* **2022**, *122*, 340-384.
- [142] *C&EN Global Enterprise* **2016**, *94*, 13-13.
- [143] S. Wilhelm, A. J. Tavares, Q. Dai, S. Ohta, J. Audet, H. F. Dvorak, W. C. W. Chan, *Nat. Rev. Mater.* **2016**, *1*, 16014.

- [144] D. Sun, S. Zhou, W. Gao, *ACS Nano* **2020**, *14*, 12281-12290.
- [145] M. Zhu, A. K. Whittaker, F. Y. Han, M. T. Smith, *Appl. Sci.* **2022**, *12*, 935.
- [146] M. Kaksonen, A. Roux, *Nat. Rev. Mol. Cell Biol.* **2018**, *19*, 313-326.
- [147] Y.-B. Hu, E. B. Dammer, R.-J. Ren, G. Wang, *Transl. Neurodegener.* **2015**, *4*, 18.
- [148] a) P. Chan, J. Lovrić, J. Warwicker, *Proteomics* **2006**, *6*, 3494-3501; b) M. J. Geisow, *Exp. Cell Res.* **1984**, *150*, 29-35; c) M. J. Geisow, W. H. Evans, *Exp. Cell Res.* **1984**, *150*, 36-46; d) R. K. Paradise, D. A. Lauffenburger, K. J. Van Vliet, *PLoS One* **2011**, *6*, e15746; e) E. C. Ruth, R. J. C. Christopher, H. Laura, J. H. Paul, J. M. Iain, L. Peter, *Drug Metab. Dispos.* **2011**, *39*, 551; f) C. Ma, S. Subramani, *IUBMB Life* **2009**, *61*, 713-722.
- [149] R. Niu, H. Jing, Z. Chen, J. Xu, J. Dai, Z. Yan, *Asia-Pacific Journal of Clinical Oncology* **2012**, *8*, 362-367.
- [150] H. Dong, L. Pang, H. Cong, Y. Shen, B. Yu, *Drug Delivery* **2019**, *26*, 416-432.
- [151] S. H. S. Boddu, P. Bhagav, P. K. Karla, S. Jacob, M. D. Adatiya, T. M. Dhameliya, K. M. Ranch, A. K. Tiwari, *J. Funct. Biomater.* **2021**, *12*, 58.
- [152] Y. Li, C. Zhang, G. Li, G. Deng, H. Zhang, Y. Sun, F. An, *Acta Pharm. Sin. B* **2021**, *11*, 2220-2242.
- [153] C. Ortiz, M. L. Ferreira, O. Barbosa, J. C. S. dos Santos, R. C. Rodrigues, Á. Berenguer-Murcia, L. E. Briand, R. Fernandez-Lafuente, *Catal. Sci. Technol.* **2019**, *9*, 2380-2420.
- [154] D. K. Kölmel, E. T. Kool, *Chem. Rev.* **2017**, *117*, 10358-10376.
- [155] P. T. Wong, S. K. Choi, *Chem. Rev.* **2015**, *115*, 3388-3432.
- [156] H. J. Forman, H. Zhang, A. Rinna, *Mol. Aspects Med.* **2009**, *30*, 1-12.
- [157] L. Flohé, *Biochim. Biophys. Acta* **2013**, *1830*, 3139-3142.
- [158] M. H. Lee, Z. Yang, C. W. Lim, Y. H. Lee, S. Dongbang, C. Kang, J. S. Kim, *Chem. Rev.* **2013**, *113*, 5071-5109.
- [159] a) R. Bej, P. Dey, S. Ghosh, *Soft Matter* **2020**, *16*, 11-26; b) H. Sun, F. Meng, R. Cheng, C. Deng, Z. Zhong, *Antioxid. Redox Signaling* **2013**, *21*, 755-767.
- [160] a) H. Sun, B. Guo, R. Cheng, F. Meng, H. Liu, Z. Zhong, *Biomaterials* **2009**, *30*, 6358-6366; b) T.-B. Ren, Y. Feng, Z.-H. Zhang, L. Li, Y.-Y. Li, *Soft Matter* **2011**, *7*, 2329-2331.
- [161] a) R. Wei, L. Cheng, M. Zheng, R. Cheng, F. Meng, C. Deng, Z. Zhong, *Biomacromolecules* **2012**, *13*, 2429-2438; b) Y. Liu, M. J. van Steenbergen, Z. Zhong, S. Oliveira, W. E. Hennink, C. F. van Nostrum, *Macromolecules* **2020**, *53*, 7009-7024; c) X. Zhang, R. M. Waymouth, *J. Am. Chem. Soc.* **2017**, *139*, 3822-3833.
- [162] N. M. Salkho, N. S. Awad, W. G. Pitt, G. A. Hussein, *Polymers* **2022**, *14*, 1286.
- [163] L. Josa-Culleré, A. Llebaria, *ChemPhotoChem* **2021**, *5*, 296-314.

- [164] W. Zhao, Y. Zhao, Q. Wang, T. Liu, J. Sun, R. Zhang, *Small* **2019**, *15*, 1903060.
- [165] B. M. Vickerman, E. M. Zywoot, T. K. Tarrant, D. S. Lawrence, *Nat. Rev. Chem.* **2021**, *5*, 816-834.
- [166] M. Grandbois, M. Beyer, M. Rief, H. Clausen-Schaumann, H. E. Gaub, *Science* **1999**, *283*, 1727-1730.
- [167] Y. Li, Y. Wang, G. Huang, J. Gao, *Chem. Rev.* **2018**, *118*, 5359-5391.
- [168] C. Tanford, *Science* **1978**, *200*, 1012-1018.
- [169] Q. Sun, *Molecules* **2022**, *27*, 7009.
- [170] P. Ma, R. J. Mumper, *J. Nanomed. Nanotechnol.* **2013**, *4*, 1000164.
- [171] C. A. Hunter, J. K. M. Sanders, *J. Am. Chem. Soc.* **1990**, *112*, 5525-5534.
- [172] A. Banerjee, A. Saha, B. K. Saha, *Cryst. Growth Des.* **2019**, *19*, 2245-2252.
- [173] K. M. Makwana, R. Mahalakshmi, *Protein Sci.* **2015**, *24*, 1920-1933.
- [174] S. K. Min, W. Y. Kim, Y. Cho, K. S. Kim, *Nat. Nanotechnol.* **2011**, *6*, 162-165.
- [175] T. Chen, M. Li, J. Liu, *Cryst. Growth Des.* **2018**, *18*, 2765-2783.
- [176] W.-R. Zhuang, Y. Wang, P.-F. Cui, L. Xing, J. Lee, D. Kim, H.-L. Jiang, Y.-K. Oh, *J. Controlled Release* **2019**, *294*, 311-326.
- [177] A. Ben-Naim, *J. Phys. Chem.* **1991**, *95*, 1437-1444.
- [178] a) C.-C. Cheng, Y.-T. Sun, A.-W. Lee, S.-Y. Huang, W.-L. Fan, Y.-H. Chiao, C.-W. Chiu, J.-Y. Lai, *Polym. Chem.* **2020**, *11*, 2791-2798; b) S. H. Kim, J. P. K. Tan, F. Nederberg, K. Fukushima, J. Colson, C. Yang, A. Nelson, Y.-Y. Yang, J. L. Hedrick, *Biomaterials* **2010**, *31*, 8063-8071.
- [179] H.-X. Zhou, X. Pang, *Chem. Rev.* **2018**, *118*, 1691-1741.
- [180] A. Harada, K. Kataoka, *Macromolecules* **1995**, *28*, 5294-5299.
- [181] I. Insua, A. Wilkinson, F. Fernandez-Trillo, *Eur. Polym. J.* **2016**, *81*, 198-215.
- [182] R. Ridolfo, S. Tavakoli, V. Junnuthula, D. S. Williams, A. Urtti, J. C. M. van Hest, *Biomacromolecules* **2021**, *22*, 126-133.
- [183] M. G. Gouveia, J. P. Wesseler, J. Ramaekers, C. Weder, P. B. V. Scholten, N. Bruns, *Chem. Soc. Rev.* **2023**, *52*, 728-778.
- [184] J. N. Israelachvili, D. J. Mitchell, B. W. Ninham, *J. Chem. Soc., Faraday Trans. 2* **1976**, *72*, 1525-1568.
- [185] C. Cao, L. Zhang, B. Kent, S. Wong, C. J. Garvey, M. H. Stenzel, *Angew. Chem., Int. Ed.* **2021**, *60*, 10342-10349.
- [186] Y. Lu, J. Lin, L. Wang, L. Zhang, C. Cai, *Chem. Rev.* **2020**, *120*, 4111-4140.
- [187] B. N. S. Thota, L. H. Uner, R. Haag, *Chem. Rev.* **2016**, *116*, 2079-2102.
- [188] a) B. List, R. A. Lerner, C. F. Barbas, *J. Am. Chem. Soc.* **2000**, *122*, 2395-2396; b) K. A. Ahrendt, C. J. Borths, D. W. C. MacMillan, *J. Am. Chem. Soc.* **2000**, *122*, 4243-4244.



- [189] a) M. K. Kiesewetter, E. J. Shin, J. L. Hedrick, R. M. Waymouth, *Macromolecules* **2010**, *43*, 2093-2107; b) N. E. Kamber, W. Jeong, R. M. Waymouth, R. C. Pratt, B. G. G. Lohmeijer, J. L. Hedrick, *Chem. Rev.* **2007**, *107*, 5813-5840.
- [190] A. Basterretxea, C. Jehanno, D. Mecerreyes, H. Sardon, *ACS Macro Lett.* **2019**, *8*, 1055-1062.
- [191] E. F. Connor, G. W. Nyce, M. Myers, A. Möck, J. L. Hedrick, *J. Am. Chem. Soc.* **2002**, *124*, 914-915.
- [192] A. P. Dove, R. C. Pratt, B. G. G. Lohmeijer, D. A. Culkin, E. C. Hagberg, G. W. Nyce, R. M. Waymouth, J. L. Hedrick, *Polymer* **2006**, *47*, 4018-4025.
- [193] B. G. G. Lohmeijer, R. C. Pratt, F. Leibfarth, J. W. Logan, D. A. Long, A. P. Dove, F. Nederberg, J. Choi, C. Wade, R. M. Waymouth, J. L. Hedrick, *Macromolecules* **2006**, *39*, 8574-8583.
- [194] a) O. Dechy-Cabaret, B. Martin-Vaca, D. Bourissou, *Chem. Rev.* **2004**, *104*, 6147-6176; b) A.-C. Albertsson, I. K. Varma, *Biomacromolecules* **2003**, *4*, 1466-1486.
- [195] a) R. C. Pratt, B. G. G. Lohmeijer, D. A. Long, R. M. Waymouth, J. L. Hedrick, *J. Am. Chem. Soc.* **2006**, *128*, 4556-4557; b) C. Sabot, K. A. Kumar, S. Meunier, C. Mioskowski, *Tetrahedron Lett.* **2007**, *48*, 3863-3866; c) M. K. Kiesewetter, M. D. Scholten, N. Kirn, R. L. Weber, J. L. Hedrick, R. M. Waymouth, *J. Org. Chem.* **2009**, *74*, 9490-9496.
- [196] A. Chuma, H. W. Horn, W. C. Swope, R. C. Pratt, L. Zhang, B. G. G. Lohmeijer, C. G. Wade, R. M. Waymouth, J. L. Hedrick, J. E. Rice, *J. Am. Chem. Soc.* **2008**, *130*, 6749-6754.
- [197] Q. Sun, X. Sun, X. Ma, Z. Zhou, E. Jin, B. Zhang, Y. Shen, E. A. Van Kirk, W. J. Murdoch, J. R. Lott, T. P. Lodge, M. Radosz, Y. Zhao, *Adv. Mater.* **2014**, *26*, 7615-7621.
- [198] T. Ojha, Q. Hu, C. Colombo, J. Wit, M. van Geijn, M. J. van Steenbergen, M. Bagheri, H. Königs-Werner, E. M. Buhl, R. Bansal, Y. Shi, W. E. Hennink, G. Storm, C. J. F. Rijcken, T. Lammers, *Biotechnol. J.* **2021**, *16*, 2000212.

## List of Abbreviations

<b>°C</b>	Degree Celsius
<b>5-FU</b>	5-Fluorouracil
<b>ABC</b>	Accelerated Blood Clearance
<b>ACUPA</b>	((S)-2-(3-((S)-5-amino-1-carboxypentyl) ureido) Pentanedioic acid
<b>AGE</b>	Allylglycidylether
<b>aROP</b>	Anionic Ring Opening Polymerization
<b>Asp</b>	Aspartic Acid
<b>BASF</b>	Badischen Anilin- & Sodafabrik
<b>BCP</b>	Block Copolymers
<b>CD44</b>	CD44 Antigen
<b>CMC</b>	Critical Micelle Concentration
<b>CPP</b>	Critical Packing Parameter
<b>CsOH</b>	Caesiumhydroxide
<b>CUR</b>	Coumarin
<b>DACHPt</b>	Dichloro(1,2-Diaminocyclohexane) Platinum(II)
<b>DLS</b>	Dynamic Light Scattering
<b>DNA</b>	Deoxyribonucleic Acid
<b>DOX</b>	Doxorubicin
<b>dPG</b>	Dendritic Polyglycerol
<b>dPGS</b>	Dendritic Polyglycerolsulfate
<b>DTX</b>	Docetaxel
<b>EEGE</b>	Ethoxy Ethyl Glycidyl Ether
<b>EMA</b>	European Medicines Agency
<b>EPR</b>	Enhanced Permeability and Retention
<b>Et</b>	Ethyl
<b>FDA</b>	Food and Drug Administration
<b>GIST</b>	Gastrointestinal Stromal Tumor
<b>Glu</b>	Glutamic Acid
<b>GPC</b>	Gel Permeations Chromatography
<b>GRAS</b>	Generally Recognized As Safe
<b>GSH</b>	Glutathione
<b>hPG</b>	Hyperbranched Polyglycerol
<b>HPMA</b>	N-(2-Hydroxypropyl) Methacrylamide
<b>HSA</b>	Human Serum Albumin

<b><i>i</i>-But<sub>3</sub>Al</b>	<i>iso</i> -Tributylaluminium
<b>IC<sub>50</sub></b>	Half Maximal Inhibitory Concentration
<b>ITC</b>	Isothermal Titration Calorimetry
<b>KB tumor</b>	Human Epithelial Carcinoma Cells
<b>I-PEI</b>	Linear Polyethyleneimine
<b>LCST</b>	Lower Critical Solution Temperature
<b>LV</b>	Leucovorin
<b>mM</b>	Mili Molar
<b>mPEG</b>	Methoxy Polyethylene glycol
<b>MST</b>	Microscale Thermophoresis
<b>NCA</b>	N-Carboxyanhydrides
<b>nm</b>	Nano Meter
<b>nM</b>	Nano Molar
<b>NMR</b>	Nuclear magnetic resonance spectroscopy
<b>ONB</b>	<i>ortho</i> -Nitrobenzyl
<b>Ox</b>	4,5-Dihydro-1,3-oxazole or 2-oxazoline
<b>OxP</b>	<i>N</i> -acylated-1,4-oxazepan-7-one
<b>P(NIPAM)</b>	Poly( <i>N</i> -isopropylacrylamide)
<b>PCL</b>	Polycaprolactone
<b>PEG</b>	Polyethylene glycol
<b>PEI</b>	Polyethyleneimine
<b>PEO</b>	Polyethylene oxide
<b>PEtOx</b>	Poly(2-ethyl-2-oxazoline)
<b>PG</b>	Polyglycerol
<b>PLA</b>	Poly lactide
<b>PLGA</b>	Poly lactide- <i>co</i> -glycolide
<b>PMeOx</b>	Poly(2-methyl-2-oxazoline)
<b>PPO</b>	Polypropylene oxide
<b>PSMA</b>	Prostate-Specific Membrane Antigen
<b>PSN</b>	Peripheral Sensory Neuron
<b>PTX</b>	Paclitaxel
<b>Py</b>	Pyrene
<b>RCC</b>	Renal Cell Carcinoma
<b>RNA</b>	Ribonucleic Acid
<b>ROCP</b>	Ring Opening Copolymerization
<b>ROP</b>	Ring Opening Polymerization

<b>RTK</b>	Receptor Tyrosine Kinase
<b>SCC7</b>	Squamous Cell Carcinoma
<b>SN-38</b>	7-Ethyl-10-hydroxycamptothecin
<b>SPR</b>	Surface Plasmon Resonance
<b>tBGE</b>	<i>tert-butyl</i> Glycidyl Ether
<b>TMP</b>	2-Ethyl-2-(hydroxymethyl)propane-1,3-diol
<b>TMSG</b>	Trimethylsilyl Glycidyl Ether
<b>UFH</b>	Unfractionated Heparin
<b>UV</b>	Ultraviolet
<b>WHO</b>	World Health Organization

# Scientific Outreach: Publications, Patents, Conferences

## Publications

1. **D. Braatz**, J. H. Peter, M. Dimde, E. Quaas, K. Ludwig, K. Achazi, M. Schirner, M. Ballauff, R. Haag Dendritic polyglycerolsulfate-SS-poly(ester amide) micelles for the systemic delivery of docetaxel: pushing the limits of stability through the insertion of  $\pi$ - $\pi$  interactions *J. Mater. Chem. B*, **2023**, 11, 3797-3807.
2. **D. Braatz**, M. Cherri, M. Tully, M. Dimde, G. Ma, E. Mohammadifar, F. Reisbeck, V. Ahmadi, M. Schirner, R. Haag Approaches to Synthetic Drug Delivery Systems for Systemic Applications *Angew. Chem. Int. Ed.* **2022**, 61, e202203942.
3. **D. Braatz**, M. Cherri, M. Tully, M. Dimde, G. Ma, E. Mohammadifar, F. Reisbeck, V. Ahmadi, M. Schirner, R. Haag Chemische Ansätze für synthetische Wirkstofftransportsysteme für systemische Anwendungen *Angew. Chem.* **2022**, 134, e202203942.
4. **D. Braatz**, M. Dimde, G. Ma, Y. Zhong, M. Tully, C. Grötzinger, Y. Zhang, A. Mavroskoufis, M. Schirner, Z. Zhong, M. Ballauff, R. Haag, *Biomacromolecules* **2021**, 22, 6, 2625–2640. Toolbox of Biodegradable Dendritic (Poly Glycerol Sulfate)-SS-poly(ester) Micelles for Cancer Treatment: Stability, Drug Release, and Tumor Targeting.
5. S. Gholami, M. Dimde, **D. Braatz**, J. Müller, R. Haag, O. Wagner, *Environmental Technology & Innovation*, **2020**, 19, 101005. Reusable Biopolymer-based Heavy Metal Filter as Plant Protection for Phytoremediation.

## Patents

WO 2021/152171: Micellar composition from an amphiphilic copolymer for tumor therapy

## Conference Contributions

### Online Speed Lecture and Poster Presentation

1. Bayreuth Polymer Symposium (BPS21), Bayreuth, Germany, 20. September – 21. September 2021; Toolbox of Biodegradable Dendritic (Poly glycerol sulfate)-SS-poly(ester) Micelles for Cancer Treatment: Stability, Drug Release, and Tumor Targeting; **Daniel Braatz**, Mathias Dimde, Guoxin Ma, Yinan Zhong, Michael Tully, Carsten Grötzinger, Yuanyuan Zhang, Alexandros Mavroskoufis, Michael Schirner, Zhiyuan Zhong, Matthias Ballauff, and Rainer Haag

### **On-site Poster Presentation**

2. Kick-Off Meeting of the IRTG2662, Berlin, Germany, 03. October – 05. October 2021; Synthesis and Evaluation of Micellar Dendritic Poly(glycerol sulfate) Systems; **Daniel Braatz**, Matthias Ballauff, and Rainer Haag
3. IRTG2662: Workshop at University of British Columbia, Vancouver, Canada, 17. July – 19. July 2022; Dendritic Polyelectrolytes to Promote Enhanced Neuronal Biocompatibility; **Daniel Braatz**, Stephan Block, Matthias Ballauff, Timothy E. Kennedy, and Rainer Haag

### **On-site Oral Presentation**

4. IRTG2662 Annual Meeting 2023, Berlin, Germany, 06. July – 07. July 2023; Dendritic Polyglycerolamine-Peptide Conjugates for Neuronal Cell Culture; **Daniel Braatz**, Matthias Ballauff, Timothy E. Kennedy, and Rainer Haag
5. ACS Fall Meeting 2023, San Francisco, California, United States of America, 13. August - 17. August 2023; Negatively Charged Dendritic Polyelectrolytes in Biomedical Applications; **Daniel Braatz**, Matthias Ballauff, and Rainer Haag